Technological Advances in Bioreporter-Based Screening for Mechanism-Informed Antibiotic Discovery in *Bacillus subtilis*

Dissertation

der Mathematisch-Naturwissenschaftlichen Fakultät

der Eberhard Karls Universität Tübingen

zur Erlangung des Grades eines

Doktors der Naturwissenschaften

(Dr. rer. nat.)

vorgelegt von

Julian Frederik Schubert

aus Würzburg

Tübingen

2026

Gedruckt mit Genehmigung der Mathematisch-Naturwissenschaftlichen Fakultät der Eberhard Karls Universität Tübingen.

Tag der mündlichen Qualifikation:	21.07.2026
Dekan:	Prof. Dr. Thilo Stehle
1. Berichterstatter/-in:	Prof. Dr. Heike Brötz-Oesterhelt
2. Berichterstatter/-in:	Prof. Dr. Wolfgang Wohlleben

Erklärung

Hiermit erkläre ich, dass ich die zur Promotion eingereichte Dissertation selbständig verfasst, nur die angegebenen Quellen und Hilfsmittel benutzt und Stellen, die wörtlich oder inhaltlich aus den Werken anderer Autoren entnommen sind, als solche gekennzeichnet habe. Eine detaillierte Abgrenzung meiner eigenen Leistungen gegenüber den Beiträgen meiner Kooperationspartner in den in dieser Arbeit diskutierten Publikationen und Manuskripten habe ich in der „Declaration of personal contribution“ vorgenommen.

_____

Tübingen, den 11.06.2026

TABLE OF CONTENTS

SUMMARY

The discovery of new antibacterial agents with potent and well-defined mechanisms of action has become essential for addressing the growing burden of antibiotic resistance. However, traditional screening pipelines remain constrained by low throughput, limited specificity, and labor-intensive dereplication. These limitations highlight the need for new screening strategies that accelerate antibacterial discovery and enable early mechanistic assessment. This dissertation describes the advancement of a bioreporter-based screening platform in *Bacillus subtilis* that combines mechanism-informed whole-cell screening with an efficient compound discovery and dereplication workflow. For this purpose, a new generation of bioreporters based on the bacterial luciferase system was developed, including a novel bioreporter specific for proteotoxic stress. In parallel, a customized workflow for the discovery and rapid dereplication of antibacterial agents was established, enabling the seamless integration of the bioreporter technology. The first study implemented the compound-resolved bioactivity-based metabolomics pipeline, which combines the bioreporter panel with high-frequency microfractionation onto microfluidic paper-analytical devices and non-targeted LC-MS/MS. This approach enabled high-throughput antibiotic screening and the identification of bioactive compounds from pure compounds, crude extracts, and producer strains, while providing early insights into their mechanisms of action. The second study expanded the mechanistic coverage of the bioreporter panel by developing a sensitive bioreporter that signals proteotoxic stress caused by the accumulation of damaged or misfolded proteins. Validation with an extensive set of antibacterial reference compounds confirmed the high specificity of the bioreporter for antibacterial agents that induce proteotoxic stress and enabled the discovery of several compounds not previously associated with this mechanism. Integration of the bioreporter with the microfractionation workflow facilitated the identification of an extensive molecular network of streptothricin derivatives from the Tübingen collection of actinomycete producer strains, including multiple putatively novel analogues. Overall, this work establishes a versatile, bioreporter-based screening platform for mechanism-informed antibiotic discovery and dereplication. By directly linking bioactivity to compound identity at early stages of screening, this approach enables efficient exploration of natural products and the discovery of new antibacterial agents.

ZUSAMMENFASSUNG

Die Entdeckung neuer antibakterieller Wirkstoffe mit potenten und klar definierten Wirkmechanismen ist angesichts der zunehmenden Belastung durch Antibiotikaresistenzen von entscheidender Bedeutung. Traditionelle Screening-Pipelines sind jedoch weiterhin durch geringen Durchsatz, begrenzte Spezifität und arbeitsintensive Dereplikationsprozesse eingeschränkt. Diese Einschränkungen verdeutlichen den Bedarf an neuen Screening-Strategien, die die Entdeckung antibakterieller Substanzen beschleunigen und eine frühzeitige mechanistische Charakterisierung ermöglichen. Diese Dissertation beschreibt die Weiterentwicklung einer Bioreporter-basierten Screening-Plattform in *Bacillus subtilis*, die Mechanismus-unterstütztes Ganzzell-Screening mit einem effizienten Workflow zur Wirkstoffentdeckung und Dereplikation kombiniert. Hierfür wurde eine neue Generation von Bioreportern auf Basis eines bakteriellen Luciferase-Systems entwickelt, einschließlich eines neuartigen Bioreporters zur Detektion von proteotoxischem Stress. Parallel dazu wurde ein individuell angepasster Workflow zur Entdeckung und schnellen Dereplikation antibakterieller Substanzen etabliert, der eine nahtlose Integration der Bioreporter-Technologie ermöglicht. Die erste Studie implementierte die wirkstoffspezifische, bioaktivitätsbasierte Metabolomics-Pipeline, die das Bioreporter-Panel mit hochfrequenter Mikrofraktionierung auf mikrofluidischen, papierbasierten Analysematerialien sowie nicht-zielgerichteter LC-MS/MS kombinierte. Dieser Ansatz ermöglichte ein hochdurchsatzfähiges Antibiotika-Screening sowie die Identifizierung bioaktiver Verbindungen aus Reinsubstanzen, Rohextrakten und Produzentenstämmen und lieferte gleichzeitig frühe Einblicke in deren Wirkmechanismen. Die zweite Studie erweiterte die mechanistische Reichweite des Bioreporter-Panels durch die Entwicklung eines sensitiven Bioreporters, der proteotoxischen Stress infolge der Akkumulation geschädigter oder fehlgefalteter Proteine detektiert. Die Validierung mit einem umfangreichen Set an antibakteriellen Referenzverbindungen bestätigte die hohe Spezifität des Bioreporters für Wirkstoffe, die proteotoxischen Stress induzieren, und führte zur Identifizierung mehrerer Verbindungen, die bislang nicht mit diesem Mechanismus in Verbindung gebracht worden waren. Die Integration der Bioreporter in den Mikrofraktionierungs-Workflow ermöglichte zudem die Identifizierung eines umfangreichen molekularen Netzwerks von Streptothricin-Derivaten aus der Tübinger

Actinomyceten-Stammsammlung, einschließlich mehrerer vermutlich neuartiger Analoga. Insgesamt etabliert diese Arbeit eine vielseitige, Bioreporter-basierte Screening-Plattform für Mechanismus-unterstützte Antibiotikaentdeckung und Dereplikation. Durch die direkte Verknüpfung von Bioaktivität und Substanzidentität in frühen Screening-Phasen schafft dieser Ansatz die Grundlage für eine effiziente Erschließung von Naturstoffen sowie die Entdeckung neuer antibakterieller Wirkstoffe.

ABBREVIATIONS

µg	microgram
µl	microliter
µm	micrometer
µPAD	microfluidic paper-analytical device
ABC	ATP-binding cassette
Ac	acetyl
Ac-CoA	acetyl-coenzyme A
AChBP	acetylcholine-binding protein
ADEP	acyldepsipeptide
ATP	adenosine triphosphate
AUC	area under the curve
BMM	Belitzky minimal medium
bp	base pair
calcd.	calculated
CAM	chloramphenicol
CCCP	carbonyl cyanide m-chlorophenylhydrazone
CER	cerulenin
CFU	colony-forming units
CIP	ciprofloxacin
Clp	caseinolytic protease
CtsR	class three stress response regulator
Da	Dalton
DAP	daptomycin
DHFA	dihydrofolic acid
DMSO	dimethyl sulfoxide
DNA	deoxyribonucleic acid
e.g.	*exempli gratia*
EF	elongation factor
ERY	erythromycin
ESI	electrospray ionization
EtOAc	ethyl acetate
EtOH	ethanol
FA	formic acid
FAS	fatty acid synthesis
$FMNH_2$	reduced flavin mononucleotide
GEN	gentamicin
GNPS2	Global Natural Products Social Molecular Networking 2
GTP	guanosine triphosphate
HPLC	high-performance liquid chromatography
i.d.	inner diameter
i.e.	*id est*
ISP2	International Streptomyces Project medium 2
ISP3	International Streptomyces Project medium 3
LB	lysogeny broth
LC	liquid chromatography
lipid II	peptidoglycan precursor lipid II

LOD	limit of detection	PLA	polylactic acid
lux	bacterial luciferase	ppm	parts per million
LZD	linezolid	RMP	rifampicin
m/z	mass-to-charge ratio	RNA	ribonucleic acid
MEF	mefloquine	RP	reversed phase
MER	meropenem	RT	room temperature
MFX	moxifloxacin	*sacA*	sucrose-6-phosphate hydrolase gene
MIC	minimum inhibitory concentration	Sats	streptothricin acetyltransferase
ml	milliliter	SD	standard deviation
mm	millimeter	SI	supplementary information
MoA	mechanism of action	SOS	DNA damage-induced SOS response
mRNA	messenger RNA	STP	streptothricin
MS	mass spectrometry	TCS	triclosan
ms	milliseconds	TET	tetracycline
MS/MS	tandem mass spectrometry	THFA	tetrahydrofolic acid
MS1	first stage of mass spectrometry	TIC	total ion current
MS2	second stage of mass spectrometry	TMAD	tetramethylazodicarboxamide
mzML	mass spectrometry markup language	TMP	trimethoprim
NAD^+	nicotinamide adenine dinucleotide	tRNA	transfer RNA
NEM	*N*-ethylmaleimide	UV	ultraviolet light
ng	nanogram	V/V	volume per volume
nm	nanometer	VAN	vancomycin
o.c.	on column	Vis	visible light
OD	optical density	XIC	extracted ion chromatogram
PCR	polymerase chain reaction		

LIST OF PUBLICATIONS

Accepted Publications

Publication I

Geibel, C.; **Schubert, J.**; Knoblauch, S.B.; Hernandez, A.; Boldt, L.; Schneider, D.C.; Papadopoulos Lambidis, S.; Vitale, G.A.; Fleischer, J.; Haussmann, M.; Gross, H.; Wang, M.; Brötz-Oesterhelt, H.; Petras, D. *High-Frequency Microfluidic Fractionation for Compound-Resolved Bioactivity-Based Metabolomics. Anal. Chem.* **2025**, 97 (43), 24093-24104. DOI: 10.1021/acs.analchem.5c04612.

Publication II

Schubert, J.; Geibel, C.; Berscheid, A.; Wex, K.W.; Vitale, G.A.; Hughes, C.C.; Petras, D.; Brötz-Oesterhelt, H. *Proteotoxic Stress Bioreporter Enables Mechanism-Informed Antibiotic Discovery. J. Nat. Prod.* **2026**, 89 (6), 1698–1710. DOI: 10.1021/acs.jnatprod.6c00112.

DECLARATION OF PERSONAL CONTRIBUTION

Publication I

The study was conceptualized and designed by Daniel Petras, Heike Brötz-Oesterhelt, Christian Geibel, and the author. The development, construction, and all experimental work associated with the bioreporters were performed by the author, except for bioreporter validation, which was conducted by Leonardo Boldt under the supervision of the author. The author carried out the cultivation, harvesting, and isolation of natural antibiotic-producing strains. The author also contributed to dereplication, data analysis, and software-based visualization. The manuscript was written collaboratively by Daniel Petras, Heike Brötz-Oesterhelt, Christian Geibel, and the author. The author prepared the figures related to the bioreporter assays, while Dana Schneider contributed the agar overlay image for bioreporter validation. All authors approved the final version.

Publication II

The study was conceptualized and designed by Heike Brötz-Oesterhelt in collaboration with the author. The development, construction, validation, and all experimental work associated with the bioreporter were performed by the author, with guidance on bioreporter design and promoter selection provided by Katharina Wex and Anne Berscheid. Cultivation, harvesting, and isolation of natural producer strains from the Tübingen strain collection were carried out by the author, with support from Marita Wurm and Sigrid Stockert. Christian Geibel conducted the microspotting. The author conducted the dereplication, data analysis, and software-based visualization, with assistance from Christian Geibel and Giovanni Andrea Vitale. The manuscript was written collaboratively by Heike Brötz-Oesterhelt and the author. The author prepared the figures presented in the manuscript. All authors approved the final version.

GENERAL INTRODUCTION

The Need for Novel Antibacterial Agents

Following the remarkable success of antibiotic development during the golden era of discovery, the identification of new antibacterial agents has become increasingly challenging.[1,2] Most antibiotic classes that are still clinically relevant to this day were discovered during this period. Since then, the antibiotic development pipeline has slowed considerably, and the introduction of novel structural scaffolds into clinical practice has become rare.[3,4] This stagnation is largely driven by the steady decline in pharmaceutical investment over recent decades, due to high research and development costs, stringent regulatory requirements, and comparatively low financial returns relative to other therapeutic areas.[5,6] As a result, most compounds currently in clinical development are derivatives or modifications of existing antibiotic classes rather than truly new chemical structures with novel mechanisms of action (MoA).[1,7,8] Notable exceptions include the depsipeptide antibiotic teixobactin and the peptide antibiotic darobactin.[9,10] At the same time, the indiscriminate use of available antibiotics in clinical, agricultural, and environmental settings has accelerated the emergence and spread of antibiotic resistance, which is now recognized as one of the most pressing global health threats.[11,12] The resulting imbalance between the diminishing pace of innovation in antibiotic discovery and the rapidly increasing rates of resistance highlights the urgent need for new antibacterial agents with potent MoAs that are unaffected by common resistance mechanisms. Natural products have historically been the primary source for antibiotic discovery, and the majority of antibacterial scaffolds are derived from or inspired by secondary metabolites.[1,13] Shaped by evolutionary pressure, natural products often exhibit physicochemical properties that are beneficial for antibacterial activity, including enzymatic stability, efficient penetration of the cell envelope, and reduced susceptibility to efflux.[13,14] Accordingly, screening of microbial producer strains or crude extract collections remains a common approach for the discovery of antibacterial natural products due to its simplicity and proven effectiveness. However, these approaches are often limited by low specificity, modest throughput, and the frequent rediscovery of previously described metabolites.[15,16] Considerable time and resources are consequently invested in the re-isolation and characterization of already known molecules, because compound

identification is typically performed only at later stages of the workflow. As a result, dereplication of abundant and widely distributed metabolites remains one of the major bottlenecks in natural product discovery. Since many readily accessible bioactive compounds have already been identified and classical natural product-based discovery has become less efficient, alternative strategies are needed to access new chemical diversity. For example, the search for natural producer strains in underexplored environments has a high likelihood of yielding previously uncharacterized secondary metabolites.[17,18] Alternative approaches focus on unlocking the biosynthetic potential of microorganisms that are not readily accessible under standard laboratory conditions or that possess promising silent biosynthetic gene clusters.[19] In this context, several strategies have been developed to enhance secondary metabolite production, including optimization of growth media, co-cultivation of producer strains, and feeding essential precursors.[20,21] In addition, advances in genome mining and bioinformatics have enabled the identification of biosynthetic gene clusters with high potential for producing novel metabolites.[22] As an alternative to whole-cell natural product screening, antibiotic discovery shifted toward target-based approaches, in which defined molecular targets were screened *in vitro* against low-molecular-weight (semi-)synthetic compound libraries. While these approaches offer direct information about target inhibition, they have yielded relatively few antibacterial leads in the past.[13] This is largely because *in vitro* binding does not necessarily translate into sufficient whole-cell target engagement, as many potential antibiotic candidates were limited by insufficient cellular uptake, active efflux, nonspecific interactions with cellular components, and unfavorable physicochemical properties.[23,24] Moreover, these assays relied on molecular targets that were often insufficiently validated in host-relevant contexts and across diverse bacterial species. In addition, the ability of bacteria to compensate for target inhibition through mutation or metabolic rewiring was often insufficiently explored.[13,16,25] To address the limitations of current antibiotic discovery pipelines and avoid the repeated identification of known compounds, mechanism-informed screening strategies represent a promising alternative. The development of such approaches, however, depends on a detailed understanding of antibacterial activity, as different antibiotic classes interfere with distinct yet interconnected cellular pathways and the resulting physiological responses reflect both primary target interactions and downstream stress adaptations.[26]

Mechanistic Basis of Antibacterial Drugs

The diversity of antibiotic classes reflects the variety of essential cellular functions that are targeted by antibacterial agents to inhibit bacterial growth or induce cell death. Most clinically relevant antibiotics interfere with highly conserved processes,[27] including DNA replication, folate synthesis, RNA synthesis, fatty acid synthesis, and protein translation or homeostasis, or disturb the integrity of the bacterial cell envelope (Fig. 1). Antibiotics either directly inhibit essential anabolic enzymatic functions and the biosynthesis of structural components, or they more generally disturb metabolic balance, energy generation, or membrane integrity. To provide an overview of this mechanistic diversity, the following sections summarize the main classes of antibiotics according to the cellular pathways they target.

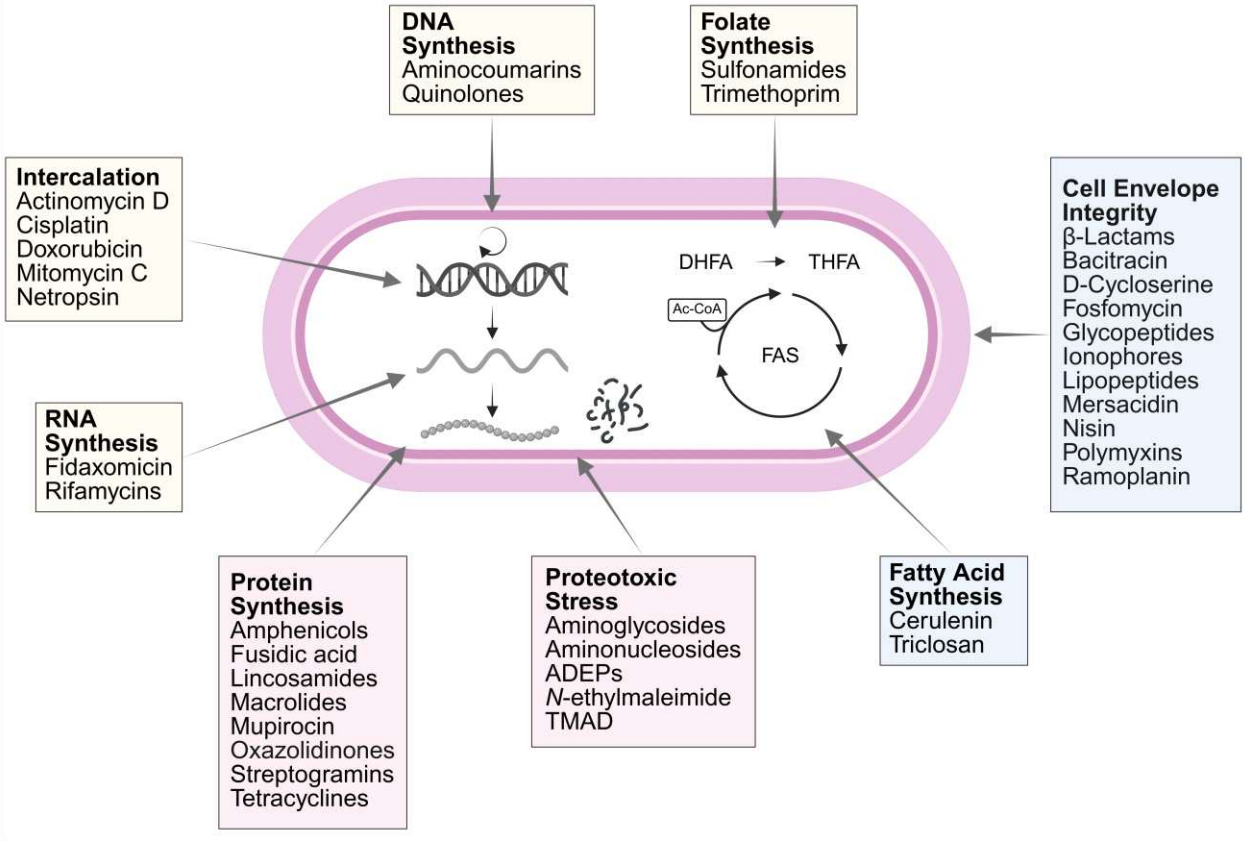

Figure 1. Overview of antibiotic mechanisms of action. Representative antibiotics were selected as examples of prominent antibacterial MoAs and are grouped by the essential metabolic pathways or structures they inhibit, including DNA synthesis, folate synthesis, RNA synthesis, and intercalation (yellow); cell envelope function and integrity, and fatty acid synthesis (blue); and protein synthesis and proteotoxic stress (red). DHFA, dihydrofolic acid; THFA, tetrahydrofolic acid; Ac-CoA, acetyl coenzyme A; FAS, fatty acid synthesis; ADEPs, acyldepsipeptide antibiotics; TMAD, tetramethylazodicarboxamide.

DNA and RNA synthesis inhibitors

Antibiotics that interfere with DNA and RNA synthesis disrupt essential processes, including DNA replication, RNA transcription, nucleotide precursor biosynthesis, and the structural integrity of the DNA template. Quinolone antibiotics, such as ciprofloxacin and other fluoroquinolones, target bacterial type II topoisomerases that regulate DNA supercoiling during replication. By stabilizing the transient enzyme–DNA cleavage complex and preventing strand re-ligation, they induce double-strand breaks that trigger the SOS stress response and lead to cell death.[28,29] Similarly, aminocoumarin antibiotics such as novobiocin competitively bind to the ATP-binding site of the GyrB subunit of the DNA gyrase, inhibiting ATP hydrolysis and preventing the conformational changes required for strand passage.[30] In addition to directly inhibiting enzymatic functions, sulfonamides and trimethoprim indirectly interfere with DNA replication by disrupting folate biosynthesis, thereby depriving bacterial cells of essential nucleotide precursors. Sulfonamides act as structural analogues of para-aminobenzoic acid and competitively inhibit dihydropteroate synthase, preventing the formation of dihydropteroate. Likewise, trimethoprim inhibits dihydrofolate reductase, blocking the reduction of dihydrofolate to tetrahydrofolate.[31,32] Rifamycin antibiotics inhibit RNA transcription by binding to the β-subunit of bacterial DNA-dependent RNA polymerase**.** This results in a steric obstruction of the RNA exit channel and prevents the elongation of the mRNA chain after transcription initiation.[33] Fidaxomicin targets transcription at an earlier stage by stabilizing the closed promoter complex, interfering with the formation of the transcriptionally competent open complex.[34] Beyond inhibiting enzymatic functions, DNA intercalators such as actinomycin D and doxorubicin directly bind to DNA and impede replication fork progression and transcription elongation.[35,36] DNA crosslinking agents, including cisplatin and mitomycin C, block DNA strand separation and DNA polymerase progression, whereas the minor-groove binder netropsin interferes with protein–DNA interactions required for transcriptional regulation.[37–39]

Cell envelope and fatty acid synthesis inhibitors

The bacterial cell envelope serves as a structural and functional barrier that maintains cell shape, protects against osmotic stress, and preserves membrane integrity. Antibiotics targeting the cell envelope either block cell wall biosynthesis or disrupt membrane

organization and permeability.[40] Cell wall biosynthesis is a highly orchestrated process that includes the synthesis of precursors in the cytoplasm, their transport across the membrane by lipid carriers, and finally the polymerization and cross-linking in the periplasm by transglycosylases and transpeptidases.[41] In the cytoplasm, the formation of UDP-MurNAc-pentapeptide precursors can be inhibited by antibiotics like fosfomycin, which blocks the MurA-catalyzed UDP-MurNAc synthesis.[42] Similarly, the structural analogue of D-alanine, D-cycloserine, prevents the synthesis of the terminal dipeptide of peptidoglycan precursors.[43] Subsequent membrane-associated processes are targeted by antibiotics such as bacitracin and ramoplanin. Bacitracin binds to undecaprenyl pyrophosphate and prevents recycling of the lipid carrier,[44] while ramoplanin binds lipid II and blocks its incorporation into the peptidoglycan layer.[45] β-lactams like penicillins and cephalosporins mimic the D-Ala-D-Ala terminus and irreversibly attach to penicillin-binding proteins in the periplasm, thereby blocking transpeptidation and the cross-linking of glycan strands. Glycopeptides such as vancomycin and teicoplanin bind the D-Ala-D-Ala terminus of lipid II, sterically hindering both transglycosylation and transpeptidation reactions.[46–48] Beyond cell wall biosynthesis, antibiotics that target the cytoplasmic membrane can either disrupt lipid organization or transmembrane electrochemical gradients. For example, ionophores cause uncontrolled ion flux across membranes. Carrier-type ionophores, such as valinomycin, shuttle specific cations across the lipid bilayer, whereas channel-forming ionophores, such as gramicidin, form small pores that allow passive diffusion of ions.[49,50] Protonophores, including carbonyl cyanide m-chlorophenyl hydrazone (CCCP), collapse the proton motive force, impairing ATP synthesis and other energy-dependent processes.[51] The lipopeptide antibiotic daptomycin binds the anionic phospholipid phosphatidylglycerol in a calcium-dependent manner and forms complexes with undecaprenyl-linked cell envelope precursors, such as lipid II, thereby perturbing membrane organization and impairing cell wall biosynthesis. These interactions are associated with membrane depolarization and ion leakage, possibly through the formation of pore-like oligomeric assemblies.[52,53] Polymyxins (e.g., polymyxin B and colistin) primarily target the lipid A core of lipopolysaccharide in the outer membrane of Gram-negative bacteria and, in addition, phospholipids in the cytoplasmic membrane, destabilizing the integrity of both membranes and leading to leakage of cellular contents and cell death.[54]

Fatty acid biosynthesis is closely linked to membrane integrity as it supplies the building blocks for membrane phospholipids. This process is carried out by the type II fatty acid synthesis (FAS II) system, which consists of separate, monofunctional enzymes that sequentially elongate acyl carrier protein (ACP)-bound intermediates. Inhibition of fatty acid biosynthesis limits membrane biogenesis and perturbs lipid homeostasis, affecting membrane function and cell division.[55] Prominent inhibitors that target key enzymatic steps of the FAS II pathway include cerulenin and triclosan. Cerulenin irreversibly inhibits the condensation reaction required for fatty acid chain elongation by covalently modifying the active-site cysteine residue of β-ketoacyl-ACP synthases such as FabB and FabF. This blocks the incorporation of malonyl-ACP into growing acyl chains, ultimately inhibiting fatty acid synthesis.[56–58] Triclosan targets the enoyl-ACP reductase FabI, which catalyzes the final reduction step of each elongation cycle. Triclosan binds within the active site of FabI and forms a stable ternary complex with the enzyme and the NAD^+ cofactor, effectively inhibiting the reduction of enoyl-ACP intermediates and thereby depleting fatty acid precursors required for membrane phospholipid production.[59]

Protein synthesis inhibitors and proteotoxic stress inducers

Protein biosynthesis represents one of the most prominent targets of clinically used antibiotics.[60] The bacterial ribosome is a highly conserved yet structurally distinct macromolecular complex that progresses through the sequential stages of initiation, elongation, termination, and ribosome recycling. First, the 30S subunit assembles a pre-initiation complex with the initiator tRNA and multiple initiation factors. Then, mRNA binding and correct codon–anticodon recognition stabilize this complex, allowing the 50S subunit to join and form the functional 70S initiation complex. During elongation, aminoacyl-tRNAs are delivered to the A site by elongation factor EF-Tu, followed by peptide bond formation that is catalyzed by the peptidyl transferase center within the 23S rRNA of the 50S subunit. Ribosomal translocation, mediated by EF-G, then shifts the mRNA–tRNA complex by one codon to allow the next elongation cycle. Finally, translation ends when a stop codon reaches the A site, followed by hydrolysis of the peptidyl-tRNA bond and the release of the newly synthesized polypeptide. Eventually, the post-termination complex is again separated into the 30S and 50S subunits by the ribosome recycling factors together with EF-G.

The essential and highly coordinated nature of the translational process provides multiple target sites for antibiotic interference.[61,62] For example, oxazolidinones such as linezolid bind to the peptidyl transferase region of the 50S ribosomal subunit. This prevents the correct positioning of the initiator tRNA, blocking the formation of the translation initiation complex.[63] Tetracyclines bind to the decoding center of the 30S ribosomal subunit, sterically occluding the aminoacyl-tRNA binding site and preventing accommodation of incoming charged tRNAs during elongation.[64,65] In contrast, amphenicols, such as chloramphenicol, inhibit peptide bond formation by binding to the peptidyl transferase center of the 50S subunit and preventing proper positioning of the aminoacyl-tRNA for peptide bond formation.[66] Macrolides (e.g., erythromycin), lincosamides (e.g., clindamycin), and streptogramine B (e.g., pristinamycin I) interact with overlapping sites in the 50S subunit, obstructing the nascent peptide exit tunnel or interfering with peptidyl transferase activity.[67–69] Elongation can also be disrupted through interference with translation factors. For instance, fusidic acid binds elongation factor EF-G on the ribosome after GTP hydrolysis, stabilizing the EF-G–GDP–ribosome complex. This prevents the translocation of tRNAs and mRNA, halts peptide elongation, and impairs subsequent ribosome dissociation and recycling.[70] Finally, mupirocin competitively inhibits bacterial isoleucyl-tRNA synthetase, depleting charged Ile-tRNA and causing ribosomal stalling at isoleucine codons, thereby indirectly blocking protein synthesis.[71]

While ribosome-stalling antibiotics shut down protein synthesis completely, there are also agents that still allow the translation machinery to proceed but interfere with proper ribosome function. Aminoglycosides, for instance, bind within the decoding center of the 16S rRNA in the 30S ribosomal subunit and promote codon misreading by stabilizing incorrect tRNA–mRNA interactions. This disruption of translational fidelity results in widespread mistranslation and the synthesis of aberrant polypeptides containing misincorporated amino acids. In addition to disrupting native protein function, many of these defective proteins either integrate into the cytoplasmic membrane or form aggregates in the cytosol, triggering membrane destabilization, oxidative stress, and activation of cellular protein quality-control pathways. Over time, this progressive disturbance of proteostasis contributes significantly to the bactericidal effects of aminoglycosides.[72,73] In addition to aminoglycoside-induced proteotoxic effects resulting

from the accumulation of damaged or misfolded proteins, the aminonucleoside puromycin represents another example of ribosome-mediated proteotoxic stress. Puromycin structurally resembles the 3′ end of aminoacyl-tRNA and binds to the ribosomal A site, where it serves as a substrate for the peptidyl transferase reaction. As a result, the nascent polypeptide chain is transferred from the P-site tRNA to puromycin. This leads to the formation of peptidyl-puromycin conjugates that rapidly dissociate from the ribosome and to the accumulation of truncated polypeptides.[74] Proteotoxic stress can also arise independently of direct ribosomal interactions. Acyldepsipeptide antibiotics (ADEPs) affect protein homeostasis through a distinct mechanism that disrupts the cellular proteolytic machinery. ADEPs target the bacterial Clp protease, which plays a key role in regulated protein quality control, thereby perturbing the balance between protein synthesis and degradation through a dual MoA. By binding to the ClpP proteolytic core and displacing its regulatory ATPase partners, ADEPs uncouple the protease from its native substrate recognition and unfolding machinery. At the same time, ADEP binding allosterically activates ClpP, opening the axial pores of the protease and enabling uncontrolled protein degradation independent of the ATPase components. As a consequence, ClpP performs nonspecific proteolysis of less-structured and nascent polypeptides, some of which are essential for bacterial survival, such as the key cell-division protein FtsZ. This dysregulation of proteolysis results in widespread degradation of cellular proteins and ultimately leads to the collapse of protein homeostasis and bacterial cell death.[75,76] Other compounds promote proteotoxic stress through direct chemical modification of proteins. Thiol-reactive electrophilic agents can induce proteotoxic stress through different mechanisms. The alkylating agent *N*-ethylmaleimide (NEM) covalently modifies cysteine residues by thiol alkylation, whereas TMAD oxidizes low-molecular-weight thiols such as glutathione and promotes inter- and intramolecular disulfide cross-linking.[77–79]

Mechanism-informed Antibiotic Discovery

Antibacterial agents that interfere with essential biosynthetic pathways trigger specific cellular stress responses that help the cell restore or rescue the targeted processes. Depending on the MoA, these responses involve coordinated signaling cascades that lead to the expression of stress-related genes, including those associated with heat-shock or SOS stress responses.[80] In *B. subtilis*, genome-wide transcriptional profiling has provided detailed insights into these responses, revealing pathway-specific expression patterns following the treatment with distinct antibiotic classes.[81,82] Although the induction of a specific stress pathway does not directly identify the molecular target of an antibiotic, it provides information about the affected metabolic pathway or cellular structure. Consequently, the associated changes in gene expression can be repurposed as functional MoA biomarkers. By coupling the promoter regions of selectively induced genes to suitable reporter systems, bioreporter strains can be generated to detect and quantify these MoA-specific responses.[82,83] Importantly, bioreporters represent a powerful tool for antibiotic discovery, as they combine the advantages of whole-cell screening approaches with a mechanism-informed bioactivity readout that enables early hypotheses about the underlying MoA. They also offer greater sensitivity than classical growth inhibition assays, facilitating the detection of antibiotic-induced stress responses already at concentrations that do not yet prevent bacterial growth.[83,84] Beyond their application in initial compound discovery, bioreporters can also guide downstream dereplication workflows, which has been shown to substantially improve the efficiency of compound identification.[84] Conventional dereplication pipelines still largely rely on iterative extract fractionation, typically performed using semipreparative HPLC.[85] During this process, the bioactivity of each fraction is assessed using growth inhibition assays until the compound of interest is isolated in sufficient quantities for structural and biochemical characterization, a process that is both time- and resource-intensive and inherently prone to rediscovery.[86] Over the past decades, significant advances in mass spectrometry-based dereplication strategies have improved the identification of bioactive metabolites. High-resolution analytical techniques enable the detection, annotation, and comparison of molecular features with steadily increasing accuracy.[87] However, the effectiveness of these approaches depends on the sensitivity and the informative content of the associated biological readouts, both

of which can be enhanced through bioreporter-based readouts relative to traditional growth inhibition assays. Chemical identities of molecules of interest can be verified by comparing UV spectra, accurate masses, molecular formulas, and MS/MS fragmentation patterns with existing databases. In parallel, bioreporters provide complementary validation by matching the observed bioactivity profiles with the reported MoAs of the identified compounds.[84] This approach is especially useful for the early identification and exclusion of previously characterized natural products, helping to prioritize potentially new compounds. In contrast, for previously uncharacterized or novel bioactive metabolites, assigning bioactivity to the underlying molecular features remains challenging due to the complexity of biological samples and the substantial signal overlap in crude extracts. To further enhance dereplication efficiency and shorten labor-intensive fractionation and iterative purification workflows, a direct association between bioreporter activity and the corresponding molecular masses of individual analytes would be beneficial. Achieving this requires technological advancements and novel integration strategies to fully exploit the potential of bioreporter-guided dereplication. For this purpose, this thesis focuses on developing an integrated bioreporter-based screening and dereplication platform that combines the physiological relevance of whole-cell assays with a sensitive, MoA-guided bioactivity profiling and high-resolution MS-based dereplication workflow. This platform utilizes a new bacterial luciferase-based bioreporter panel that enables autonomous and continuous monitoring of bioreporter activity in both solid and liquid media and integrates this readout with a high-resolution microfractionation workflow to generate bioactivity-guided metabolomics data. Additionally, the mechanistic coverage of the bioreporter panel is expanded in this work by incorporating a novel proteotoxic stress bioreporter, enabling the detection of a widespread antibacterial mechanism not previously captured by the existing bioreporters. Collectively, this platform is designed to help overcome key limitations of traditional natural product discovery and facilitate the direct identification of antibacterial natural products.

Aim of the Dissertation

Natural products remain the major source of novel antibiotics, but traditional whole-cell screening approaches typically provide limited mechanistic insight and sensitivity. In combination with inefficient dereplication strategies, this often leads to substantial effort invested into the repeated discovery of known compounds. To overcome these limitations, there is a need for rapid, sensitive, and efficient strategies that combine bioactivity assessment, early MoA profiling, and reliable dereplication. The aim of this dissertation was to establish an integrated, bioreporter-based screening platform in *B. subtilis* that accelerates the mechanism-informed discovery and dereplication of urgently needed antibacterial agents. To achieve this, this work was structured around four complementary objectives:

(I) The construction of a novel bacterial luciferase-based bioreporter panel for MoA-informed antibiotic screening;

(II) The development of a dedicated proteotoxic stress bioreporter to expand the mechanistic coverage of the bioreporter panel;

(III) The design and validation of a bioreporter-guided compound discovery and dereplication workflow; and

(IV) The application of this workflow to screen natural producer strains from the Tübingen actinomycetes collection for antibacterial agents that induce proteotoxic stress.

The following publications contribute to these objectives. Publication I describes how the bioreporter panel and the bioreporter-guided discovery and dereplication platform were established, thereby addressing aims (I) and (III). Publication II presents the development of the proteotoxic stress bioreporter and its use in screening a natural product library and the Tübingen strain collection, together with the discovery and dereplication platform established in the first publication, fulfilling aims (II) and (IV). Together, these studies contribute to the development of a versatile platform for mechanism-informed antibiotic discovery.

PUBLICATION I – HIGH-FREQUENCY MICROFLUIDIC FRACTIONATION FOR COMPOUND-RESOLVED BIOACTIVITY-BASED METABOLOMICS

Published in *Analytical Chemistry*, 2025, 97(43), 24093–24104. Published by the American Chemical Society. This article is licensed under CC BY 4.0. Copyright © 2025 The Authors. DOI: 10.1021/acs.analchem.5c04612

Manuscript Context

This study addresses the need for efficient antibiotic screening and dereplication strategies by developing a bioreporter-guided platform for the mechanism-informed discovery of antibacterial compounds. The platform combines non-targeted LC-MS/MS, high-resolution microfractionation-based metabolomics, and the sensitive, mechanism-informed readout of a bioreporter panel. To develop the platform, the author constructed a novel panel of bacterial luciferase-based bioreporters based on the established antibiotic stress-sensing promoter regions *fabHB, yorB, ypuA, liaI,* and *bmrC*. This bioreporter panel enables continuous monitoring of luminescence signals and detects dynamic and time-resolved bacterial stress responses induced by antibiotics that disrupt key metabolic processes, including fatty acid synthesis, DNA and folate synthesis, cell envelope integrity, lipid-II cycling, and translation arrest. In addition, a custom high-speed microfractionation device (microspotter) and a suitable microfluidic paper-analytical device (µPAD) were designed. The author contributed to the design of the µPAD and its integration into the bioreporter workflow. Finally, the combined bioreporter-guided platform was validated for throughput, sensitivity, and robustness in screening and identifying bioactive metabolites. Here, the author conducted all bioreporter-based experimental analyses and contributed to data analysis and visualization for the combined platform. The bioreporter-guided antibiotic discovery and dereplication platform accelerates natural product screening and dereplication by combining functional metabolomics approaches with automated high-frequency microfractionation and high-content bioreporter readouts. This approach improves the identification of known compounds, increasing screening throughput and enabling a stronger focus on novel scaffolds. In combination with molecular networking, the workflow also enables the identification of structurally related analogues based on fragmentation similarity, thereby extending the accessible chemical space.

analytical chemistry

Open Access
This article is licensed under CC-BY 4.0

pubs.acs.org/ac
Article

High-Frequency Microfluidic Fractionation for Compound-Resolved Bioactivity-Based Metabolomics

Christian Geibel, Julian Schubert, Simon B. Knoblauch, Albert Hernandez, Leonardo Boldt, Dana C. Schneider, Stilianos Papadopoulos Lambidis, Giovanni Andrea Vitale, Jakub Fleischer, Manuela Haussmann, Harald Gross, Mingxun Wang, Heike Brötz-Oesterhelt,* and Daniel Petras*

Cite This: *Anal. Chem.* 2025, 97, 24093−24104

Read Online

ACCESS | Metrics & More | Article Recommendations | Supporting Information

ABSTRACT: Specialized metabolites represent a prolific source of potential drug candidates. However, the process from detecting bioactivity in a crude metabolite extract to unambiguously identifying the active agent is a tedious and expensive endeavor. Speeding up this procedure is crucial, as new drugs, such as antibiotics, are urgently needed. Furthermore, the systematic functional assessment of complex metabolome samples represents a key bottleneck in nontargeted metabolomics, which once solved, holds the potential to fundamentally advance our systematic understanding of biology. To tackle this central bioanalytical challenge, we developed a compound-resolved bioactivity-based metabolomics workflow that combines nontargeted liquid chromatography tandem mass spectrometry (LC-MS/MS), high frequency fractionation on microfluidic devices and subsequent readout with luminescent bioreporter strains. Central for this workflow is a custom high-speed (∼1 Hz frequency) fractionation device that spots the mobile phase onto a microfluidic paper-analytical device (μPAD) in parallel to MS/MS data acquisition. Subsequently, the μPAD can be overlaid with a bioreporter strain, which displays cellular stress by expressing luciferase. The luminescence signal can then be correlated to MS signals through their chromatographic profiles. We evaluated five different luciferase-expressing bioreporter strains which provide information about different antibacterial modes of action, and tested the workflow with different antibiotic standards and mixtures thereof, as well as crude extracts from the known antibiotic producer *Saccharopolyspora erythraea*. Our results demonstrated high sensitivity (up to 1 ng/spot, depending on compound and bioreporter) and the rapid identification of multiple antimicrobial compounds out of crude extracts, highlighting the practicality and high-throughput capability of this compound-resolved bioactivity-based metabolomics approach.

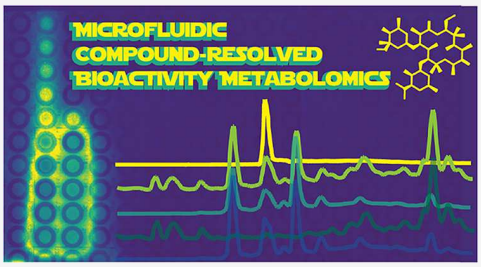

INTRODUCTION

Specialized metabolites (often referred to as natural products) from plants, bacteria, fungi, and other organisms have long served as a rich source of bioactive compounds. Natural products have inspired drug development for decades, either through direct use or by mimicking and optimizing their structures to improve potency, stability, or target binding.[1−3] Given nature's vast chemical diversity, it is believed that many specialized metabolites remain undiscovered.[4] The urgent need for new pharmaceutical lead structures is particularly evident in the case of antibiotics, where nearly 5 million deaths associated with antibiotic resistance were reported in 2019 alone.[5] At the same time, the ongoing loss of biodiversity threatens to erase natural sources of potential new drugs before they are discovered.[6] To counter this, rapid screening of natural extracts for bioactive metabolites is of high importance for future drug discovery and fundamental understanding of biological mechanisms. Understanding the structure and pharmacological mode of action of promising compounds allows for their synthesis, optimization and potential medical use.

Despite recent reductions in natural product programs in the pharmaceutical industry, natural products remain a prime resource for drug discovery, although most low-hanging fruit seem to have already been picked, i.e., the potent, highly produced and easy to purify bioactive agents from lab strains. However, this trend is largely driven by challenges in accessing uncultivable taxa, and to fully trigger the biosynthetic potential of cultivable ones.[7−9] A recent shift in focus includes screening whole microbial communities and field-grown organisms, which are more likely to produce defensive chemicals than laboratory grown strains.[10] Such approaches hold promise but they require concomitant technology development to increase resolution, sensitivity and throughput. The traditional process of finding new active metabolites is tedious as well as time- and

Received: July 28, 2025
Revised: October 17, 2025
Accepted: October 17, 2025
Published: October 25, 2025

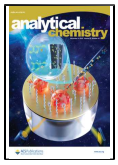

© 2025 The Authors. Published by American Chemical Society

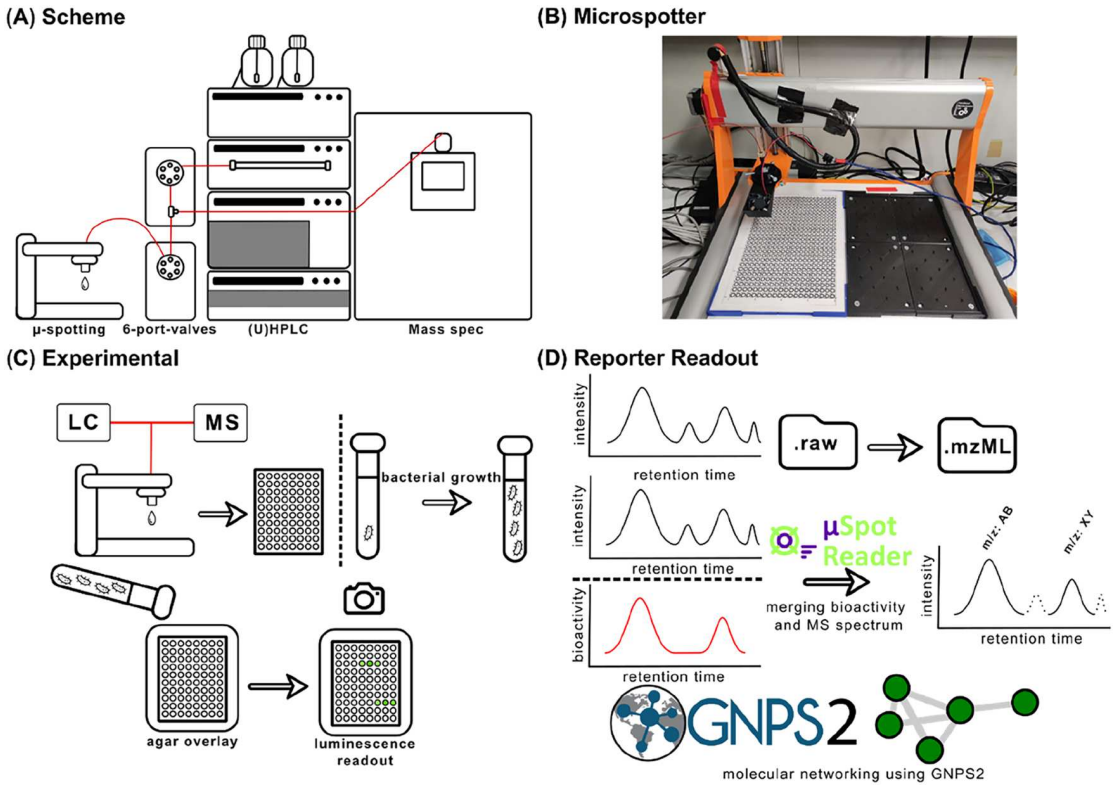

Figure 1. (A) Instrumental setup used for the experiments. Relevant capillaries are shown in red. Extracts are separated on an HPLC system and eluted into a double 6-port-valve setup. Between both valves is a T-piece. Here, the flow gets diverted between the MS and the Microspotter. (B) Image of the Microspotter. For detailed operation of the instrument, see Video S1 or https://www.youtube.com/watch?v=PTC9epQNzow. (C) Wet lab workflow for the use of the Microspotter. The extract is separated by LC. Subsequently, MS spectra are recorded and the eluate is spotted on a μPAD. In parallel, the bacterial bioreporters are grown. A spotted and dried μPAD is overlaid with agar containing the bioreporter strain. Luminescence readout can be performed after 180 min. (D) Dry lab workflow. The MS output-file is converted to .mzML format and fed into the MicrospotReader app, which is able to create a chromatogram based on the bioactivity data from the luminescence readout. Furthermore, it merges this chromatogram with the MS output file to filter only relevant m/z-values for the bioactivity. The app output file can be used for molecular networking using GNPS2.

resource-intensive, consisting of an extract being fractionated, and each fraction containing a putative novel and interesting bioactive agent to be subfractionated until the molecule/s responsible for the activity is/are isolated in sufficient amount/s and purity for structure elucidation and biological assessment. This process is usually performed on semipreparative HPLC systems without concomitantly recording mass spectra or obtaining any other information on the fraction, except for the retention time and UV spectra. The antibacterial activity of fractions is usually assessed by inhibition zone tests. This assay is comparably insensitive as it relies on bacterial growth inhibition and does not detect the stress responses experienced by the cells at lower, sublethal concentrations. In this traditional approach, the molecule of interest is identified only at the end of this time-consuming process, often leading to rediscovery of already known bioactive compounds.

Over the last decades, significant progress was made in the high-throughput screening of bioactive compounds. As affinity is a prerequisite to bioactivity, many experimental setups focus on the affinity between natural products and a target. Here, mainly native MS and affinity-selection MS methods have been used.[8] In native metabolomics, the eluting metabolites from an HPLC system are tested for their affinity against purified proteins, which are infused postcolumn.[11,12] Affinity-selection MS uses an incubation step as the first step. After incubation, nonbinders are removed either by size-exclusion chromatography or pulsed ultrafiltration. Subsequently, the binder is released by denaturing the protein. This binder can then be detected in an LC-MS run.[13] Building up from traditional bioactivity-guided natural product discovery,[14] offline methods for the determination of bioactivity have been widely used. Here, bioactive extracts are separated by LC and fractionated into a deep-well plate. A mass spectrum is then recorded in parallel by infusing a small amount of the eluate in the MS. The results from the offline biotesting are overlaid to the mass spectrum to find possible bioactive compounds.[15] In this way, e.g., antiprotozoic compounds were identified.[16,17] While offline approaches are inherently lower throughput, new workflows have been developed to screen extracts in an online manner, e.g., against acetylcholine binding protein (AChBP).[15] Simultaneously to micro fractionation, mass spectra were recorded via a postcolumn T-piece and infusing a small amount of the eluate into the MS. Other sample-centric metabolomics-based approaches use sets of LC-MS/MS samples, analyze them with molecular networking,[18] and correlate the bioactivity of the samples to the intensity of metabolite features within the samples.[19−21] A key feature to identify the active components is hereby the correlation between the intensity of the metabolites and their activity signal. However, analyzing complex samples, or large fraction sizes, typically results in substantial signal overlap, which limits the unambiguous identification of the active component.

https://doi.org/10.1021/acs.analchem.5c04612
Anal. Chem. 2025, 97, 24093−24104

Here, we report on the development of a compound-resolved bioactivity-based LC-MS/MS approach radically shrinking the fraction size to achieve high-resolution bioactivity data, at the same frequency as the scanning of MS duty cycle. This enables more precise correlation of MS features to bioactivity signals and reduces ambiguity when associating with analytes. Our technology makes use of four components: 1. A custom high-speed fractionation device that is coupled to a commercial LC-MS/MS system. 2. Paper-based microfluidic devices (μPAD) that serve as microfractionation wells. 3. Bioreporter strains which can be deployed onto the μPAD and which produce a luminescence signal. And 4. custom software to read out the luminescent signal and correlate it to MS features. A conceptual overview of the system and approach is shown in Figure 1. After the development of the instrumentation, bioreporter strains and software, we validated the workflow with a panel of antibiotic standards. To showcase the practicality of the method we further screened bacterial crude extracts for antibiotics, during which we identified multiple metabolites with antimicrobial activities.

EXPERIMENTAL SECTION

Materials. Chromatographic separation was performed on a Kinetex EVO LC column by Phenomenex (Torrance, California, USA). Specifications of the column were as follows: 150 mm × 4.6 mm (l. × i.d.), equipped with fully porous 2.6 μm particles with a pore size of 100 Å. Water was of Optima LC/MS-grade quality and was supplied by Fisher Chemical (Fisher Scientific, Hampton, NH, USA). Acetonitrile and formic acid was LC-MS grade and was supplied by Thermo Fisher Scientific (Bremen, Germany). All used antibiotic standards can be found in Table S1. The polylactic acid (PLA) filament for the 3D-printer was supplied by Labists (Shenzhen, China). Used oligonucleotides can be found in Table S2.

Instrumentation. The microfluidic paper analytical device (μPAD) was printed using a wax printer (Xerox Colorqube 8580) from Xerox (Norwalk, CT, USA) or a thermal transfer printer (HPRT MT800) from Xiamen Hanin Electronic Technology Co., Ltd. (Xiamen, China). Hydrophobic "caps" were printed using the toner printer TASKalfa 352ci from Kyocera (Kyoto, Japan). The Microspotter is a three-axis robot, a modified milling machine from Stepcraft GmbH & Co. KG (Meden, Germany). 3D printing was performed using an i3 mega printer from Anycubic (Shenzhen, China) using polylactic acid (PLA) filaments. As HPLC, an Agilent 1260 Infinity II system from Agilent Technologies (Waldbronn, Germany) with a quaternary pump, an autosampler, and a UV/Vis detector was used. MS measurements were performed on a Q Exactive orbitrap system from Thermo Fisher Scientific (Bremen, Germany). Two 6-port valves were used in the instrumental setup, both Rheodyne valves from Idex (Northbrook, IL, USA). The imaging system for luminescence pictures was a ChemiDoc MP by Bio-Rad (Hercules, CA, USA).

Fabrication of μPADs. Microfluidic paper-based analytical devices (μPADs) have gained a certain popularity since their introduction in 2007.[22] They are inexpensive, easy to manufacture, and offer a versatile platform for biosensing, similar to the "lab-on-a-chip" approach.[23] While colorimetric detection is commonly used,[24] μPADs also support electrochemical[25] and fluorescent methods,[26,27] broadening their range of applications. A key advantage is their customizability: μPADs can be tailored to specific analytical needs. The operating mode is straightforward: a desired design is printed onto a commercially available sheet of paper using a solid ink printer. This forms a thin layer of a waxy resin-based polymer on top of the paper that is sensitive towards heat. When placing the printed paper into an oven at 110 °C for 1 min, the "wax" melts and migrates into the paper, forming a hydrophobic barrier. Here, 500 small circles were printed onto the paper, forming space for up to 500 fractions from the eluate in one LC-run. For high resolution fractionation with a spotting frequency of 1 Hz, a total of 8 min and 20 s of the LC run can be covered. The number of spots can individually be changed, but should be in accordance with the LC method. A sampling frequency of 1 Hz was chosen, as we expected the width of elution peaks to be wider than 1 s. When diverting the dead time (1 min) into the waste, almost the whole gradient time of 10 min can be covered by 500 spots.

To prevent compounds from migrating through the paper, "caps" were printed on the back of the μPAD after curating it at 110 °C. Those caps were not heated and stayed on the lower surface of the μPAD to prevent the spotted compounds from bleeding through the paper and diffusing into the agar under the PAD. Several different setups were tested, with this "capped" μPAD resulting in the most promising approach. A laser printer was used for the printing of hydrophobic caps. To be able to replace outdated solid-ink printers, a comparable workflow was also performed with a thermal transfer printer (see SI).

Fabrication of High-Speed Microspotting Device (Microspotter). We built the Microspotter on the basis of a commercial CNC milling machine (STEPCRAFT D.600 CNC System). For our purpose, the milling head was removed and replaced by a tailor-made 3D-printed head, with an adjustable PEEK capillary holder. The spotter head of the Microspotter precisely positions the outlet of the capillary through its three-axis motion from one spot to the next spot. For precise positioning of the eluent on the μPAD, we engineered a nozzle consisting of a PEEK capillary (i.d. 0.13 mm) within a 3D-printed spotter head. The spotter head consists of four parts (see Figures S2 and S3 and CAD files in data sharing section). Reliable hardware synchronization is essential for reproducible results and to avoid delay errors while spotting. To synchronize the MS with the Microspotter, a C++ embedded program was written to control an Esp32 microcontroller, which provided the contact closure for the spotter start. The code is publicly available and can be found in the data sharing section.

LC-MS/MS and Microspotter Instrumental Setup. For the LC system, mobile phase A consisted of water +0.1% formic acid (V/V) and mobile phase B was acetonitrile +0.1% formic acid (V/V). Runtime was 15 min with the gradient as follows: 0.00 min: 5% B, 10.00 min: 95% B, 12.00 min: 99% B, 13.00 min: 99% B, 13.01 min: 5% B, flow rate 1 mL/min. Mass spectrometer conditions: full MS, scan range: m/z 150 to 2,000, resolution: 35,000, positive ion mode. Sheath gas: 35 psi, aux gas: 5 psi, sweep gas: off, spray voltage: 3.5 kV, capillary temperature: 250 °C, aux gas heater temperature: 250 °C.

Postcolumn, an automatic, time-programmable 6-port valve was installed. Here, the eluate can be directed either to the waste or to the MS and the Microspotter. In the latter line, a T-piece diverts the flow, 10% are infused in the MS, 90% are diverted to a second 6-port valve. This valve can be switched between waste and the Microspotter. When the first valve is in

https://doi.org/10.1021/acs.analchem.5c04612
Anal. Chem. 2025, 97, 24093−24104

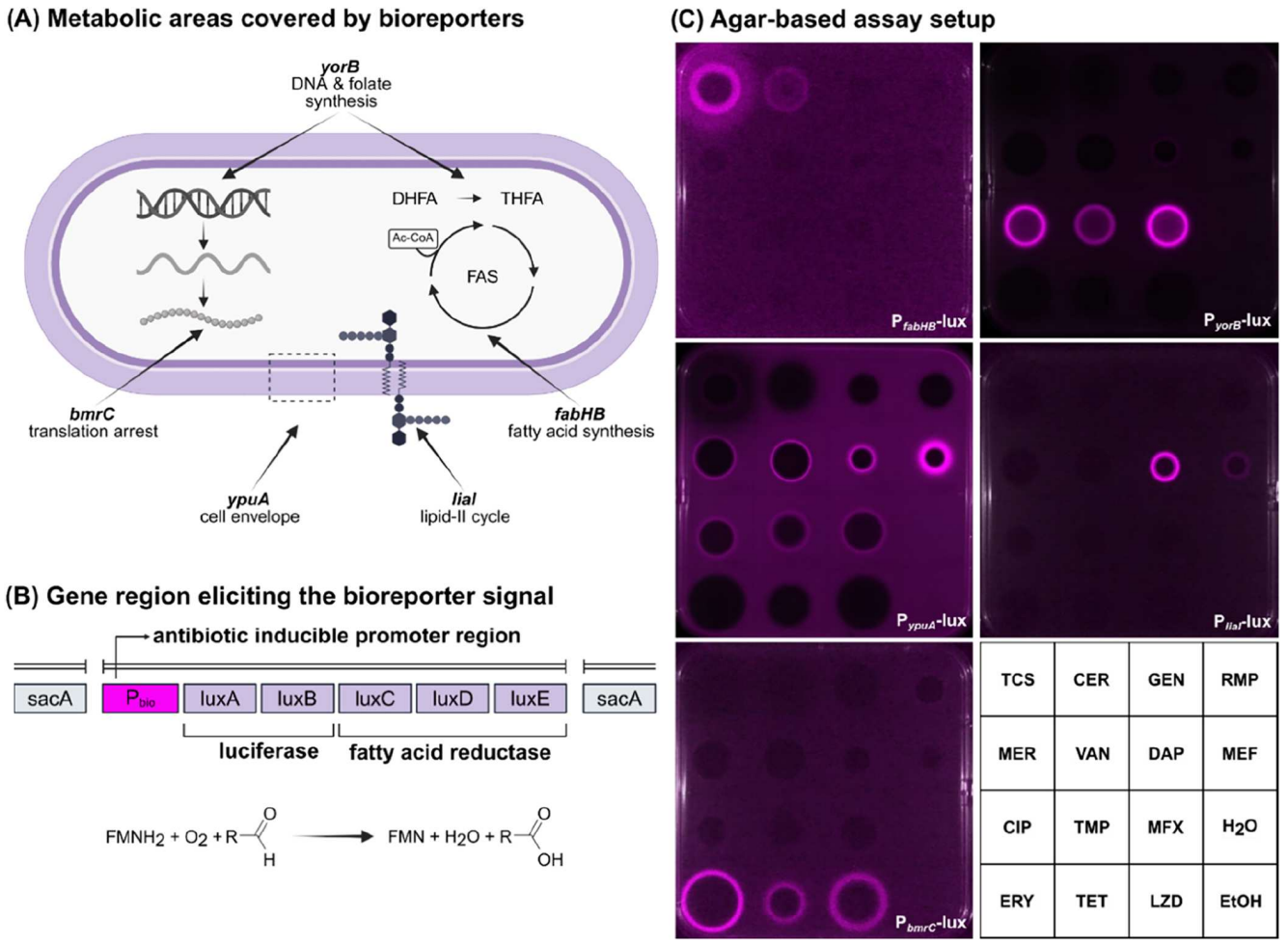

Figure 2. Biosynthetic pathway coverage, construction and validation of the bioreporter panel. (A) Schematic overview of the key biosynthetic processes covered by the bioreporter panel. Each bioreporter enables rapid detection of antimicrobial compounds interfering with the depicted major biosynthetic pathways: *yorB* (DNA and folate synthesis), *bmrC* (translation arrest), *liaI* (lipid II cycle), *ypuA* (cell envelope integrity), *fabHB* (fatty acid synthesis). DHFA, dihydrofolic acid; THFA, tetrahydrofolic acid; Ac-CoA, acetyl coenzyme A; FAS, fatty acid synthesis. (B) Schematic illustration of the gene region eliciting the bioreporter signal, integrated into the *sacA* locus of the sporulation-deficient *B. subtilis* 1S34 strain. For each bioreporter, the respective antibiotic-inducible promoter region (P_{fabHB}, P_{yorB}, P_{ypuA}, P_{liaI}, P_{bmrC}) was cloned upstream of the *P. luminescens luxABCDE*-operon, consisting of a heterodimeric luciferase protein (LuxAB) and a fatty acid reductase complex (LuxCDE).[37] Enzymatic conversion of long-chain fatty aldehydes in the presence of molecular oxygen and reduced flavin mononucleotide ($FMNH_2$) promotes an autonomous production of light with a wavelength of 490 nm.[31,37] (C) Representative images of the agar-based bioreporter assay exemplifying inductions of the bioreporter panel (P_{fabHB}-lux, P_{yorB}-lux, P_{ypuA}-lux, P_{liaI}-lux, P_{bmrC}-lux) following exposure to 14 exemplary reference compounds with diverse mechanisms of action; for results on additional 36 agents, see Figure S5A. Antibiotics, denoted by their three-letter codes, were spotted onto the bioreporter lawn in a 4 × 4 grid at the following concentrations: triclosan (TCS), 2 μg; cerulenin (CER), 5 μg; gentamicin (GEN), 1 μg; rifampicin (RMP), 0.5 μg; meropenem (MER), 0.5 μg; vancomycin (VAN), 15 μg; daptomycin (DAP), 2 μg; mefloquine (MEF), 10 μg; ciprofloxacin (CIP), 1 μg; trimethoprim (TMP), 0.5 μg; moxifloxacin (MFX), 0.5 μg; erythromycin (ERY), 2 μg; tetracycline (TET), 20 μg; linezolid (LZD), 3 μg. Water and ethanol (5 μL each) served as solvent controls. Bioreporter induction was quantified by luminescence imaging at 180 min after antibiotic treatment, with luminescent halos indicating bioreporter activation.

analysis-mode, the second valve can be switched to waste after spotting one μPAD. This ensures further infusion to the MS for the monitoring of, e.g., extremely lipophilic compounds that elute (under the chosen circumstances) only in very high percentage of organic solvent, usually at the end of a standard LC gradient. The arm of the spotter can be programmed for the *x*-, *y*- and *z*-axis and can precisely drive and stop over the printed spots of the μPAD. To precisely control the head of the three-axis-robot, HPLC outlet, and microspotting, the Microspotter was controlled using the CNC Drive software. Its real-time 3D toolpath viewer, friendly user-interface, and flexible machine control (programmable and manual) made it ideal for troubleshooting, testing, and ultimately programming a Microspotter motion profile. The motion profile is driven by G-code and coordinate-based commands to drive the robot's movement. To streamline the coding process across similar motion profiles (e.g.,: same pattern but different starting coordinates or speed), a template was created using an R script.

Bioreporter Design. Based on a sporulation-deficient mutant of the Gram-positive model organism *Bacillus subtilis* and established antibiotic stress-sensing promoters of the genes *fabHB, yorB, ypuA, liaI* or *bmrC*,[28−32] we constructed five bioreporter strains that signal promoter activity using the bacterial luciferase system as a sensitive readout (Figure 2A).

https://doi.org/10.1021/acs.analchem.5c04612
Anal. Chem. 2025, 97, 24093−24104

The genes for the β-ketoacyl−acyl carrier protein synthase III *fabHB* were identified as a specific biomarker for fatty acid biosynthesis inhibition.[29,32−34] While the primary function of YorB remains unknown, it is regulated by LexA and associated with the bacterial SOS response, serving as an indicator of DNA damage and folate synthesis interference, the latter via inhibition of nucleic acid synthesis.[28,32,35] YpuA is implicated in general cell envelope stress responses and detects antibiotics disrupting the cell wall and membrane, whereas LiaI is more specific for undecaprenyl phosphate cycling inhibition ("lipid II cycle").[28,29,31,32] The subunit of a multidrug ABC transporter BmrC is natively expressed during late-exponential and stationary growth phase and serves as a biomarker for translation-arresting antibiotics.[29,36] For each bioreporter, the corresponding antibiotic-inducible promoter (P_{fabHB}, P_{yorB}, P_{ypuA}, P_{liaI}, P_{bmrC}) was cloned upstream of the *Photorhabdus luminescens luxABCDE*-operon and integrated into the nonessential *sacA* locus of the *B. subtilis* chromosome, enabling the stable detection of promotor induction. The *luxABCDE*-operon encodes a heterodimeric luciferase (LuxAB) and a fatty acid reductase complex (LuxCDE), enabling an autonomous production of luminescence through the oxidation of long-chain aliphatic aldehydes (Figure 2B). Details on the cloning procedure for the new bioreporter set are provided in the Supporting Methods section.

Autonomous light production by the stressed bacteria, i.e., independent of the addition of an external substrate, combined with the use of a sporulation-deficient *B. subtilis* background, avoiding the contamination of instrumentation by heat-resistant endospores, makes the new bioreporter set particularly suitable for the Microspotter application.

The bacterial luciferase-based bioreporters offer continuous self-sustained signal output, enabling a dynamic, time-resolved analysis, eliminating the necessity of external substrate addition as required for conventional firefly luciferase or β-galactosidase reporters. This novel bioreporter panel supports convenient whole-cell screening in both liquid and solid media.

Bioreporter Assay Setup. Bioreporters are suitable in an agar-based assay format as exemplified in Figure 2C (for the full data set, see Figure S5A) and in a liquid assay setup (Figure S5B). Bioreporter cultivation was generally performed in lysogeny broth (LB; 1% NaCl, 1% tryptone, 0.5% yeast extract, pH 7.25) supplemented with 5 μg/mL chloramphenicol at 37 °C and shaking (190 rpm). For the agar-based assay, a liquid preculture was initiated for each bioreporter from a glycerol stock and incubated for 18 h, followed by inoculation of a main culture to an initial OD_{600} of 0.05, which was subsequently grown to an OD_{600} of approximately 1.0. From the main culture, soft agar (0.75% agar, without chloramphenicol) was inoculated to achieve a final cell count of 3×10^6 colony-forming units (CFU)/mL. LB soft agar was used for P_{fabHB}-lux, P_{yorB}-lux, P_{ypuA}-lux, P_{liaI}-lux, while BMM soft agar[38] was used for P_{bmrC}-lux. The bioreporter soft agar, containing an individual bioreporter strain was poured over the μPAD, which had been previously placed into a square 120 mm × 120 mm Petri dish (Sarstedt) covered with a thin bottom layer of soft agar without bacterial cells. After a solidification period of 20 min, the bioreporter plates were incubated for 180 min at 37 °C. Luminescence was recorded using a ChemiDoc MP system (Bio-Rad) with an exposure time of 600 s in Chemiluminescent Blot 647SP mode, capturing light emission produced at a wavelength of 490 nm. Postimaging, the bioreporter plates were further incubated for 18 h to identify antimicrobial effects (inhibition zones). Incubation was performed at 30 °C for the strains P_{fabHB}-lux, P_{yorB}-lux, P_{ypuA}-lux, P_{liaI}-lux, while P_{bmrC}-lux was incubated at 37 °C. For bioreporter validation by reference compounds, the bioreporter soft agar was poured into an empty Petri dish and pure compounds (≤3 μL, dissolved in DMSO) were directly spotted on the solidified soft agar and left to dry for 5 min before incubation. For the procedure of the liquid assay format see Supporting Methods.

***Saccharopolyspora erythraea* Cultivation and Extraction.** *Saccharopolyspora erythraea* was cultivated on ISP2 agar plates (0.4% D-glucose, 1% malt extract, 0.4% yeast extract, 2% agar, pH 7.3) for 7 days at 28 °C. Biomass was harvested using a cell scraper (Sarstedt) and transferred into a mixture of water and ethyl acetate (50/50, V/V). Extraction was performed in an overhead shaker for 18 h, followed by phase separation via centrifugation (4000*g*, 10 min, 4 °C). The organic phase was lyophilized and reconstituted in 80% (V/V) methanol.

Data Analysis via the MicrospotReader and GNPS2. We developed a Python-based web application called MicrospotReader for data processing and integration of bioluminescence readouts and MS/MS data. The software is built as a streamlit web application and uses the NumPy,[39] pandas,[40,41] SciPy,[42] scikit-image,[43] Numba[44] and pyOpenMS[45,46] packages. The data processing is split into three steps: (I) Image analysis (II) activity data preparation and (III) LC-MS feature detection and correlation with activity data. We provide jupyter notebooks for each step of the process as well as a browser-based web app built using the streamlit framework.

(I) During image analysis activity values are derived automatically from the luminescence readout for each fraction by taking the mean pixel intensity of a given spot. The sizes of luminescent halos can be quantified if present in the image. In addition to overall luminescence intensity, the sizes of halos can be used to provide a semiquantitative estimate of bioactivity. Bioactivity values for all fractions are normalized by the median bioactivity of the image, ensuring comparability among samples.

(II) From the bioactivity data an activity chromatogram is constructed by assigning each fraction a retention time based on experimental parameters. The chromatogram is smoothed using a one-dimensional Gaussian kernel with a sigma-value of 1.

(III) We detected mass spectrometry features in the .mzML files using an untargeted metabolomics workflow provided by the pyOpenMS library.[45,46] Bioactivity peaks are detected within the bioactivity chromatogram and correlated with mass features based on retention time and peak-shape correlation using a Pearson correlation. The retention time overlap is determined by considering a set bias and time window. Correlated features are ranked based on the Pearson correlation coefficient and correlations above 0.8 were kept. A visual representation of the processing workflow is shown in Figure S1.

Molecular networking was performed in GNPS2 (gnps2.org), using the classical networking workflow. Parameters were as follows: Precursor and fragment ion tolerance: 0.002, min cluster size: 2, min cosine (library and network): 0.7, min matched peaks (library and network): 6.

https://doi.org/10.1021/acs.analchem.5c04612
Anal. Chem. 2025, 97, 24093−24104

RESULTS AND DISCUSSION

Microspotter Workflow. The concept of the presented compound-resolved bioactivity-based metabolomics workflow is based on parallelizing LC-MS/MS and biological activity data streams. The combination of both MS/MS and bioactivity signals over a chromatographic time dimension (Figure 1D) is achieved through high-frequency microfractionation and simultaneous MS and MS/MS analysis of the split LC flow (Figure 1A). To achieve fractionation frequencies in the same range as the MS/MS duty cycle time (∼1 Hz), we built a custom Microspotter device based on a commercial CNC milling instrument (Stepcraft, see experimental section, Figures 1B and S2 for details). The stepping motors of the Microspotter allow for a fast and precise switching between the spots without losing eluate despite constant flow (without an additional valve at the capillary outlet). Due to the spotting speed droplets are formed on the tip of the capillary at the spotter head and are deposited onto the μPAD before droplet separation takes place. Transfer of the hanging drops is performed by a lowering of the spotting head into *z*-axis direction, so that the drop, but not the capillary comes into spatial contact with the μPAD (for details, see Video S1 or https://www.youtube.com/watch?v=PTC9epQNzow). The hydrophobic barriers of the μPAD contain the fractions of LC, where the mobile phase can rapidly evaporate, before they can be further tested for their bioactivity. This is crucial, as organic solvents can lead to false positive hits by interfering with bacterial cell viability. To assess possible spot-to-spot carryover and diffusion, we performed further experiments using flow injections (see Figure S8 and subchapter "spot-to-spot carryover in the SI), which indicated that division effects of the Microspotter and related spot-to-spot carry over, were in a similar range as for the ESI-MS part of our setup. In the here described search for antibacterial activity, we overlaid the dry μPADs with bioreporter-containing agar for rapid and sensitive detection of cellular stress that is indicated through the expression of luciferase and the emission of light. The individual steps of the procedure (Figure 1C) may be split into two separate workflows and can be performed in parallel.

The use of bioreporters has several benefits compared to the nonengineered wild-type strains commonly used in bioactivity assays. Reading out a rapid physiological reaction by sensitive luminescence detection yields reliable data already after 180 min, while standard bioactivity assays are generally assessed after 18−24 h. The stress responses signaled by the bioreporters are already triggered at sublethal antibiotic concentrations, resulting in higher sensitivity than the classical growth inhibition readout (see Figure S4). Consequently, bioreporters are superior to classical test strains in detecting low abundant or weakly active agents. Another advantage results from our use of not a single bioreporter, but a defined set of closely related strains that report on different cellular modes of action of antibacterial agents. An individual light-emitting strain among the set informs about the target area of the antibacterial compound, which can assist in the dereplication of known compounds and guide potential downstream assays to identify the molecular target(s) of novel compounds.

After incubating the μPADs with the bioreporter strains, luminescence images are taken, and together with the corresponding LC-MS/MS files, serve as input files for the subsequent computational data analysis. We developed a web application (microspotreader.gnps2.org) to first perform a densitometry analysis of the bioluminescence image, which is then transformed into a bioactivity chromatogram that can be correlated against all extracted ion chromatograms (XICs) from the LC-MS/MS data to identify overlapping features (Figure 1D). The app's output data can then be used to perform molecular networking in GNPS2. In this way, it can be seen if spectra of compounds that are already known to the database were acquired. Furthermore, compounds with spectral similarity cluster in a network and can be interpreted as derivatives.

Bioreporter Induction Specificity. To validate the specificity of the bioreporter panel, we used a collection of 50 reference antibiotics with well-characterized and diverse mechanisms of action (Table S1). Figure 2C exemplifies a representative subset of reference agents in the agar-based setup, and the full data set is shown in Figure S5A. In the agar-based assay, bioreporter induction was quantified by luminescence imaging after 180 min of antibiotic exposure. Within this time frame, the bioreporter signals related specifically and robustly to the agents with the corresponding mechanisms of action, while prolonged incubation occasionally resulted in nonspecific responses. In the agar-based assay, luminescent halos indicating bioreporter activation appeared at the margin of zones of growth inhibition, i.e., at compound concentrations in the diffusion gradient that triggered the bacterial stress responses but still allowed for bacterial metabolism to generate the luciferase signal. The luminescent halos were subsequently superimposed as a pink colorization onto an epi-luminescence image capturing zones of growth inhibition. By relying exclusively on bioluminescence instead of fluorescence, the current system also avoids interference from autofluorescent natural products.

The specificity of the bioreporters was validated in previous studies[28,29] using over 100 reference antibiotics with defined modes of action, ensuring that only promoters responding selectively to their intended target areas were used. In the current work, the same validated promoters were used to drive bacterial luciferase expression, and their specificity was reconfirmed with reference antibiotics, confirming the absence of leakiness or crosstalk.

The bioreporter P_{fabHB}-lux was selectively induced by the fatty acid synthesis inhibitors triclosan[47] and cerulenin[48,49] (Figures 2C and S5A). The activity of DNA gyrase inhibitors, nucleotide synthesis inhibitors, and DNA intercalating agents were detected by P_{yorB}-lux (Figure S5A). In Figure 2C, both DNA gyrase inhibitors ciprofloxacin and moxifloxacin,[50−53] as well as the nucleotide synthesis inhibitor trimethoprim[54,55] show strong inductions. Additionally, P_{yorB}-lux responded to nitrofurantoin, a pleiotropic antibiotic known to also interfere with DNA.[56,57] The general cell envelope stress bioreporter P_{ypuA}-lux reacted to compounds interfering with enzymes and precursors in peptidoglycan synthesis, cell membrane disruptors and certain ionophores (Figure S5A). The phospholipid-binding membrane disruptor mefloquine[58] elicited the strongest signal, followed by the lipid II cycle inhibitors vancomycin[59] and daptomycin,[60,61] and the peptidoglycan transpeptidase inhibitor meropenem.[62] Notably, P_{ypuA}-lux was also induced, albeit weakly, by DNA-active agents as a secondary mechanism of action, consistent with previous observations.[28] This response may result from the activity of the SOS-induced cell division inhibitor YneA, which binds peptidoglycan and interacts with late divisome proteins,

https://doi.org/10.1021/acs.analchem.5c04612
Anal. Chem. 2025, 97, 24093−24104

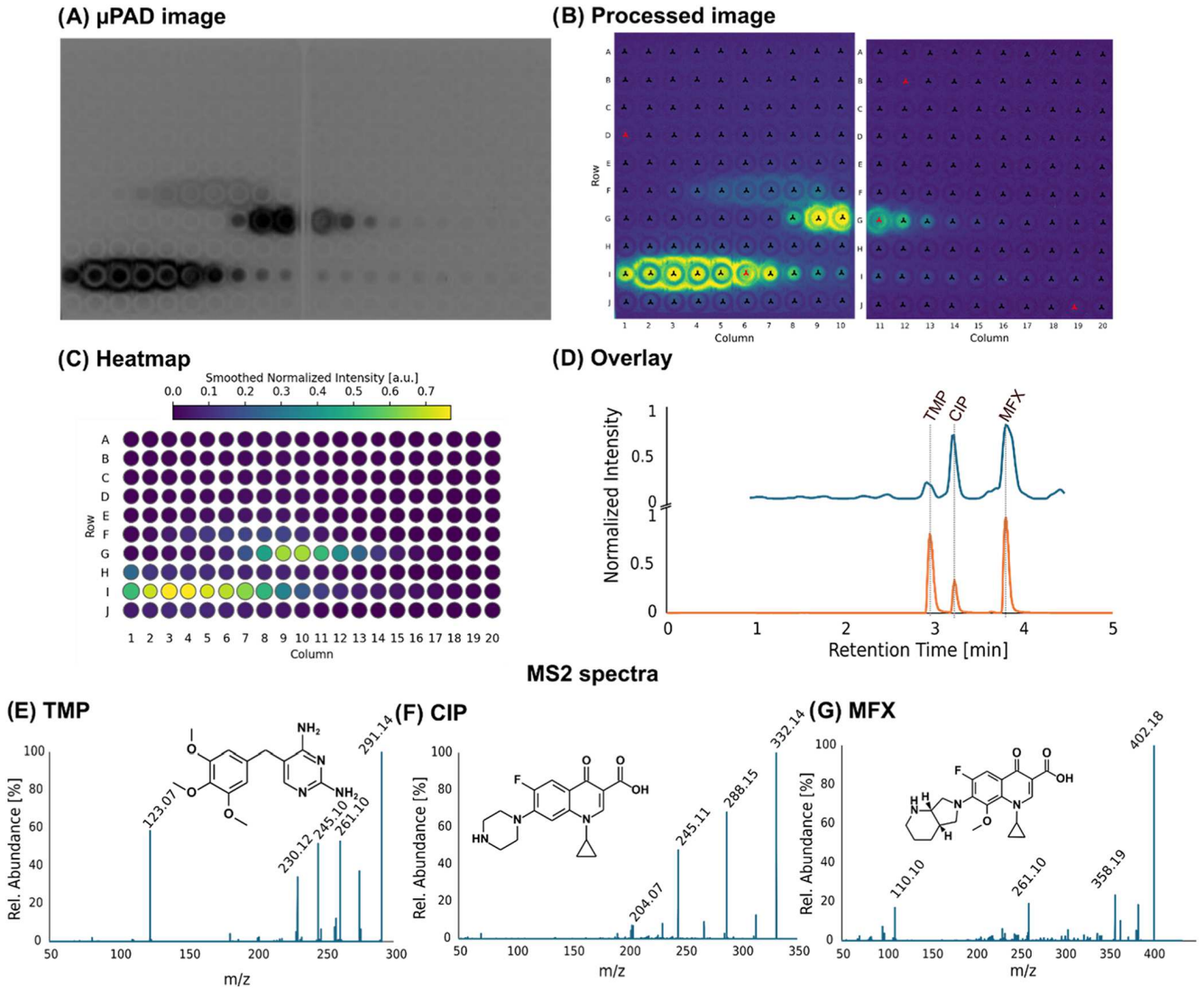

Figure 3. Workflow of the densitometric analysis of a spotted μPAD and its translation into a bioactivity chromatogram. (A) An image of the μPAD is generated, where luminescence can be displayed (here, colors are inverted to increase contrast). (B) The image is recognized by the app, spots are assigned to coordinates. The images will subsequently be transformed into a heatmap (C). By correlating every spot to a distinct retention time, a bioactivity chromatogram (D, blue trace) can be obtained. A comparison to the total ion current (TIC) as obtained with the MS (orange trace) can be performed by overlaying both chromatograms and by comparing the peak shape at a distinct retention time (D) (TMP, trimethoprim; CIP, ciprofloxacin; MFX, moxifloxacin). (E−G) shows the MS2 spectra (positive mode) of trimethoprim (E), ciprofloxacin (F) and moxifloxacin (G); collision energy for all: 35 eV.

thereby inhibiting septal cell wall synthesis and cell division following DNA damage.[63] In contrast, the bioreporter P_{liaI}-lux was induced on agar only by the lipid II cycle inhibitor daptomycin (DAP) as well as mefloquine (MEF) (Figures 2C and S5A). The P_{bmrC}-lux bioreporter was activated by antibiotics that cause translational arrest through diverse mechanisms (Figure S5A). In Figure 2C, bioreporter induction by the exit channel blocker erythromycin,[64] tRNA binding inhibitor tetracycline,[65] and translation initiation inhibitor linezolid[66] is exemplified. Notably, the activation of P_{bmrC}-lux was specific to translational arrest, whereas agents causing miscoding (e.g., gentamicin), general protein-stress (e.g., acyldepsipeptides, ADEPs), abortive translation (e.g., puromycin) or tRNA synthetase inhibitors (e.g., mupirocin) did not induce P_{bmrC}-lux (Figure S5A), corroborating previous findings.[28,29] The bioreporter panel was further assessed in a second, independent whole-cell screening assay in liquid culture applying the same set of reference antibiotics (see Figure S5B and Supporting Methods). In summary, each bioreporter strain demonstrated a selective activation profile in accordance with the established modes of action of the reference antibiotics.

Validation of the Microspotter-LC-MS/MS System. A primary investigation of the bioactive capabilities of the sample of interest is an important step to help reduce the downstream workload. For this purpose, we directly tested crude extracts on the entire bioreporter panel, by manually spotting 10−20 μL of the sample onto the μPAD, repeated once for each bioreporter strain (Figure S4). Generally, one of the bioreporters gave a response, rarely two due to overlapping modes of action. We recommend performing this as a first step in assessing unknown extracts, as it helps to efficiently pinpoint the bioactivities of the sample of interest.

https://doi.org/10.1021/acs.analchem.5c04612
Anal. Chem. 2025, 97, 24093−24104

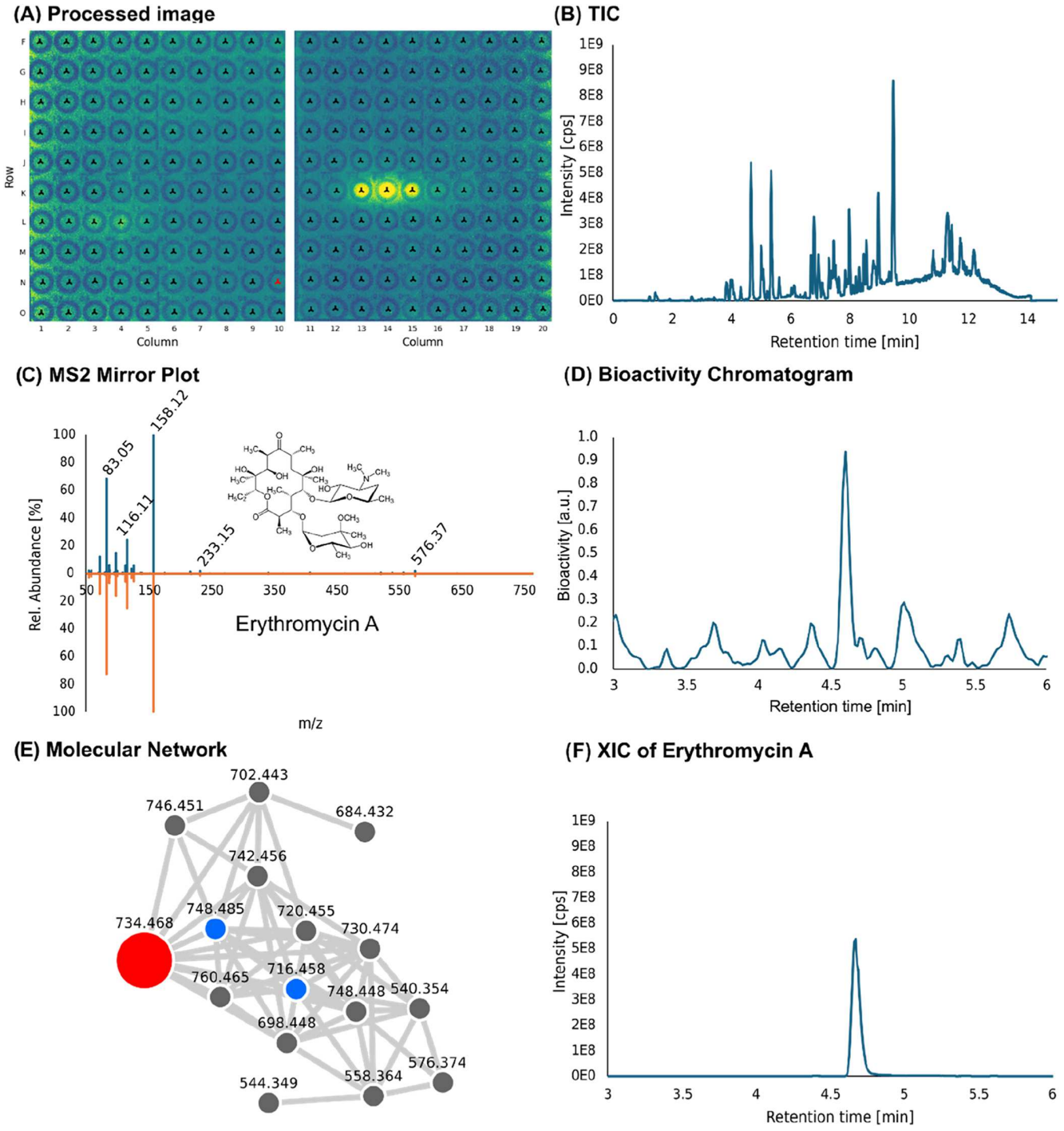

Figure 4. (A) Overview of the observed bioactivity on the μPAD spotted with bacterial extract from *S. erythraea*, shown are spots with a retention time of ∼2.6−6 min. (B) Total ion current (TIC) of the crude extract. (C) MS2 (mirror plot) of an authentic erythromycin A standard (upper part in blue) and the bioactive compound found in the crude extract (lower part, orange). (D) Bioactivity chromatogram obtained from (A). (E) Section of the molecular network generated with the data obtained with the extract from *S. erythraea*. The red highlighted node translates to a spectral match to erythromycin A, the blue nodes are spectral matches to an erythromycin derivative (anhydroerythromycin A) and erythromycin E. (F) extracted ion chromatogram (XIC) of erythromycin A.

Next, we validated the Microspotter setup using a mixture of three commercially available antibiotic compounds and the P_{yorB}-lux bioreporter strain (DNA synthesis stress). The mixture containing ciprofloxacin (500 ng on column (o.c.)), moxifloxacin (250 ng o.c.) and trimethoprim (250 ng o.c.) was spotted applying the HPLC gradient described above. The data analysis pipeline is displayed in Figure 3, beginning with the luminescence image generated by incubating the μPAD for 3 h with the respective bioreporter strain (Figure 3A). From the 500 spots on the μPAD, only the first 200 are shown here. While the first minute (which roughly translates to the dead time of the system) was not spotted, the shown 200 spots represent the elution time from 1.00 to 4.33 min. Spotting was

https://doi.org/10.1021/acs.analchem.5c04612
Anal. Chem. 2025, 97, 24093−24104

performed in a serpentine way to not lose resolution while changing to another row.

Figure 3A clearly shows the luminescence traces that are baseline separated from each other. Figure 3B shows the recognition of the luminescence by performing a densitometric analysis by the use of the MicrospotReader web application (see Chapter 2.9 and Figure S1). As the spotted μPADs were incubated in squares of 10 × 10 spots, two images were taken separately to acquire the images shown in (A) and (B). In a next step, the app merges the information gained from the images to provide a heatmap of detected bioactivity, as the sum of luminescence signal and halo diameter (Figure 3C). By aligning the information shown in the heatmap with the retention time for each spot, the app can provide a bioactivity chromatogram (Figure 3D, blue trace). Using this noncomplex sample, a simple overlay of the bioactivity chromatogram with the total ion current (TIC, orange trace) leads to the detection of the bioactive masses. While the manual inspection is fairly easy in noncomplex samples, it can be hard to perform in complex samples. For this reason, the app uses further information, like peak shape, for the identification of the bioactive peak in complex samples with a multitude of coeluting features. The recording of MS2 spectra gives further valuable information on the detected bioactive compounds and facilitates the structure elucidation when a previously unknown compound is shown to be bioactive. In Figure 3E−G, the recorded MS2 spectra of the three bioactive compounds are shown.

Assessment of Limits of Detection of the Bioactivity Readout. The strength of response by the bioreporter is dependent on the activity (i.e., antibacterial potency and specific mode of action) of the compound, as well as its concentration in the eluted fraction. Compounds with low bioactivity may yield a high signal if present in high amounts; contrarily compounds with high bioactivity may give rise to low signal if not present at sufficient concentration in the sample.

Here, substances with different modes of action were used, and a 2-fold dilution series was performed and manually spotted using a pipet. To simulate the spotting with the Microspotter—and by this the higher volume (roughly 15 μL per spot) and more homogeneous distribution of the substance over the surface of the spot—first 10 μL of a mixture of water/methanol (50/50, V/V) was manually spotted on the μPAD. Thereafter, 5 μL of the antibiotic were pipetted into the water/methanol mixture on the μPAD. Subsequently, the μPADs were left drying and then incubated with the bacteria. For each used bioreporter strain, one antibiotic was chosen, from which the lower limit of detection (LOD) values for luminescence readout, as well as inhibition zone, were determined from the same sheet. In Figure S4, it can clearly be seen that the LOD of the luminescence signal of the bioreporter-strains is lower than the LOD of a classical inhibition zone test. The inhibition zone after 18 h is most probably also dependent on the thickness of the agar layer, as classical inhibition zone tests are performed by spotting the antibiotic on top of the agar, not the other way round as in this case. Nevertheless, this result indicates that the sensitivity of the bioreporter based method is higher. This is mechanistically plausible, as the inhibition zone requires full growth inhibition of the bacteria, while the bioreporter strain-based method produces signals when the bacteria are stressed, but can still grow. This lowers the lower detection threshold, in accordance with previous observations.[28] The plot of the area under the curve (AUC) as obtained by densitometric analysis against concentration reaches a plateau at a distinct concentration. This shows the reached saturation and by this the upper detection limit. LODs were as follows: moxifloxacin (1 ng/spot), erythromycin (1 ng/spot), triclosan (2 ng/spot), vancomycin (59 ng/spot), and daptomycin (125 ng/spot) (see Figure S4).

Identification of Erythromycin as a Bioactive Component in the Extract from *Saccharopolyspora erythraea*. Next, we evaluated the usability of the Microspotter workflow by screening crude extracts from *S. erythraea*, a natural producer of macrolide antibiotics from the erythromycin family. An agar plate of *S. erythraea* was extracted, and the extract was spotted and subsequently overlaid and incubated with P_{bmrC}-lux (translational arrest). After luminescence readout, we could identify bioactivity as shown in Figure 4A.

A strong luminescence signal can clearly be seen in row K. In addition, spots L2−L4 show very light luminescence. Figure 4B shows the TIC of the extract, with (due to the extraction protocol) mostly mid- to nonpolar compounds. While D shows the bioactivity chromatogram, F shows the XIC of the correlating natural product, which corresponds to the mass of erythromycin A. Figure 4C shows a mirror plot of an MS2 spectrum of an authentic erythromycin A standard (upper part, blue) in comparison to the MS2 spectrum gained from the bioactive mass found in the extract, which further confirms the identity of erythromycin as level 2 ID.

In addition to erythromycin A, molecular networking (Figure 4E) showed that multiple compounds with spectral similarity were found in the extract as well. Here, the red node shows the bioactive compound that was annotated by library search on GNPS as erythromycin. Two further erythromycin derivatives were identified here via exact mass and MS/MS spectrum-library matching, namely anhydroerythromycin A and erythromycin E (see Figure S6).[67] These results show that our bioactivity-based microfractionation approach, in combination with molecular networking is a powerful tool to quickly identify bioactive compounds, provide insights on their mode of action, and dereplicate their structure, or prioritize new chemical scaffolds for subsequent structure elucidation.

CONCLUSION

We introduced a novel compound-resolved bioactivity-based metabolomics workflow, including customized open-source hard- and software for the accelerated discovery of bioactive metabolites. While the Microspotter was used in the discovery of antibiotic compounds in this study, it could also be exploited for other applications with other bioassays and formats. The μPAD can be adjusted to meet different assay needs, fit commercial fraction collectors, or be exchanged with 96 or 384 microwell plates for bioactivity assay in liquid state. Focusing on antibiotic activity, we constructed five non-sporulating bioreporter strains that respond to different cellular stress modes of action by autonomous light emission. We validated and tested the bioreporters and the Microspotter workflow with a panel of antibiotic standard compounds as a proof of principle. We could hereby unambiguously assign bioactivity to the masses and MS2 spectra of all standards. While further evaluating the performance and practicality of our approach with complex crude extracts from the actinomycete bacterium *S. erythraea*, we could rapidly identify the known macrolide antibiotic erythromycin A and derivatives.

https://doi.org/10.1021/acs.analchem.5c04612
Anal. Chem. 2025, 97, 24093−24104

In summary, our results demonstrate that LC-MS/MS coupled microfractionation on μPADs at high frequency and in combination with luminescent bioreporter strains is a powerful strategy for the search for novel bioactive compounds. We anticipate that its versatility and high-throughput capability will contribute to accelerate the discovery of bioactive metabolites from complex extracts.

■ ASSOCIATED CONTENT

Data Availability Statement

All LC-MS/MS raw and processed files as well as luminescence images are available through the Zenodo (10.5281/zenodo.10800808) and MassIVE (MSV000094260) repositories. CAD files for the 3D printable parts of the Microspotter are available through the Zenodo repository (10.5281/zenodo.15796942) as well as on Thingiverse (thingiverse.com/thing:7077237/). GNPS2 molecular networking results of the crude extract of *S. erythraea* is available under: https://gnps2.org/status?task=0df811f274154242a7b349ac5e8d4b91. Code of the MicrospotReader (Knoblauch, S. (2025)). MicrospotReader WebApp (Version v0.1.1) can be found at: https://github.com/Functional-Metabolomics-Lab/MicrospotReader and a release has been deposited at Zenodo with the following DOI: 10.5281/zenodo.15494998. Executable files for local installations can be downloaded at: https://github.com/sknesiron/MicrospotReader/releases/tag/v0.1.1. Code for the Autostart (Fleischer, J. (2025) Microspotter-Synchronizing hard-/Software) can be found at https://github.com/Functional-Metabolomics-Lab/UCCNC_api_test and a release has been deposited at Zenodo with the following DOI: 10.5281/zenodo.15756837.

Supporting Information

The Supporting Information is available free of charge at https://pubs.acs.org/doi/10.1021/acs.analchem.5c04612.

Antibiotics used in this study, primers, microplate reader settings, figures for the app's workflow, close-up picture of the tailor-made Microspotter head, images of the 3D-printable files, validation of the assay and determination of LODs, structure of erythromycin and derivatives, comparison of wax printed and thermal transfer printed μPADs, determination of possible spot-to-spot carryover and diffusion, methods for cloning of lux bioreporters and liquid based bioreporter assay, notes on comparison of wax printed and thermal transfer printed μPADs, Microspotter head fabrication and spot-to-spot carryover (PDF)

Microspotter working (Video S1) (MP4)

■ AUTHOR INFORMATION

Corresponding Authors

Heike Brötz-Oesterhelt − *Department of Microbial Bioactive Compounds, Interfaculty Institute of Microbiology and Infection Medicine (IMIT), University of Tübingen, 72076 Tübingen, Germany; Cluster of Excellence Controlling Microbes to Fight Infections (CMFI), University of Tübingen, 72076 Tübingen, Germany; German Center for Infection Research (DZIF), Partner Site Tübingen, 72076 Tübingen, Germany;* orcid.org/0000-0001-9364-1832; Email: heike.broetz-oesterhelt@uni-tuebingen.de

Daniel Petras − *Cluster of Excellence Controlling Microbes to Fight Infections (CMFI), University of Tübingen, 72076 Tübingen, Germany; Department of Biochemistry, University of California Riverside, Riverside, California 72521, United States;* orcid.org/0000-0002-6561-3022; Email: dpetras@ucr.edu

Authors

Christian Geibel − *Department of Microbial Bioactive Compounds, Interfaculty Institute of Microbiology and Infection Medicine (IMIT), University of Tübingen, 72076 Tübingen, Germany; Cluster of Excellence Controlling Microbes to Fight Infections (CMFI), University of Tübingen, 72076 Tübingen, Germany;* orcid.org/0009-0002-2044-9422

Julian Schubert − *Department of Microbial Bioactive Compounds, Interfaculty Institute of Microbiology and Infection Medicine (IMIT), University of Tübingen, 72076 Tübingen, Germany; Cluster of Excellence Controlling Microbes to Fight Infections (CMFI), University of Tübingen, 72076 Tübingen, Germany*

Simon B. Knoblauch − *Cluster of Excellence Controlling Microbes to Fight Infections (CMFI), University of Tübingen, 72076 Tübingen, Germany*

Albert Hernandez − *Cluster of Excellence Controlling Microbes to Fight Infections (CMFI), University of Tübingen, 72076 Tübingen, Germany*

Leonardo Boldt − *Department of Microbial Bioactive Compounds, Interfaculty Institute of Microbiology and Infection Medicine (IMIT), University of Tübingen, 72076 Tübingen, Germany; Cluster of Excellence Controlling Microbes to Fight Infections (CMFI), University of Tübingen, 72076 Tübingen, Germany;* orcid.org/0009-0009-7743-605X

Dana C. Schneider − *Department of Microbial Bioactive Compounds, Interfaculty Institute of Microbiology and Infection Medicine (IMIT), University of Tübingen, 72076 Tübingen, Germany; Cluster of Excellence Controlling Microbes to Fight Infections (CMFI), University of Tübingen, 72076 Tübingen, Germany; German Center for Infection Research (DZIF), Partner Site Tübingen, 72076 Tübingen, Germany*

Stilianos Papadopoulos Lambidis − *Cluster of Excellence Controlling Microbes to Fight Infections (CMFI), University of Tübingen, 72076 Tübingen, Germany; Department of Microbiome Science, Max Planck Institute for Biology, 72076 Tübingen, Germany*

Giovanni Andrea Vitale − *Department of Microbial Bioactive Compounds, Interfaculty Institute of Microbiology and Infection Medicine (IMIT), University of Tübingen, 72076 Tübingen, Germany; Cluster of Excellence Controlling Microbes to Fight Infections (CMFI), University of Tübingen, 72076 Tübingen, Germany;* orcid.org/0000-0002-7143-6317

Jakub Fleischer − *University of Innsbruck, 6020 Innsbruck, Austria*

Manuela Haussmann − *Pharmaceutical Institute, Department of Pharmaceutical Biology, University of Tübingen, 72076 Tübingen, Germany*

Harald Gross − *Cluster of Excellence Controlling Microbes to Fight Infections (CMFI) and Pharmaceutical Institute, Department of Pharmaceutical Biology, University of Tübingen, 72076 Tübingen, Germany; German Center for Infection Research (DZIF), Partner Site Tübingen, 72076 Tübingen, Germany;* orcid.org/0000-0002-0731-821X

https://doi.org/10.1021/acs.analchem.5c04612
Anal. Chem. 2025, 97, 24093−24104

Mingxun Wang − *Department of Computer Science and Engineering, University of California Riverside, Riverside, California 92521, United States*

Complete contact information is available at: https://pubs.acs.org/10.1021/acs.analchem.5c04612

Author Contributions

H.B.O. and D.P. conceptualized the approach and the study. C.G., S.K., A.H., S.P.L., J.F., and D.P. developed the Microspotter hardware. J.S., L.B., D.C.S., and H.B.O., developed the bioreporter strains. S.K. and M.W. developed software. C.G., J.S., S.K., G.A.V., M.H., D.P., and L.B., DCS performed the experiments. C.G., J.S., S.K., L.B., and D.P. analyzed the data. H.G., H.B.O., and D.P. provided materials and instrumentation. C.G., J.S., S.K., H.B.O., and D.P. wrote the manuscript. All authors edited and approved the final manuscript.

Notes

The authors declare the following competing financial interest(s): Mingxun Wang is a co-founder of Ometa labs LLC.

■ ACKNOWLEDGMENTS

We thank Chambers Hughes for helpful discussions. We thank Tatiana and Pieter Dorrestein for providing the crayons for the first μPAD prototype. This study was supported by the Deutsche Forschungsgemeinschaft (German Research Foundation, DFG) via the Cluster of Excellence EXC 2124: Controlling Microbes to Fight Infection (CMFI, project ID 390838134) to H.B.O. and D.P. and via TRR 261 (project ID 398967434) to H.G., H.B.O., and D.P. We are thankful for the support of the Simons Foundation International through an Simons Early Career Investigator in Aquatic Microbial Ecology and Evolution Award (SFI-LS-ECIAMEE-00013858) to D.P. This work was supported in part by the National Institute of General Medical Sciences, GM160154 to D.P., the National Institute of Diabetes and Digestive and Kidney Diseases, 5U24DK133658-02 to M.W., and by the U.S. Department of Energy Joint Genome Institute (https://ror.org/04xm1d337), a DOE Office of Science User Facility, supported by the Office of Science of the U.S. Department of Energy operated under Contract No. DE-AC02-05CH11231.

■ REFERENCES

(1) Gagare, S.; Patil, P.; Jain, A. *Future J. Pharm. Sci.* **2024**, *10*, No. 55.
(2) Xiao, Z.; Morris-Natschke, S. L.; Lee, K. *Med. Res. Rev.* **2016**, *36*, 32−91.
(3) Zhang, L.; Song, J.; Kong, L.; et al. *Pharmacol. Ther.* **2020**, *216*, No. 107686.
(4) Gavriilidou, A.; Kautsar, S. A.; Zaburannyi, N.; et al. *Nat. Microbiol.* **2022**, *7*, 726−735.
(5) Murray, C. J. L.; Ikuta, K. S.; Sharara, F.; et al. *Lancet* **2022**, *399*, 629−655.
(6) Newman, D. J. *Expert Opin. Drug Discovery* **2019**, *14*, 521−525.
(7) Vitale, G. A.; January, G. G.; Oppong-Danquah, E.; et al. *PNAS Nexus* **2023**, *2*, No. pgad221.
(8) Vitale, G. A.; Geibel, C.; Minda, V.; et al. *Nat. Prod. Rep.* **2024**, *41*, 885−904.
(9) Bağcı, C.; Nuhamunada, M.; Goyat, H.; et al. *Nucleic Acids Res.* **2025**, *53*, D618−D624.
(10) Li, C.; Han, Y.; Zou, X.; et al. *Synth. Syst. Biotechnol.* **2024**, *9*, 775−783.
(11) Wagner, B. C.; Geibel, C.; Stadelmann, A.et al.Native metabolomics identifies pteridines as CutA ligands and modulators of copper binding *bioRxiv* 2025 DOI: 10.1101/2025.04.03.647050.
(12) Reher, R.; Aron, A. T.; Fajtová, P.; et al. *Nat. Commun.* **2022**, *13*, No. 4619.
(13) Prudent, R.; Annis, D. A.; Dandliker, P. J.; Ortholand, J.-Y.; Roche, D. *Nat. Rev. Chem.* **2021**, *5*, 62−71.
(14) Atanasov, A. G.; Zotchev, S. B.; Dirsch, V. M.; et al. *Nat. Rev. Drug Discovery* **2021**, *20*, 200−216.
(15) Kool, J.; Heus, F.; de Kloe, G.; et al. *SLAS Discovery* **2011**, *16*, 917−924.
(16) Mahmoud, A. B.; Danton, O.; Kaiser, M.; et al. *Front. Pharmacol.* **2020**, *11*, No. 1246.
(17) Akaberi, M.; Danton, O.; Tayarani-Najaran, Z.; et al. *J. Nat. Prod.* **2019**, *82*, 958−969.
(18) Wang, M.; Carver, J. J.; Phelan, V. V.; et al. *Nat. Biotechnol.* **2016**, *34*, 828−837.
(19) Bazzano, C. F.; de Felicio, R.; Alves, L. F. G.; et al. *Anal. Chem.* **2024**, *96*, 7460−7469.
(20) Nothias, L.-F.; Nothias-Esposito, M.; da Silva, R.; et al. *J. Nat. Prod.* **2018**, *81*, 758−767.
(21) von Eckardstein, L.; Petras, D.; Dang, T.; et al. *Chem. − Eur. J.* **2017**, *23*, 15316−15321.
(22) Martinez, A. W.; Phillips, S. T.; Butte, M. J.; Whitesides, G. M. *Angew. Chem., Int. Ed.* **2007**, *46*, 1318−1320.
(23) Das, S.; Gagandeep; Bhatia, R. *Rev. Anal. Chem.* **2022**, *41*, 112−136.
(24) Tan, W.; Zhang, L.; Jarujamrus, P.; Doery, J. C. G.; Shen, W. *Microchem. J.* **2022**, *180*, No. 107562.
(25) Ataide, V. N.; Mendes, L. F.; Gama, L. I. L. M.; De Araujo, W. R.; Paixão, T. R. L. C. *Anal. Methods* **2020**, *12*, 1030−1054.
(26) Arai, M. S.; de Camargo, A. S. S.; Carrilho, E. Fluorescent Paper-Based Analytical Devices. In *Paper-Based Analytical Devices for Chemical Analysis and Diagnostics*; Elsevier, 2022; pp 183−212.
(27) Zhang, W.-Y.; Tian, T.; Peng, L. J.; et al. *Biosensors* **2022**, *12*, No. 893.
(28) Wex, K. W.; Saur, J. S.; Handel, F.; et al. *Cell Chem. Biol.* **2021**, *28*, 1242−1252.e4.
(29) Urban, A.; Eckermann, S.; Fast, B.; et al. *Appl. Environ. Microbiol.* **2007**, *73*, 6436−6443.
(30) Freiberg, C.; Brunner, N.; Macko, L.; Fischer, H. P. *Mol. Cell. Proteomics* **2006**, *5*, 2326−2335.
(31) Mascher, T.; Zimmer, S. L.; Smith, T.-A.; Helmann, J. D. *Antimicrob. Agents Chemother.* **2004**, *48*, 2888−2896.
(32) Hutter, B.; Fischer, C.; Jacobi, A.; Schaab, C.; Loferer, H. *Antimicrob. Agents Chemother.* **2004**, *48*, 2588−2594.
(33) Lai, C.-Y.; Cronan, J. E. *J. Biol. Chem.* **2003**, *278*, 51494−51503.
(34) Schujman, G. E.; Paoletti, L.; Grossman, A. D.; De Mendoza, D. *Dev. Cell* **2003**, *4*, 663−672.
(35) Au, N.; Kuester-Schoeck, E.; Mandava, V.; et al. *J. Bacteriol.* **2005**, *187*, 7655−7666.
(36) Torres, C.; Galián, C.; Freiberg, C.; Fantino, J.-R.; Jault, J.-M. *Biochim. Biophys. Acta, Biomembr.* **2009**, *1788*, 615−622.
(37) Radeck, J.; Kraft, K.; Bartels, J.; et al. *J. Biol. Eng.* **2013**, *7*, No. 29.
(38) Stülke, J.; Hanschke, R.; Hecker, M. *J. Gen. Microbiol.* **1993**, *139*, 2041−2045.
(39) Harris, C. R.; Millman, K. J.; van der Walt, S. J.; et al. *Nature* **2020**, *585*, 357−362.
(40) The pandas development team. pandas-dev/pandas *Pandas* 2023 DOI: 10.5281/ZENODO.10045529. Zenodo.
(41) McKinney, W. In *Data Structures for Statistical Computing in Python*, Proceedings of the Python in Science Conference 56−61; SciPy: Austin, TX, 2010.
(42) Virtanen, P.; Gommers, R.; Oliphant, T. E.; et al. *Nat. Methods* **2020**, *17*, 261−272.
(43) Van Der Walt, S.; Schönberger, J. L.; Nunez-Iglesias, J.; et al. *PeerJ* **2014**, *2*, No. e453.

(44) Lam, S. K.; Pitrou, A.; Seibert, S. In *Numba: a LLVM-Based Python JIT Compiler*, Proceedings of the Second Workshop on the LLVM Compiler Infrastructure in HPC; ACM: Austin Texas, 2015; pp 1−6.
(45) Röst, H. L.; Schmitt, U.; Aebersold, R.; Malmström, L. *Proteomics* **2014**, *14*, 74−77.
(46) Röst, H. L.; Sachsenberg, T.; Aiche, S.; et al. *Nat. Methods* **2016**, *13*, 741−748.
(47) Heath, R. J.; Rubin, J. R.; Holland, D. R.; et al. *J. Biol. Chem.* **1999**, *274*, 11110−11114.
(48) D'Agnony, G.; Rosenfeld, I. S.; Awaya, J.; Ōmura, S.; Vagelos, P. R. *Biochim. Biophys. Acta, Lipids Lipid Metab.* **1973**, *326*, 155−166.
(49) Buttke, T. M.; Ingram, L. O. *Biochemistry* **1978**, *17*, 5282−5286.
(50) Madurga, S.; Sánchez-Céspedes, J.; Belda, I.; Vila, J.; Giralt, E. *ChemBioChem* **2008**, *9*, 2081−2086.
(51) LeBel, M. *Pharmacotherapy* **1988**, *8*, 3−30.
(52) Drlica, K.; Zhao, X. *Microbiol. Mol. Biol. Rev.* **1997**, *61*, 377−392.
(53) Pan, X. S.; Ambler, J.; Mehtar, S.; Fisher, L. M. *Antimicrob. Agents Chemother.* **1996**, *40*, 2321−2326.
(54) Hitchings, G. H. *J. Infect. Dis.* **1973**, *128*, S433−S436.
(55) Gleckman, R.; Blagg, N.; Joubert, D. W. *Pharmacotherapy* **1981**, *1*, 14−19.
(56) McOsker, C. C.; Fitzpatrick, P. M. *J. Antimicrob. Chemother.* **1994**, *33*, 23−30.
(57) Kettlewell, R.; Jones, C.; Felton, T. W.; Lagator, M.; Gifford, D. R. *npj Antimicrob. Resist.* **2024**, *2*, No. 41.
(58) Chevli, R.; Fitch, C. D. *Antimicrob. Agents Chemother.* **1982**, *21*, 581−586.
(59) Reynolds, P. E. *Eur. J. Clin. Microbiol. Infect. Dis.* **1989**, *8*, 943−950.
(60) Pogliano, J.; Pogliano, N.; Silverman, J. A. *J. Bacteriol.* **2012**, *194*, 4494−4504.
(61) Taylor, S. D.; Palmer, M. *Bioorg. Med. Chem.* **2016**, *24*, 6253−6268.
(62) Craig, W. A. *Clin. Infect. Dis.* **1997**, *24*, S266−S275.
(63) Masser, E. A.; Burby, P. E.; Hawkins, W. D.; et al. *Mol. Microbiol.* **2021**, *116*, 707−722.
(64) Kanoh, S.; Rubin, B. K. *Clin. Microbiol. Rev.* **2010**, *23*, 590−615.
(65) Chopra, I.; Roberts, M. *Microbiol. Mol. Biol. Rev.* **2001**, *65*, 232−260.
(66) Wilson, D. N.; Schluenzen, F.; Harms, J. M.; et al. *Proc. Natl. Acad. Sci. U.S.A.* **2008**, *105*, 13339−13344.
(67) Deubel, A.; Fandiño, A. S.; Sörgel, F.; Holzgrabe, U. *J. Chromatogr. A* **2006**, *1136*, 39−47.

https://doi.org/10.1021/acs.analchem.5c04612
Anal. Chem. 2025, 97, 24093−24104

Supplemental Information

High-frequency microfluidic fractionation for compound-resolved bioactivity-based metabolomics

Christian Geibel[1,2], Julian Schubert[1,2], Simon B. Knoblauch[2], Albert Hernandez[2], Leonardo Boldt[1,2], Dana C. Schneider[1,2,3], Stilianos Papadopoulos Lambidis[2,4], Giovanni Andrea Vitale[1,2], Jakub Fleischer[5], Manuela Haussmann[6], Harald Gross[2,3,6], Mingxun Wang[7], Heike Brötz-Oesterhelt[1,2,3,*], Daniel Petras[2,8,*]

1. Department of Microbial Bioactive Compounds, Interfaculty Institute of Microbiology and Infection Medicine (IMIT), University of Tübingen, 72076 Tübingen, Germany
2. Cluster of Excellence Controlling Microbes to Fight Infections (CMFI), University of Tübingen, 72076 Tübingen, Germany
3. German Center for Infection Research (DZIF), Partner Site Tübingen, 72076 Tübingen, Germany
4. Department of Microbiome Science, Max Planck Institute for Biology, 72076 Tübingen, Germany
5. University of Innsbruck, 6020 Innsbruck, Austria
6. Pharmaceutical Institute, Department of Pharmaceutical Biology, University of Tübingen, 72076 Tübingen, Germany
7. Department of Computer Science and Engineering, University of California Riverside, Riverside, California 92521, USA
8. Department of Biochemistry, University of California Riverside, Riverside, California 72521, USA

* Correspondence: heike.broetz-oesterhelt@uni-tuebingen.de or dpetras@ucr.edu

Table of Contents

Table S1: Antibiotics used in this study.

Antibiotic	Solvent	Supplier
Fatty acid synthesis inhibitors		
Cerulenin	DMSO	Cayman Chemicals
Triclosan	DMSO	LKT Laboratories
DNA synthesis inhibitors		
DNA gyrase binders		
Ciprofloxacin	H_2O	AppliChem
Moxifloxacin	H_2O	Fluka
Norfloxacin	DMSO	Fluka
Nalidixic acid	DMSO	Roth
Novobiocin	H_2O	AppliChem
Intercalators		
Phleomycin	H_2O	Invitrogen
Proflavine	H_2O	Sigma-Aldrich
Nucleotide synthesis inhibitors		
Azaserine	H_2O	Cayman Chemicals
Sulfamethoxazol	DMSO	Sigma-Aldrich
Trimethroprim	DMSO	Sigma-Aldrich
Pleiotropic effects		
Nitrofurantoin	DMSO	Sigma-Aldrich
Cell envelope inhibitors		
Peptidoglycan synthesis enzyme inhibitors		
Fosfomycin	H_2O	Sigma-Aldrich
Penicillin G	H_2O	Fluka
Methicillin	H_2O	Sigma-Aldrich
Ampicillin	H_2O	Roth
Cefadroxil	H_2O	Sigma-Aldrich
Cefotaxime	H_2O	Sigma-Aldrich
Cefuroxime	H_2O	Sigma-Aldrich
Meropenem	H_2O	Fluka
Peptidoglycan precursor binders		
Vancomycin	H_2O	AppliChem
Teicoplanin	H_2O	Aventis Pharma
Daptomycin	H_2O	Cayman Chemicals
Cell membrane disruptors		
Colistin	H_2O	Cayman Chemicals
Mefloquine	DMSO	Sigma-Aldrich
Ionophores		
Salinomycin	Ethanol	Cayman Chemicals
CCCP	DMSO	Sigma-Aldrich
Efflux pump inhibitors		
Reserpine	DMSO	Fluka

Antibiotic	Solvent	Supplier
Protein synthesis inhibitors		
Translation stallers		
Linezolid	DMSO	Acros Organics
Anhydrotetracycline	DMSO	Cayman Chemicals
Tetracycline	DMSO	Sigma-Aldrich
Doxycycline	H_2O	AppliChem
Chloramphenicol	Ethanol	Sigma-Aldrich
Clindamycin	H_2O	Cayman Chemicals
Lincomycin	H_2O	Alfa Aesar
Erythromycin	DMSO	AppliChem
Telithromycin	DMSO	Cayman Chemicals
Fusidic acid	H_2O	AppliChem
Hygromycin B	H_2O	Roth
Thiostrepton	DMSO	AppliChem
Miscoding inducers		
Gentamycin	H_2O	AppliChem
Kanamycin	H_2O	Roth
Tobramycin	H_2O	Acros Organics
Abortive translation inducer		
Puromycin	H_2O	Sigma-Aldrich
Protein stress inducer		
TMAD	H_2O	Sigma-Aldrich
tRNA synthetase inhibitors		
Mupirocin	H_2O	Sigma-Aldrich
Antibiotic	Solvent	Supplier
RNA polymerase binders		
Fidaxomicin	Methanol	Cayman Chemicals
Rifampicin	DMSO	AppliChem
Diverse mechanism of action		
Clp protease dysregulators		
Acyldepsipeptide 2	DMSO	EMC Microcollections
Acyldepsipeptide 7	DMSO	EMC Microcollections

Table S2: Primers.

PCR primer	Nucleotide sequence (5'-3')
PyheI-forward	GATAAGCTGTCAAACATGAGAATTCTTCTTACTATTTTCACTTCCGTCAAACG
PyheI-reverse	TTTCATAGAGAGTCCTCCTGTCGACCTCATCAGCCGCCTTCTATTTTTTC
PfabHB-forward	GATAAGCTGTCAAACATGAGAATTCTCATAGATTCCTATCTACACTTCTC
PfabHB-reverse	TTTCATAGAGAGTCCTCCTGTCGACCACTCCTTATGGTCAGATTATAACAC
PliaI-forward	GATAAGCTGTCAAACATGAGAATTCCGGGTATCGGAATCTTGCTGTTTAC
PliaI-reverse	TTTCATAGAGAGTCCTCCTGTCGACTCCAAAAAAGACGGAGATCCCAAATAC
PyorB-forward	GATAAGCTGTCAAACATGAGAATTCCGGGATATATTGGGATAAAGATTCAG
PyorB-reverse	TTTCATAGAGAGTCCTCCTGTCGACTTTTGAAATTTTTGGTACTACTAAATTAT ATACC
PypuA-forward	GATAAGCTGTCAAACATGAGAATTCGCGGGCATCCGCCTTGGCTGACGAA
PypuA-reverse	TTTCATAGAGAGTCCTCCTGTCGACCAATTTCACAAGCAGCTGGATAGTGCTG CTTTGTG

Sequencing primer	Nucleotide sequence (5'-3')
Insert-control-forward	TTCGTTTGTTGAACTAATGGGTGC
Insert-control-reverse	AAACCACACTCCTCAGAGATG
Insert-yheI-reverse	TCGACCTCATCAGCCGCCTTC
Insert-fabHB-reverse	TCCTGTCGACCACTCCTTATG
Insert-liaI-reverse	AAGACGGAGATCCCAAATAC
Insert-yorB-reverse	TGCACCAATACCTTGAACATC
Insert-ypuA-reverse	TCGACCAATTTCACAAGCAGC

Colony PCR primer	Nucleotide sequence (5'-3')
SacA-Int-forward	CTGATTGGCATGGCGATTGC
SacA-Int-reverse	ACAGCTCCAGATCCTCTACG

Table S3: Microplate reader settings.

Parameter	Settings
Lid	Yes
Humidity cassette	No
Temperature control	On - wait for temperature
Temperature	37°C [min: 36°C, max: 38°C]
Measurement duration	Three hours
Interval time	Five minutes
Interval ▼	
Shaking	60 s, double orbital, amplitude 2.5 mm (108 rpm)
Wait	10 s
Luminescence	Integration time 1000 [ms]
Absorbance	Wavelength 600 nm, bandwidth 3.5, Flashes 10, settle time 100 [ms], multiple reads per well: XY-line 3x3, border 2400 [µm]
Wait	Wait for interval restart

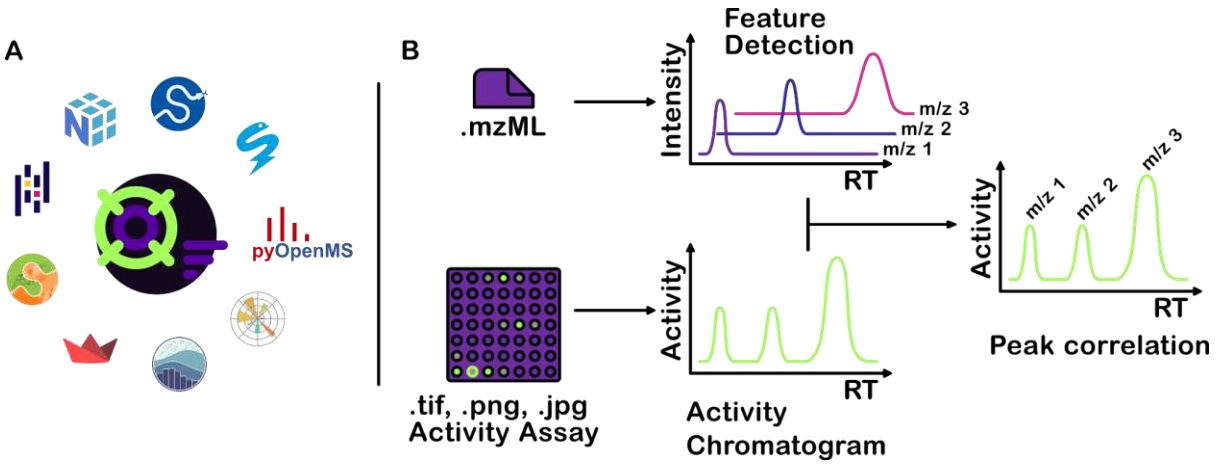

Figure S1: A) MicrospotReader leverages multiple optimized libraries for data processing (pandas, NumPy, SciPy, Numba, scikit-image, pyOpenMS), data visualization (Seaborn, matplotlib) and streamlit as a web app framework. B) Feature detection in LC-MS data (top), construction of an activity chromatogram from a bioactivity assay on LC-fractions (bottom) and correlation of activity peaks with LC-MS features (right).

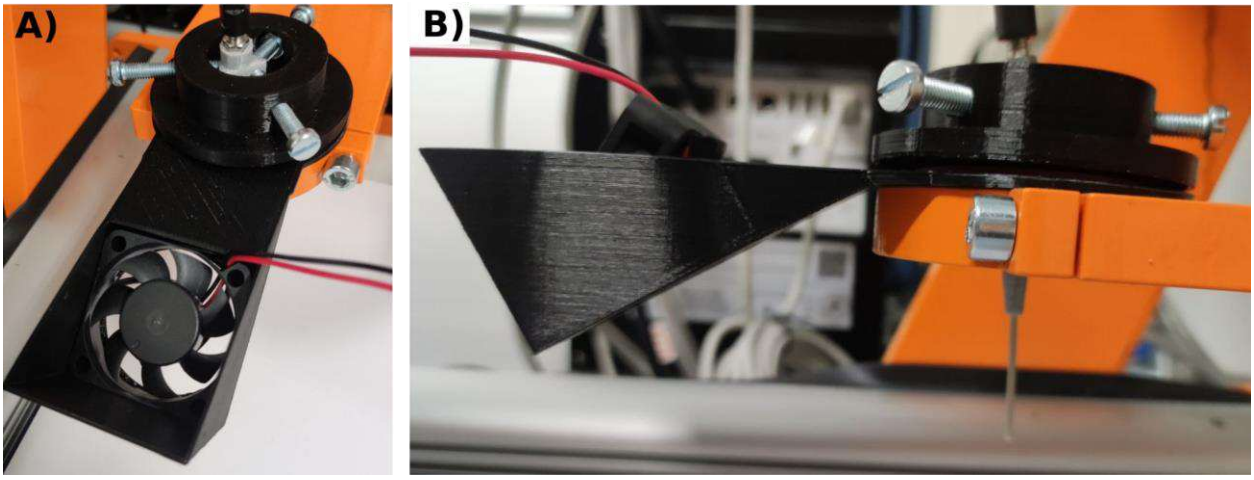

Figure S2: Tailor-made Microspotter head, A) top view with cooling fan (lower part) and adjustable capillary holder (between screws, light grey). B) Side view of the head, the truncated cone of the adjustable capillary holder as well as the capillary can be seen (light grey) as well as the angled fan holder.

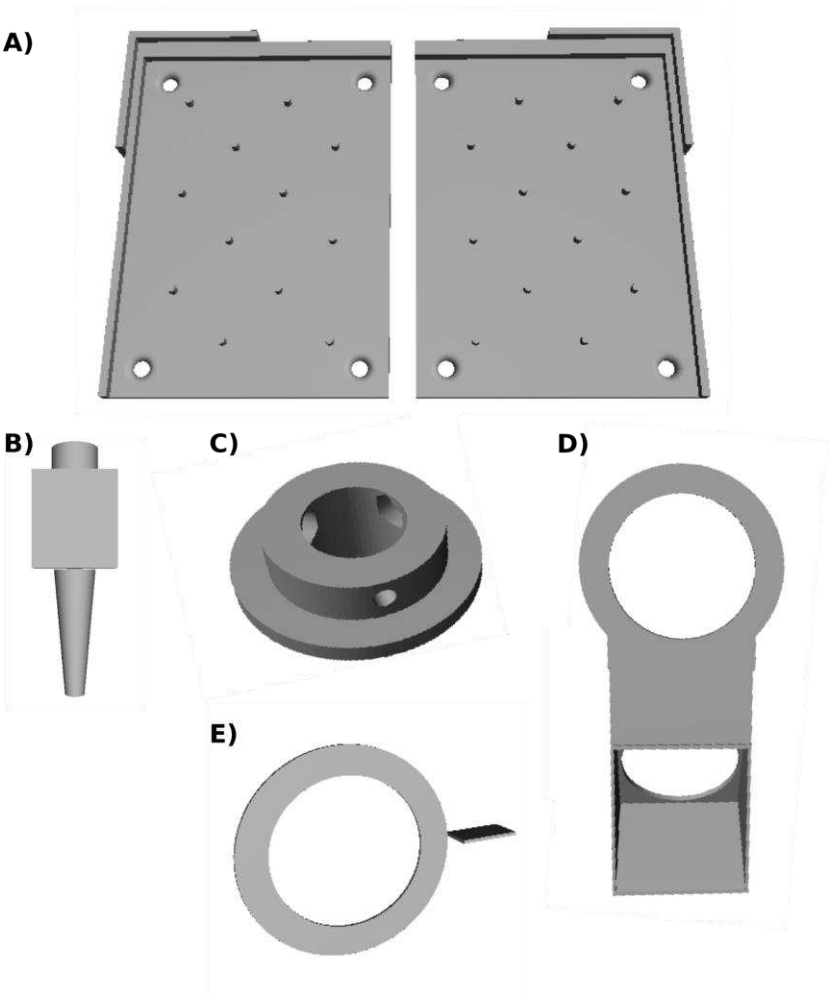

Figure S3: Drawing of the 3D printable parts as uploaded on Zenodo and Thingiverse (see data sharing section in main document). A) Paper holder, designed for one DIN A4 paper (needs to be printed twice). This holder keeps the µPAD in place and elevates it to facilitate drying. Can be installed on the bench surface of the milling machine. B) Spotter head, designed to lead the capillary. The upper part is designed to hold a crimped capillary fitting. C) Inner ring, which holds B) in place. Three holes can be equipped with screws to hold B) in place and to finetune its position. D) Angled fan holder, optional part, can be equipped with a small computer fan to speed up drying of the mobile phase while spotting. Should be installed under C). E) Optional part: a small ring that can be placed beneath part D) and secured using the flap in the small opening of the milling machine holder (see Fig. S2, orange part—gap secured with a screw). This prevents the spotter head from rotating within the milling holder.

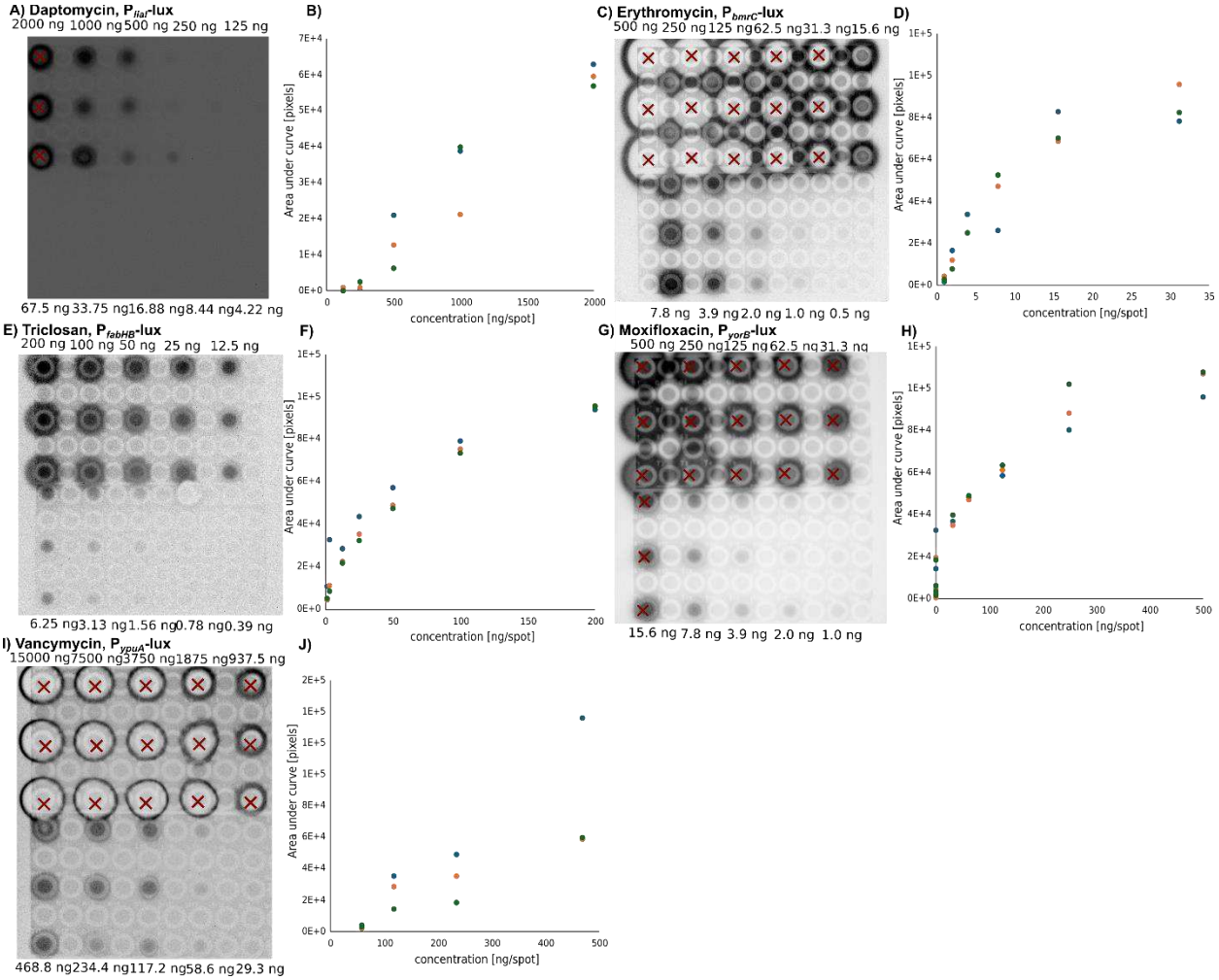

Figure S4: Dilution series of all tested antibiotic standards. The values indicate the concentration of the antibiotic in ng/spot. All concentrations were spotted manually in triplicates. Left side shows the luminescence readout after 3 h. Red crosses indicate spots in which an inhibition zone could be seen by the naked eye after 18 h of incubation. Right side shows the AUC of the spots in pixels plotted against the concentration. (A) and (B): daptomycin, incubated with P*liaI*-lux reporter strain. (C) and (D): erythromycin, incubated with P*bmrC*-lux reporter strain. (E) and (F): triclosan, incubated with P*fabHB*-lux reporter strain. (G) and (H): moxifloxacin, incubated with P*yorB*-lux reporter strain. (I) and (J): vancomycin, incubated with P*ypuA*-lux reporter strain.
Of note, it is established that the antibacterial activity of daptomycin is enhanced when Ca^{2+} is added to growth media, per its MoA that involves Ca^{2+} binding. To better simulate „real life conditions“ under which such a specific requirement would not be known when discovering a novel natural product, we refrained in experiment A) from adding Ca^{2+} to the agar for more sensitive daptomycin detection.

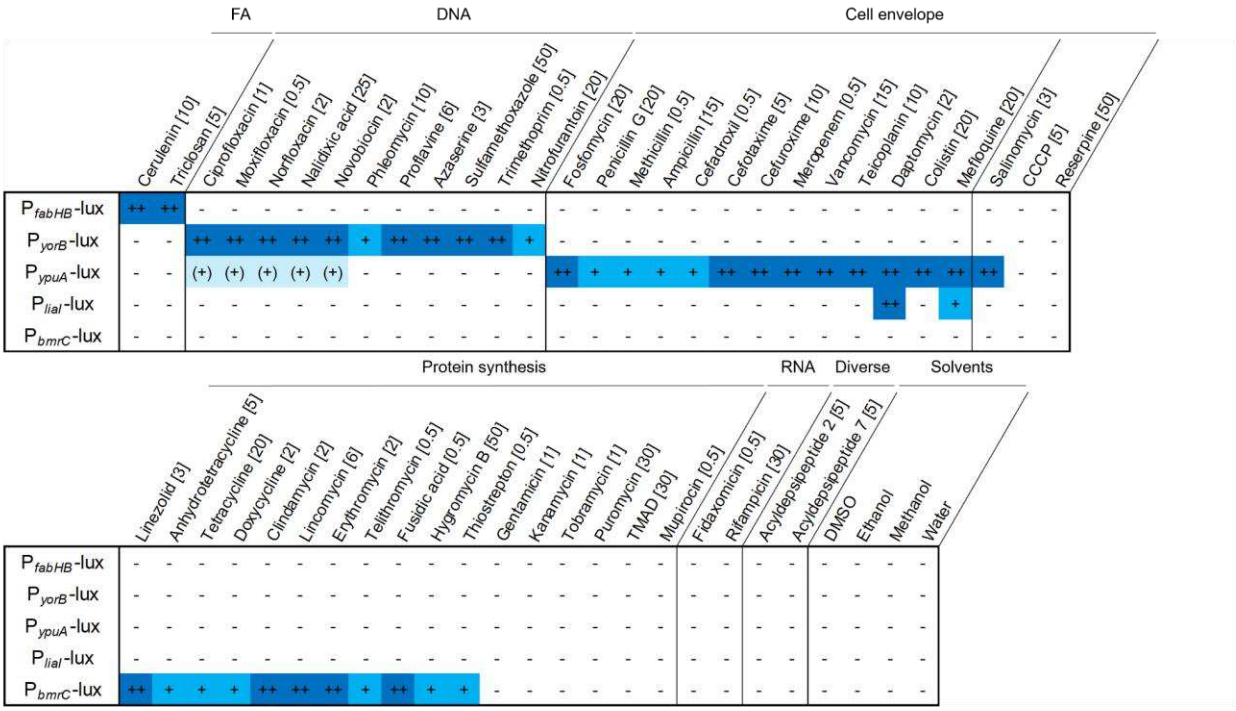

Figure S5A: Agar-based specificity validation. The bioreporter panel was tested in an agar-based setup against 50 reference antibiotics with well-characterized and diverse mechanisms of action, interfering with the depicted major biosynthetic pathways: fatty acid synthesis (FA), DNA and folate synthesis (DNA), cell envelope integrity, protein synthesis, and RNA synthesis (RNA). Likewise, solvent controls (2 µL) were included and showed no effect. Bioreporter induction was quantified by luminescence imaging at 180 min following antibiotic addition and categorized using a four-tier scale: dark blue (++, strong induction), blue (+, good induction), light blue ((+), weak induction) and white (-, no induction). Pure antibacterial agents were directly spotted onto the solidified bioreporter lawn at specified concentrations (µg; amounts denoted in brackets).

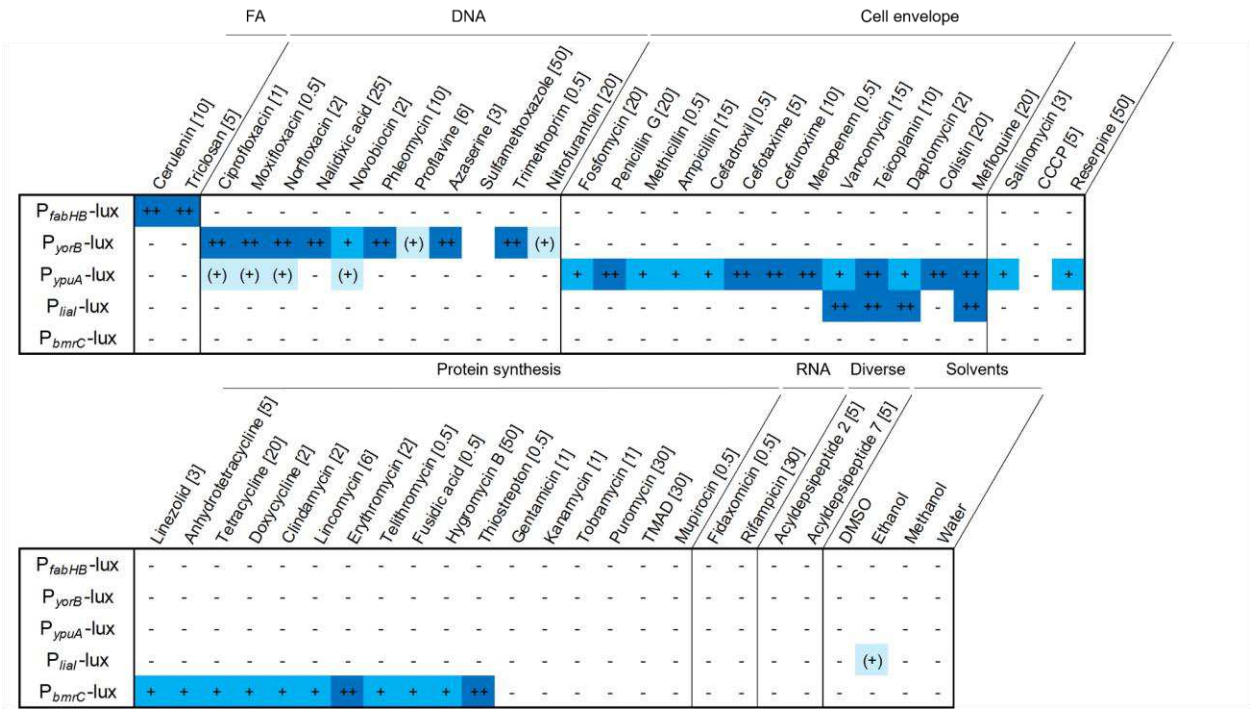

Figure S5B: Liquid-based specificity validation. The bioreporter panel was tested in an liquid-based setup against 50 reference antibiotics with well-characterized and diverse mechanisms of action, interfering with the depicted major biosynthetic pathways: fatty acid synthesis (FA), DNA and folate synthesis (DNA), cell envelope integrity, protein synthesis, and RNA synthesis (RNA). Likewise, solvent controls (4%) were included and showed no effect. Bioreporter induction was quantified as normalized fold increase relative to untreated controls over a period of 60 min for P_{lial}-lux, 90 min for P_{fabHB}-lux, 120 min for P_{ypuA}-lux and 180 min for P_{bmrC}-lux and P_{yorB}-lux, based on two biological replicates. Induction levels were categorized using a four-tier scale: dark blue (++, strong induction), blue (+, good induction), light blue ((+), weak induction) and white (-, no induction). Pure antibacterial agents were tested in a two-fold dilution series starting from the indicated concentrations (µg; amounts in brackets).

In general, results from the liquid setup matched the results from the agar-based setup, with the following few exceptions: Lack of P_{yorB}-lux induction by the nucleotide synthesis inhibitor sulfamethoxazole[1] in liquid culture, which may be attributed to the reduced antimicrobial efficacy of sulfamethoxazole observed in this setup. Lack of P_{ypuA}-lux induction by nalidixic acid in liquid culture.[2] The P_{ypuA}-lux bioreporter was induced by the efflux pump inhibitor reserpine[3] in the liquid assay, but not in the agar-based setup. The P_{lial}-lux bioreporter was induced by the glycopeptides vancomycin and teicoplanin[4] in the liquid assay, but not in the agar-based setup. Exposure to high concentrations of ethanol (≥8% V/V) resulted in a weak induction of P_{lial}-lux in the liquid setup, consistent with previous reports describing ethanol as a weak P_{lial} inducer.[5]

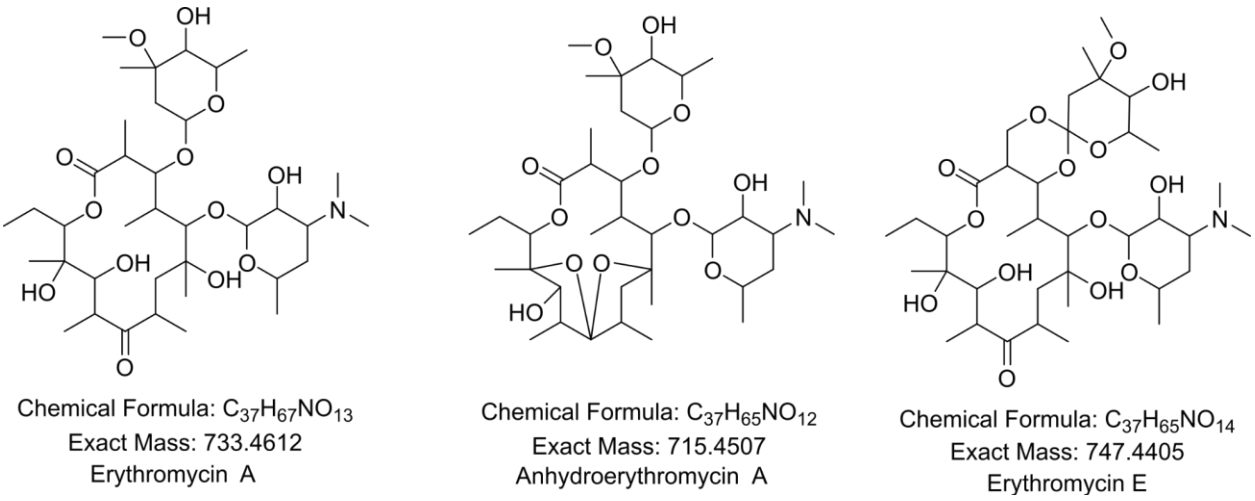

Figure S6: Compounds determined in the crude extract of *S. erythraea* that clustered together in the molecular network as shown in Fig. 4. While erythromycin A gives the main activity peak, anhydroerythromycin A and erythromycin E are present as minor compounds.[6]

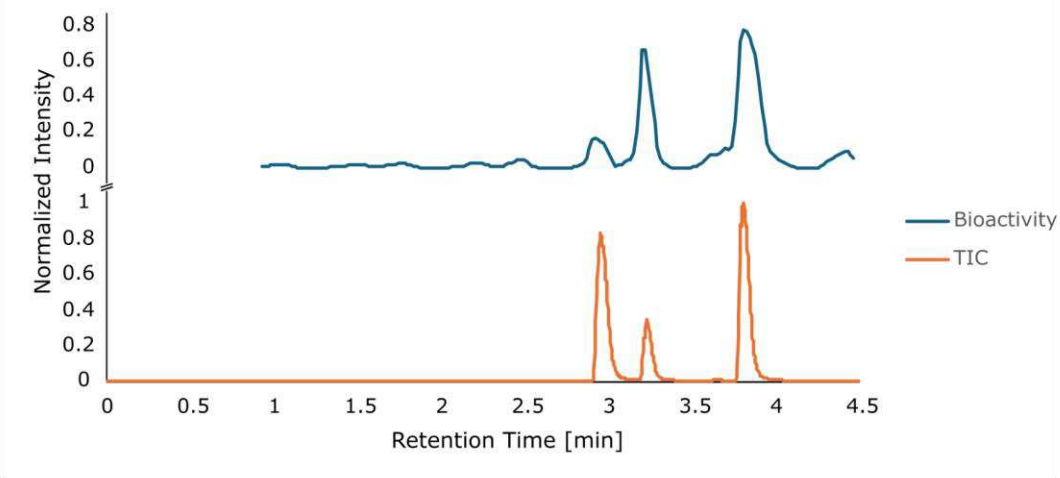

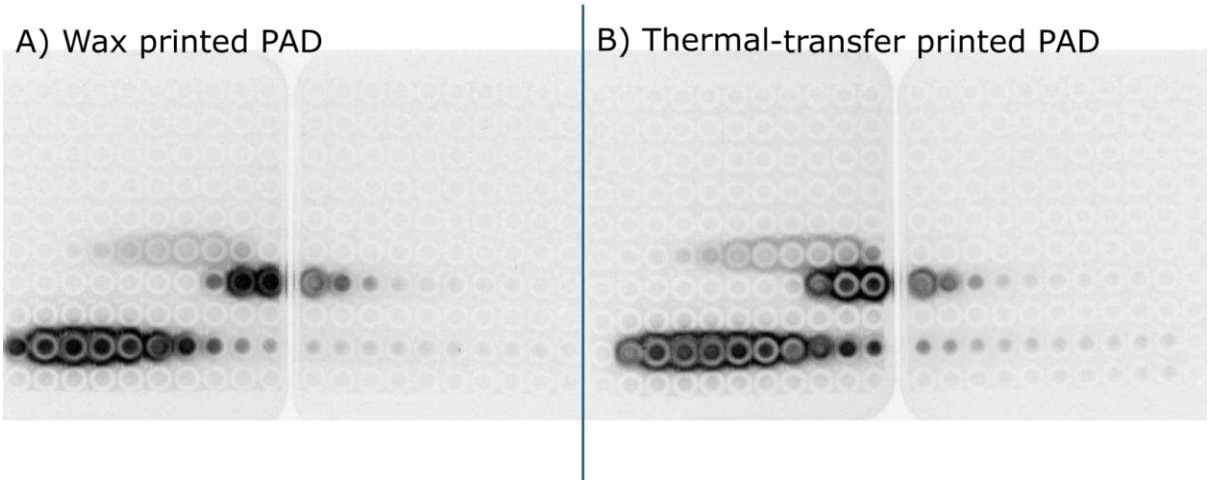

Figure S7: Comparison of PADs printed with wax printer (A) and thermal transfer printer (B). Elution order: Trimethoprim, Ciprofloxacin, Moxifloxacin. See also Fig. 3 and chapter 3.3 in the main document.

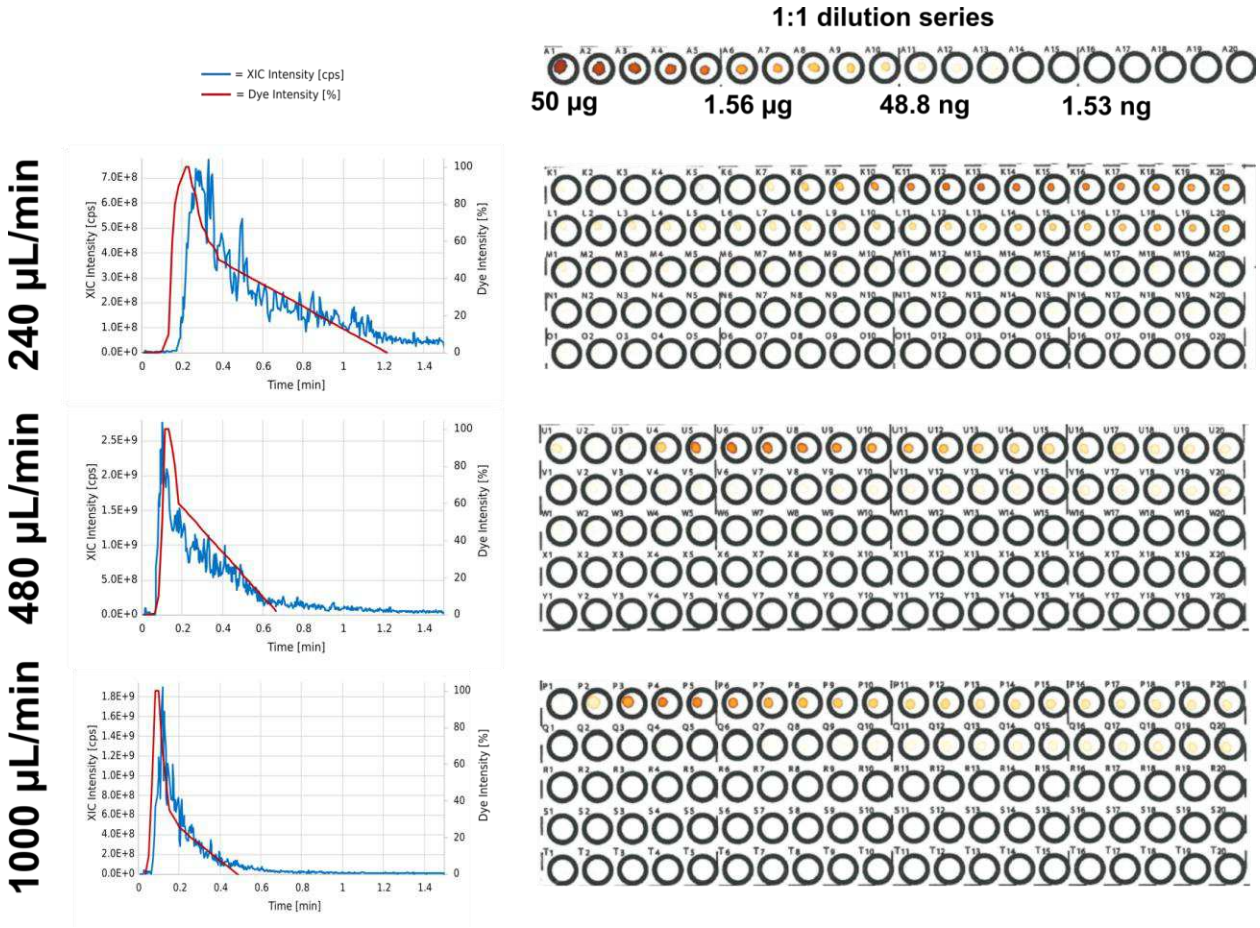

Figure S8: Determination of diffusion effects between MS and Microspotter. To test for possible peak broadening effects and spot-to-spot carryover due to diffusion effects, a sample of a dye (methyl red, 10 mg/mL) was injected in-flow without column at three different flow rates (240, 480, and 1000 µL/min). Upper part: Overview on the spot intensity by manual spotting of a dilution series. Left side: extracted ion chromatograms (XICs) of the sodium adduct of methyl red ($C_{15}H_{15}N_3O_2Na$, ***m/z*** = 292.1062 ± 10 ppm, blue curves). Curves were smoothed manually applying a 5-point Savitzky-Golay-smoothing. Red curves show the manual readout of the spot intensities Right side: Respective spotted µPADs.

SUPPLEMENTARY METHODS

Cloning of the Lux bioreporters

Bioreporters were constructed by transforming a sporulation-deficient *Bacillus subtilis* 1S34 with a modified version of the integrative reporter vector pBS3Clux.[7,8] This vector harbors an ampicillin resistance gene for selection in *Escherichia coli* on the non-integrative plasmid region, and a chloramphenicol resistance gene situated between the integration sites to facilitate selection in *B. subtilis*. Promoter regions specific to each bioreporter (P_{fabHB}, P_{yorB}, P_{ypuA}, P_{lial}, P_{bmrC}) were amplified from *B. subtilis* 1S34 genomic DNA and cloned into the pBS3Clux shuttle vector via common restriction-ligation protocols combined with Gibson assembly. Each promoter region was integrated 19 bp upstream of the *Photorhabdus luminescens luxABCDE*-operon, exercising the original mRFP1 red fluorescent protein. Vectors were propagated in *E. coli* XL-10, cultured in lysogeny broth (LB; 1% NaCl, 1% tryptone, 0.5% yeast extract, pH 7.25) containing 100 µg/mL ampicillin, and purified using a GeneJET Plasmid Miniprep Kit (Thermo Scientific). Successful integration of the promoter regions was verified by Sanger sequencing (LGC Genomics GmbH). Naturally competent *B. subtilis* 1S34 cells were prepared by nutrient starvation[9] and transformed with the assembled vectors, which integrated into the chromosomal *sacA* locus. Transformants were selected on 5 µg/mL chloramphenicol, and integration was confirmed via colony PCR. Primers utilized in this study are listed in Table S2. Bioreporter strains were cultivated in LB supplemented with 5 µg/mL chloramphenicol at 37°C and shaking (190 rpm).

Liquid-based bioreporter assay

For each bioreporter a pre-culture was initiated from a glycerol stock and incubated for 18 h, followed by inoculation of a main culture to an initial OD_{600} of 0.05, which was subsequently grown to an OD_{600} of approximately 1.0. Reference antibiotics were prepared in a two-fold serial dilution using a white, clear-flat bottom 96-well plate (Brand) in LB medium for the bioreporter P_{fabHB}-lux, P_{yorB}-lux, P_{ypuA}-lux, P_{lial}-lux, while BMM[7] was utilized for P_{bmrC}-lux. For solvent controls, 4% of solvent were added to the first well and serially diluted in the same manner. The bioreporters were transferred onto the pre-warmed well plate to a final cell count of $0.95x10^7$ CFU/mL, diluted in the respective media (without chloramphenicol). The final assay volume was 120 µL. Luminescence and absorbance measurements at 600 nm were performed at five-minute intervals over an incubation period of 3 h at 37°C using a SPARK multimode microplate reader (Tecan), with the incubation parameters listed in Table S3.

Bacterial growth and bioreporter luminescence were continuously monitored in a microplate reader over a period of 60 min for P_{lial}-lux, 90 min for P_{fabHB}-lux, 120 min for P_{ypuA}-lux, and 180 min for P_{bmrC}-lux and P_{yorB}-lux following antibiotic addition. These incubation times were selected to ensure specific bioreporter activation, as extended incubation occasionally resulted in nonspecific signals, like in the agar-based assay. Antibiotics were tested in a two-fold dilution series starting at 1x the minimal inhibitory concentration (MIC) or higher. Induction was quantified relative to untreated controls and normalized to both baseline luminescence and the optical density at 600

nm (OD_{600}; as a measure of bacterial growth) of each well. Results from independent biological replicates were reported as mean fold induction values. For assay validation, significant induction thresholds were defined as a ≥500%-fold increase for P_{fabHB}-lux, P_{yorB}-lux, P_{lial}-lux and P_{bmrC}-lux, and a ≥200%-fold increase for the less responsive promotor P_{ypuA}-lux. Each bioreporter displayed a distinct and selective activation profile that was largely consistent with the results obtained in the agar-based assay. For instances where the two assay formats diverged, see Fig. S5B. Inherent differences in baseline expression and natural differences in promotor regulation preclude direct quantitative comparison between the different bioreporters. Also, an individual bioreporter reacted to different compound classes to a different extent, as a consequence of the diverging mechanisms of action. In summary, each bioreporter strain demonstrated high specificity for its respective mechanisms of action area in both the agar-based and liquid-based bioreporter assay.

Comparison of wax-based and thermal transfer PAD

The wax-based PADs have a long standing history in analytical chemistry.[10] They are extremely cheap and easy to produce, and commercially available printer paper can be used. When a wax printer is at hand, the printing of a PAD only takes seconds, and the design can be freely chosen, which makes it attractive for several applications. As the wax lies on top of the paper, it just has to be heated to ~110°C for about 1 minute, so that the wax melts into the paper and hydrophobizes the paper in the form of the printed wax. Unfortunately, wax printers are, to our knowledge, not produced anymore. As the lack of PADs would be a drawback for this project, we searched for alternative possibilities for the production of PADs. In the publication of Ruiz et al.,[11] we found a comparison of different possibilities to print PADs. We decided to systematically investigate the printing of PADs using a thermal-transfer printer. All chosen timepoints and temperatures for the conditioning of the PADs (90, 105, 120°C and 5, 10, 30 min) were analyzed by spotting 20 µL pure acetonitrile manually into the spots and see if the spots are able to hold the acetonitrile so that it dries inside the ring before running out. The optimum in those conditions was conditioning for 30 minutes at 120°C. A drawback of the printer used in our case was that the printing itself was not always accurate. The first pages often had to be discarded as some circles were not fully printed, and the printer had no proper paper feed; a paper fed askew led to a scheme of circles to-be-spotted in that was not centered and oblique. This could partly be avoided by carefully feeding the paper one by one. Nevertheless, as after conditioning the backing had to be printed to the paper to avoid a migration of the compounds in the agar below, an oblique printing can lead to problems. This printing device might therefore not be as ideal as a wax printer; given the fact that wax printers are outdated and that the thermal transfer printer is cheap and small, we believe that it poses a sufficient replacement. To verify the usability of the PADs obtained from this printer, an antibiotic mixture (ciprofloxacin, trimethoprim, moxifloxacin) was spotted in the same concentration with the same method on both PADs. Both were incubated with P_{yorB}-lux bioreporter to display DNA stress. As seen in Fig. S7, both results are comparable. All antibiotics can be seen in both PADs with comparable intensity. When focusing on the tail of the signals, thermal-transfer PAD might even be superior as it might lower the limit of detection; for all three compounds, more

spots are visible on the thermal-transfer PAD. This indicates that it is a suitable alternative to the wax printed PADs.

Microspotter head fabrication

The 3D printed spotter head consists of four parts (see Figure S2, S3 and CAD files in data sharing section in the main document). Fig. S3B shows the capillary holder, designed as a ring that tapers into a truncated cone to secure the capillary outlet at the bottom. The top end features a crimped capillary fitting connected to a union that can be attached to the outlet capillary of the HPLC. Fig. S3C depicts the outer ring, which includes three holes fitted with screw nuts. These allow screws to be inserted for securing the inner capillary holder. The capillary holder is freely movable along the x- and y-axis by the screws.
Furthermore, a third part was 3D-printed (Fig. S3D), holding a small fan at an angle that allows the fan to blow air over the µPAD to dry it faster while the spotter head is moving. The 5V power supply for the fan is realized by a USB cable.
The fourth part is a small ring that locks the spotter head into the milling machine arm, preventing it from rotating during operation. All of the parts for the spotter head were tailor-made in-house using a 3D-printer with PLA as filament and CAD files are publicly available under the Zenodo repository as well as via Thingiverse (see data sharing section in main document).

Spot-to-spot carryover

Carryover of eluate from one spot to the next on the µPAD can be a drawback for the determination of bioactivity based on retention time. Therefore, spot-to-spot carryover should be critically assigned and avoided if possible. As the capillary tip on the Microspotter in our setup does not come into contact with the µPAD, a contamination or carryover due to contact is unlikely. The hanging drop is transferred by capillary forces onto the µPAD and should lead to a complete detachment once the spotter head is moving back up before continuing to the next spot. However, to experimentally evaluate this, we performed flow injections at different flow rates to compare detector responses of the MS and compound deposition on the µPAD. To do so, we used methyl red (10 mg/mL) as a test compound, as it allows for easy optical evaluation of compound deposition. Three different flow rates were evaluated (240, 480, 1000 µL/min), spotting frequency was 1 Hz. As both detectors reacted to the flow rate resp. peak width changes comparably (see Fig. S8), we argue that the prolonged signal for broader peaks at low flow rates on the µPAD arises not from a significant spot-to-spot carryover but rather from diffusion effects within the capillary. This is also supported by the flow rate dependence of the MS signal. At higher flow rates, the peak is significantly sharper in both the MS trace and the µPAD. In accordance to Fick's first law of diffusion, broadening of the injection band can be described by $\sigma^2 = 2Dt$ (with σ^2 being the injection band variance, D being the diffusion coefficient and t the residence time in the capillary), as the injection band moves in open tubular capillaries. This equation shows a time dependence, which can directly be translated into a flow rate dependence. No column was used

in this experiment, hence refocusing of the injection band on the column head did not take place. Post-column diffusion effects are typically smaller than the diffusion seen in this experiment. For flow rates used in our experiments (1 mL/min), post-column diffusion is low, since the residence time in the capillary is short. While spot-to-spot carryover cannot fully be ruled out, the result of this experiment shows that the carryover can be expected to be low or insignificant when working at a flow rate of 1 mL/min.

Supplementary References

1. Hitchings, G. H. Mechanism of Action of Trimethoprim-Sulfamethoxazole--I. *J. Infect. Dis.* **128**, S433–S436 (1973).
2. Anderson, V. E., Zaniewski, R. P., Kaczmarek, F. S., Gootz, T. D. & Osheroff, N. Quinolones Inhibit DNA Religation Mediated by Staphylococcus aureus Topoisomerase IV. *J. Biol. Chem.* **274**, 35927–35932 (1999).
3. Li, G. *et al.* Antimycobacterial activity of five efflux pump inhibitors against Mycobacterium tuberculosis clinical isolates. *J. Antibiot. (Tokyo)* **69**, 173–175 (2016).
4. Reynolds, P. E. Structure, biochemistry and mechanism of action of glycopeptide antibiotics. *Eur. J. Clin. Microbiol. Infect. Dis.* **8**, 943–950 (1989).
5. Mascher, T., Zimmer, S. L., Smith, T.-A. & Helmann, J. D. Antibiotic-Inducible Promoter Regulated by the Cell Envelope Stress-Sensing Two-Component System LiaRS of *Bacillus subtilis*. *Antimicrob. Agents Chemother.* **48**, 2888–2896 (2004).
6. Deubel, A., Fandiño, A. S., Sörgel, F. & Holzgrabe, U. Determination of erythromycin and related substances in commercial samples using liquid chromatography/ion trap mass spectrometry. *J. Chromatogr. A* **1136**, 39–47 (2006).
7. Stülke, J. & Hanschke, R. Temporal activation of β-glucanase synthesis in Bacillus subtilis is mediated by the GTP pool. *J. Gen. Microbiol.* **139**, 2041–2045 (1993).
8. Radeck, J. *et al.* The Bacillus BioBrick Box: generation and evaluation of essential genetic building blocks for standardized work with Bacillus subtilis. *J. Biol. Eng.* **7**, 29 (2013).
9. Newcastle iGEM Project Wiki (2009). Transforming into Bacillus subtilis 168. https://2009.igem.org/Team:Newcastle/Project/Labwork/OurProtocols/TransformBac, accessed 2025-07-08.
10. Martinez, A. W., Phillips, S. T., Butte, M. J. & Whitesides, G. M. Patterned Paper as a Platform for Inexpensive, Low-Volume, Portable Bioassays. *Angew. Chem. Int. Ed.* **46**, 1318–1320 (2007).
11. Ruiz, R. A., Gonzalez, J. L., Vazquez-Alvarado, M., Martinez, N. W. & Martinez, A. W. Beyond Wax Printing: Fabrication of Paper-Based Microfluidic Devices Using a Thermal Transfer Printer. *Anal. Chem.* **94**, 8833–8837 (2022).

PUBLICATION II – PROTEOTOXIC STRESS BIOREPORTER ENABLES MECHANISM-INFORMED ANTIBIOTIC DISCOVERY

Published in *Journal of Natural Products*, 2026, 89(6), 1698–1714. Published by the American Chemical Society and American Society of Pharmacognosy. This article is licensed under CC BY 4.0. Copyright © 2026 The Authors. DOI: 10.1021/acs.jnatprod.6c00112

Manuscript Context

This study focuses on the development and validation of the novel proteotoxic stress bioreporter P_{clpE}-lux to expand the mechanistic coverage of the established bioreporter panel. This bioreporter addresses a mechanistic gap by selectively detecting bacterial stress caused by the accumulation of damaged or misfolded proteins. The study further highlights the advantages of bioreporter-guided screening and mechanism-informed dereplication workflows. The bioreporter was used to screen a diverse natural product library and a collection of natural producer strains for antibacterial compounds that induce proteotoxic stress. In the former, several natural products were identified to induce proteotoxic stress, some of which had not previously been associated with this mechanism, warranting further investigation. In the latter, the bioreporter rapidly identified promising producer strains directly from agar plates, without requiring extensive sample preparation. Finally, the bioreporter was integrated into the antibiotic discovery and dereplication platform established in Publication I to guide the dereplication of the natural producer strains. Notably, this study represents the first large-scale application of the platform in a screening campaign, providing important insights into its dereplication capabilities. The approach revealed an extensive network of structurally diverse streptothricin derivatives, including analogues with putatively novel acetylation modifications. The author constructed and validated the P_{clpE}-lux bioreporter, performed all experimental work associated with the bioreporter and producer strain cultivation, and conducted the dereplication, data analysis, and visualization. The results demonstrate that P_{clpE}-lux is a sensitive tool for discovering proteotoxic stress-inducing antibacterial compounds across diverse sample types. In addition, making the streptothricin dataset generated in this work publicly available provides a valuable resource for future dereplication studies, given that streptothricins are commonly encountered in screening campaigns.

JOURNAL OF NATURAL PRODUCTS

pubs.acs.org/jnp

Article

Open Access

This article is licensed under CC-BY 4.0

Proteotoxic Stress Bioreporter Enables Mechanism-Informed Antibiotic Discovery

Julian Schubert, Christian Geibel, Anne Berscheid, Katharina W. Wex, Giovanni Andrea Vitale, Chambers C. Hughes, Daniel Petras,* and Heike Brötz-Oesterhelt*

Cite This: *J. Nat. Prod.* 2026, 89, 1698–1710

Read Online

ACCESS | Metrics & More | Article Recommendations | Supporting Information

ABSTRACT: Antibiotic resistance poses a major global health challenge, which is intensified by the decline in antibiotic discovery efforts. This highlights the urgent need for innovative antibacterial agents. Natural products remain a key source of antibiotics, yet early mechanistic insights are often lacking. Classical whole-cell screening identifies growth inhibition but provides no mechanistic information. Bioreporter strains combine bioactivity detection with preliminary mechanistic profiling; however, they remain unavailable for several promising antibiotic target areas. We developed a sensitive bioreporter that signals the induction of the heat-shock Clp-ATPase gene *clpE* in *Bacillus subtilis*. ClpE serves as a specific biomarker for proteotoxic stress, resulting from the accumulation of damaged or misfolded proteins. The self-sustained luminescence of the P_{clpE}-lux bioreporter enables monitoring of proteotoxic stress in both solid and liquid assay formats and supports high-throughput screening. Consolidated through extensive validation with reference antibiotics, the bioreporter also identified antibacterial agents that were not previously associated with proteotoxic stress. Coupling the bioreporter with a microfractionation-based metabolomics workflow accelerated the identification of hydrophilic antibacterial metabolites from complex natural product extracts, thereby uncovering an extensive group of streptothricin derivatives, including putatively novel analogues. This study demonstrates that the P_{clpE}-lux bioreporter is a versatile tool for mechanism-informed antibiotic discovery, enhancing the detection sensitivity and dereplication efficiency.

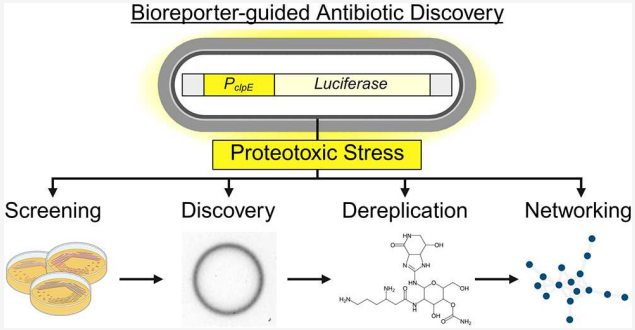

The global threat of antibiotic-resistant pathogens necessitates the development of new antibacterial agents, yet the discovery of novel antibiotic classes remains rare, and approval rates continue to decline.[1,2] Sustained clinical efficacy requires a robust discovery and development pipeline capable of delivering antibiotic candidates that meet essential criteria, including novelty in chemical classes and mechanisms of action (MoAs) and the absence of cross-resistance.[3,4] In past decades, high-throughput screening campaigns with synthetic libraries and purified protein targets conducted by the pharmaceutical industry have yielded very few new antibacterial leads. Severe limitations included a lack of whole-cell activity due to limited cell penetration, nonspecific activity, and pharmacokinetic liabilities.[5,6] To revitalize antibiotic discovery, contemporary drug discovery programs employ a broad range of complementary strategies. Assessment of microbial diversity in underexplored environments expands natural product discovery,[7] while bioinformatic genome mining provides access to novel, silent, or cryptic biosynthetic pathways.[8] The integration of multiomics, machine learning, and artificial intelligence further accelerates compound discovery, drug design, and target prediction.[9,10] In parallel, ongoing advances in mass spectrometry-based dereplication strategies have improved efficiency in identifying antibacterial agents. Metabolic engineering increases secondary metabolite yields, supports heterologous expression of biosynthetic gene clusters, and enables cultivation of challenging producer strains.[11] Semisynthetic optimization of natural products improves their potency, pharmacokinetics, or resistance profiles, while synthetic chemistry enables the rational design and total synthesis of new molecular scaffolds.[12] Combination therapies exploit synergistic interactions,[13] and drug repurposing uncovers additional antibacterial applications for drugs approved for other indications.[14,15]

Classical growth inhibition assays remain the primary approach in antibacterial natural product screening workflows due to their simplicity and proven effectiveness but are limited by labor-intensive sample preparation, modest throughput, low specificity, and frequent rediscovery of known compounds.[16,17] Whole-cell assays evaluate compound efficacy in the

Received: January 26, 2026
Revised: May 8, 2026
Accepted: May 11, 2026
Published: May 15, 2026

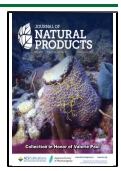

ACS Publications

© 2026 The Authors. Published by American Chemical Society and American Society of Pharmacognosy

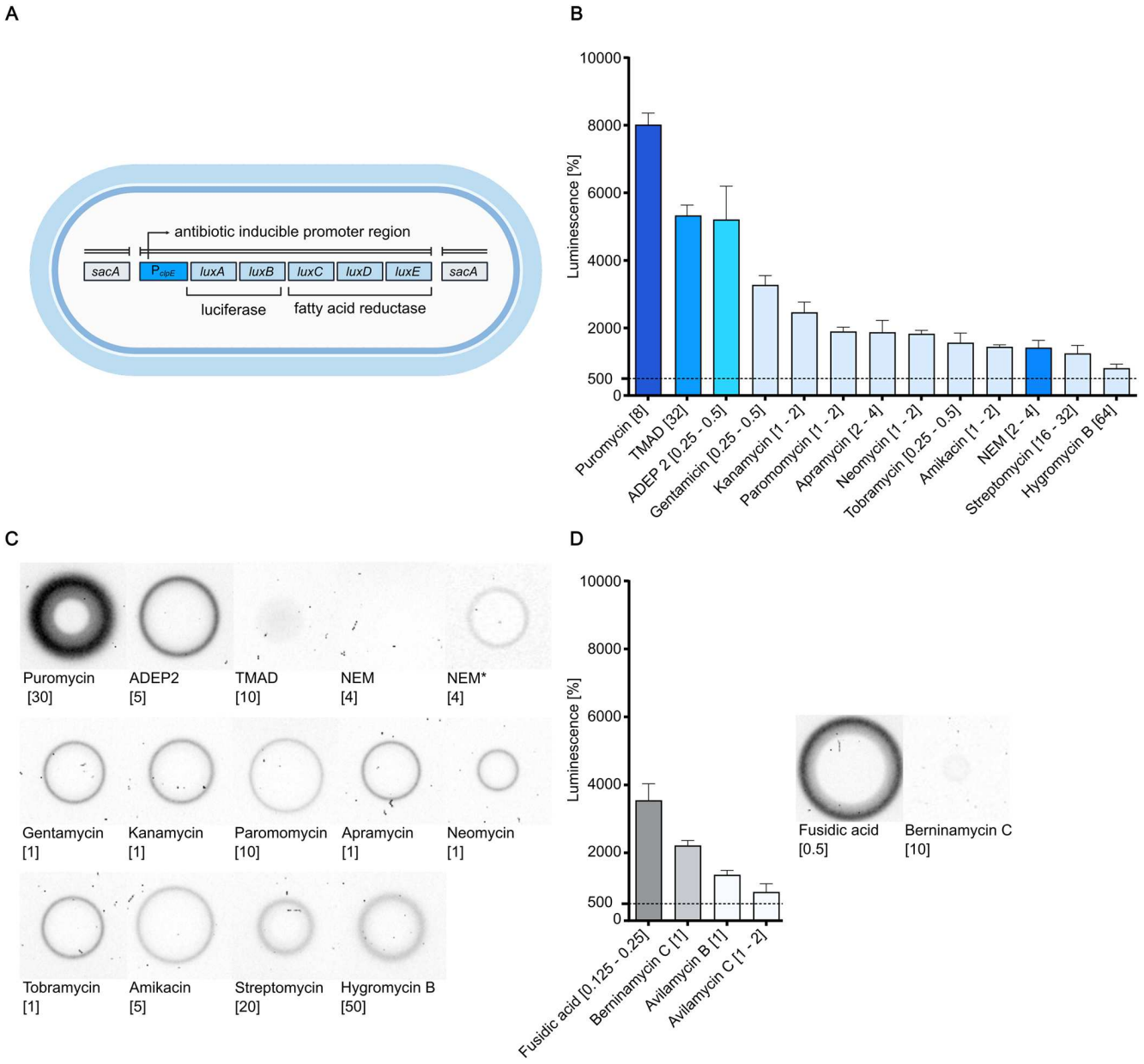

Figure 1. P_{clpE}-lux bioreporter construction and validation. (A) Schematic of the P_{clpE}-lux bioreporter integrated into the *B. subtilis* 1S34 *sacA* locus. P_{clpE} promoter insertion upstream of the *Photorhabdus luminescens luxABCDE* operon.[45] (B) P_{clpE}-lux induction by reference compounds in the liquid assay format, color-coded according to MoA: puromycin (dark blue), TMAD and NEM (blue), ADEP 2 (turquoise), and aminoglycosides (light blue). Compounds were tested in 2-fold serial dilutions, from below to above their minimal inhibitory concentration (MIC). Luminescence and OD_{600} (cell mass) were monitored for 180 min, and induction was normalized to the baseline luminescence of the untreated control (100%) and OD_{600}. The induction threshold was defined as ≥500% luminescence within 90 min of antibiotic exposure (black dotted line). Extended incubation times occasionally resulted in nonspecific activation. Bars represent maximal normalized luminescence (mean ± standard deviation (SD)), and values in brackets indicate the compound concentration range at which those inductions occurred in independent biological replicates. (C) P_{clpE}-lux induction by reference compounds in the agar-based assay format, with amounts [μg] spotted onto the bioreporter lawn. Luminescence imaging after 180 min showed bioreporter induction as luminescent halos at the margins of growth inhibition zones, with size and intensity depending on the amount of compound applied and its diffusion characteristics through the agar matrix. Transient NEM induction at 90 min (asterisk). (D) P_{clpE}-lux induction by reference compounds not previously associated with proteotoxic stress: fusidic acid (dark gray), berninamycin C (gray), and avilamycin B and C (light gray) in liquid; fusidic acid and berninamycin C on agar. Bars and values in brackets are as in panel (B).

physiological context of the bacterial cell, thereby accounting for key barriers such as cell envelope penetration and intracellular retention.[18,19] A promising development in whole-cell screening involves the use of bioreporters, engineered bacterial strains that generate measurable reporter signals in response to antibiotic-induced stress. Antibiotic interference with biosynthetic processes triggers the upregulation of specific genes as a compensatory mechanism. Such genes can be repurposed to probe the stress-bearing pathway by fusing their promoters to reporter genes such as β-galactosidases or luciferases. Consequently, bioreporters provide a direct readout of antibacterial activity while

https://doi.org/10.1021/acs.jnatprod.6c00112
J. Nat. Prod. 2026, 89, 1698−1710

simultaneously indicating the type of cellular stress and the affected target pathway. Additionally, bioreporters detect physiological damage at compound concentrations well below growth-inhibitory levels,[20] enabling the identification of promising candidates that are overlooked by traditional inhibition assays.[21]

The Gram-positive model organism *Bacillus subtilis* was chosen for the development of antibiotic stress bioreporters due to its rapid growth, natural competence, broad antibiotic susceptibility, and well-characterized physiological stress responses to antibiotic exposure.[22−24] Genome-wide analyses of antibiotic-induced mRNA expression profiles revealed modular gene expression patterns linked to distinct antibiotic mechanisms and identified promoters responsive to specific kinds of antibiotic-induced stress.[23,25] Based on these insights, Urban et al. engineered a panel of firefly luciferase-based whole-cell bioreporters that detect cell envelope damage and inhibition of RNA, DNA, fatty acid, and protein syntheses.[22] However, the protein synthesis bioreporter *bmrC* (formerly *yheI*) detects only ribosomal stalling (translation arrest) and does not sense proteotoxic stress caused by mistranslation, protein misfolding, or other forms of protein damage.[20−22] Consequently, many natural products that induce proteotoxic stress, including clinically relevant aminoglycosides, remain undetected by the existing bioreporter panel. To address this gap in bioreporter coverage, we revisited the transcriptome data. We selected the heat-shock Clp-ATPase gene *clpE* as a candidate biomarker for proteotoxic stress in *B. subtilis* because it showed strong induction in response to aminoglycosides and *N*-ethylmaleimide.[23] Under nonstress conditions, *clpE* is tightly repressed by the global stress regulator CtsR. Upon heat shock or proteotoxic stress, ClpE is rapidly upregulated and, in conjunction with the proteolytic core ClpP, forms the ClpEP protease complex. This protease contributes to protein quality control and the restoration of cellular proteostasis by degrading heat-denatured or otherwise damaged proteins.[26−30] Given its functional role and its induction by agents that cause protein damage or misfolding, we evaluated *clpE* as a specific biomarker of proteotoxic stress.

Here, we report the construction and validation of a novel *B. subtilis* bioreporter based on the *clpE* gene, which is selectively induced by proteotoxic stress arising from the accumulation of damaged or misfolded proteins. By fusing the *clpE* promoter region (P_{clpE}) to a bacterial luciferase operon, we generated the P_{clpE}-lux bioreporter construct and established two complementary whole-cell assay formats in solid and liquid media. These assays enable convenient high-throughput screening of pure compounds, crude extracts, and natural producer strains without extensive sample preparation. Application of the P_{clpE}-lux bioreporter to a library of diverse natural products identified several antibacterial agents that had not previously been linked to proteotoxic stress. Integration of the P_{clpE}-lux bioreporter into a high-resolution microfractionation-based dereplication workflow[20] enabled simultaneous dereplication and mechanistic characterization of antibacterial metabolites, including those present in highly hydrophilic fractions. This approach uncovered a substantial network of diverse streptothricin derivatives among 53 bacterial isolates from the Tuebingen collection of actinomycete producer strains, including analogues with putatively novel acetylation patterns.

RESULTS AND DISCUSSION

Validation of the P_{clpE}-lux Bioreporter Induction Profile

The P_{clpE}-lux bioreporter was designed to expand the detection capabilities of our bioreporter panel by selectively identifying antibiotics that induce proteotoxic stress. For this purpose, the antibiotic-inducible P_{clpE} promoter was cloned upstream of a self-sustained bacterial luciferase operon (Figure 1A). Following chromosomal integration into a sporulation-deficient *B. subtilis* strain,[31] induction specificity was validated against a panel of 99 antibacterial reference compounds with diverse, well-characterized MoAs (Table S4). The bioreporter enabled the selective detection of proteotoxic stress in liquid and solid assay formats. In the liquid format, luminescence signals were continuously monitored across a serial dilution of each reference compound through several generations of exponential growth. The agar-based assay format enabled higher throughput by detecting luminescence signals at a single time point and utilizing concentration gradients generated by compound diffusion in the agar. In both formats, the bioreporter showed robust induction in response to all tested compounds known to trigger proteotoxic stress (Figures 1B,1C and S1). P_{clpE}-lux inducers include antibiotics with ribosome-dependent MoAs, such as aminoglycosides, which trigger translational misreading by compromising codon−anticodon recognition,[32] and puromycin, which causes premature peptide chain termination through covalent incorporation into nascent polypeptides.[33] Additionally, compounds with protein-damaging mechanisms independent of ribosomal interaction induce the bioreporter, including acyldepsipeptide antibiotics (ADEPs), *N*-ethylmaleimide (NEM), and tetramethylazodicarboxamide (TMAD). ADEPs deregulate the Clp protease, compromising protein homeostasis and regulatory proteolysis as well as promoting nonspecific degradation of unstructured and nascent polypeptides.[34,35] Thiol-reactive electrophilic compounds, such as NEM and TMAD, covalently modify or oxidize cysteine residues and induce disulfide cross-linking.[36−39] Compared with other reference compounds, NEM produced an unusually early bioreporter signal in the liquid assay. Also on agar, the luminescence signal was already detectable after 90 min but not at 180 min, indicating a rapid but short-lived proteotoxic stress response (Figure 1C).

None of the reference compounds targeting DNA replication, RNA transcription, cell wall synthesis, or fatty acid biosynthesis induced the P_{clpE}-lux bioreporter, nor did most agents that were classified as translation stallers. Such negative responses were characterized by luminescence signals well below the defined induction threshold in the liquid assay and no detectable luminescence signals on agar plates (Table S4, Figures S2−S5). Interestingly, induction of the P_{clpE}-lux bioreporter was also observed for four compounds, among them two from the same class, whose primary MoAs were reported to be translation inhibition via ribosomal stalling rather than induction of proteotoxic stress. Fusidic acid, berninamycin C, and avilamycin B and C induced the bioreporter in the liquid assay, and fusidic acid and berninamycin C produced inductions on agar (Figures 1D, S2, and S5A,B). Fusidic acid targets elongation factor G (EF-G) bound to the ribosome, stabilizing EF-G in a conformation that prevents its dissociation after the guanosine triphosphate (GTP) hydrolysis. This inhibition stalls translocation and blocks subsequent ribosomal subunit recycling by locking EF-G in a posttranslocation state,[40,41] leading to induction of the

https://doi.org/10.1021/acs.jnatprod.6c00112
J. Nat. Prod. 2026, 89, 1698−1710

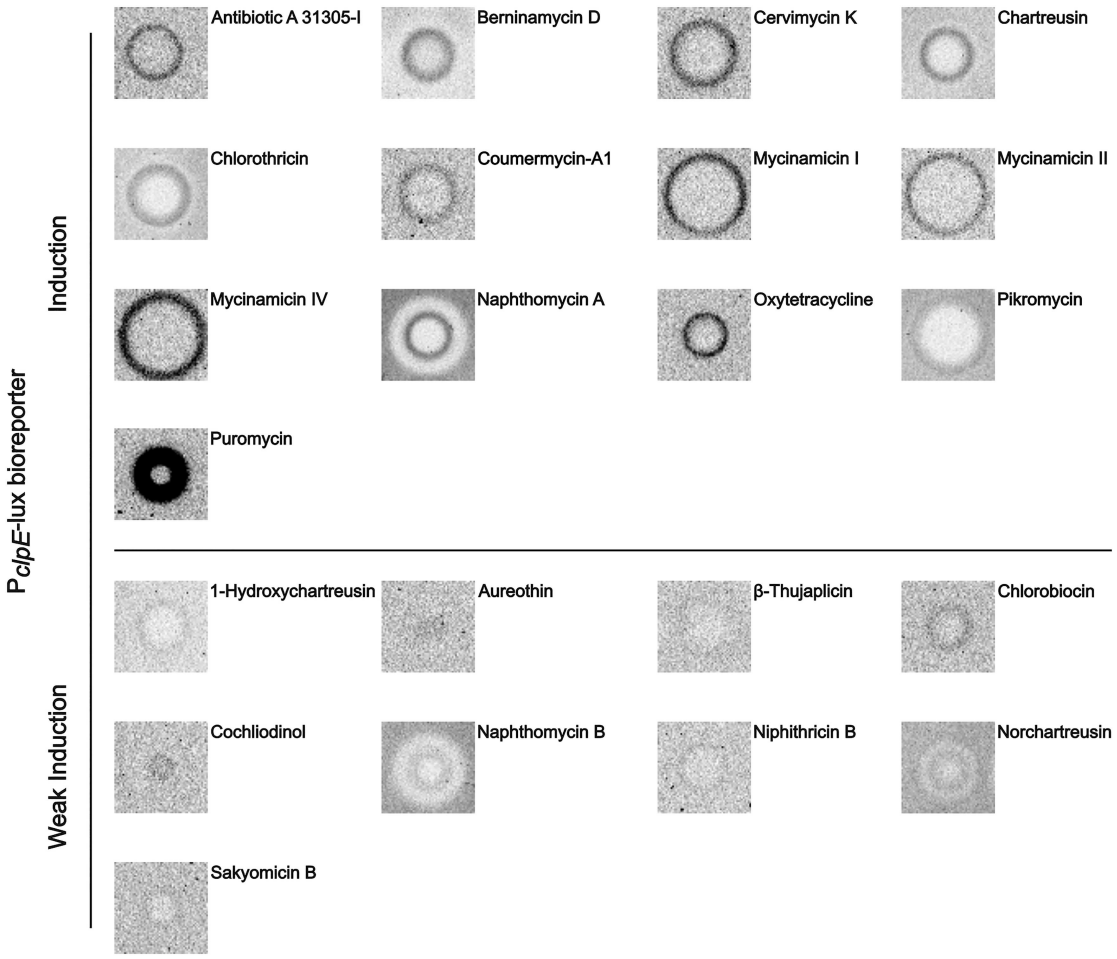

Figure 2. Proteotoxic stress induction by diverse natural products. Among the Tuebingen subset of the DZIF library (complete list of the 340 tested compounds provided in Supporting Information File 1), 22 natural products showed reproducible P_{clpE}-lux induction, among them 13 strong and 9 weak inducers. Compounds were directly spotted onto the bioreporter lawn. Luminescence was imaged after 180 min and normalized to the untreated background. Representative uncropped screening plates are provided in Figure S6.

translation arrest biomarker *bmrC*.[21,22] The P_{clpE}-lux induction that we observed here aligns with increased *clpE* expression in previously reported transcriptomic data,[23] thereby confirming *clpE* upregulation in response to fusidic acid and suggesting proteotoxic stress as an additional component of its MoA. For fusidic acid, it is reported that inhibition of ribosome recycling leads to the accumulation of ribosomes arrested in the posttermination ribosomal complex,[40] which may explain the observed P_{clpE}-lux induction, as similar secondary effects are also characteristic of aminoglycoside-induced stress.[42] The cyclic thiopeptide berninamycin C also induced *bmrC*,[21] in agreement with its established MoA of ribosome stalling through inhibition of amino acid incorporation into nascent polypeptides,[43] but the induction of proteotoxic stress noted here has not been reported before. Berninamycin C contains dehydroalanine, a thiol-reactive moiety that could explain the occurrence of proteotoxic stress. However, other dehydroalanine-containing thiopeptides, such as thiostrepton and sulfomycin I, did not activate the P_{clpE}-lux bioreporter, distinguishing berninamycin C as a notable exception in this class (Table S4). The orthosomycin antibiotics avilamycin B and C are known to disrupt both translation initiation and elongation by inhibiting formyl-methionyl-tRNA recruitment to the initiation complex and aminoacyl-tRNA positioning, respectively.[44] P_{clpE}-lux induction by fusidic acid, berninamycin C, and the avilamycins was consistently well above the induction threshold, with the signal strength comparable to those of agents with established proteotoxic MoAs. This argues against nonspecific bioreporter activation and encourages the hypothesis that damaged proteins may accumulate as an additional aspect of their MoA. The role of the bioreporter as an easy-to-handle entry assay is to point to such putative effects, which must be validated in follow-up studies by using orthogonal assay technologies.

The previously characterized translation arrest biomarker *bmrC*[20−22] and the new *clpE* biomarker exhibit complementary activation patterns. To date, only fusidic acid, berninamycin C, and hygromycin B[21] have been documented to induce both bioreporters. Avilamycins may be another example, but they have not yet been tested on *bmrC*. Hygromycin B is an atypical aminoglycoside that primarily stalls the ribosome rather than promotes translational misreading,[42] consistent with its low induction of P_{clpE}-lux. These results underscore that the two bioreporters respond to distinct cellular stress pathways and can be used to distinguish proteotoxic stress from that of translation arrest. Taken together, our findings indicate that the P_{clpE}-lux bioreporter functions as a physiological readout of proteotoxic stress by reporting the intracellular accumulation

https://doi.org/10.1021/acs.jnatprod.6c00112
J. Nat. Prod. 2026, 89, 1698−1710

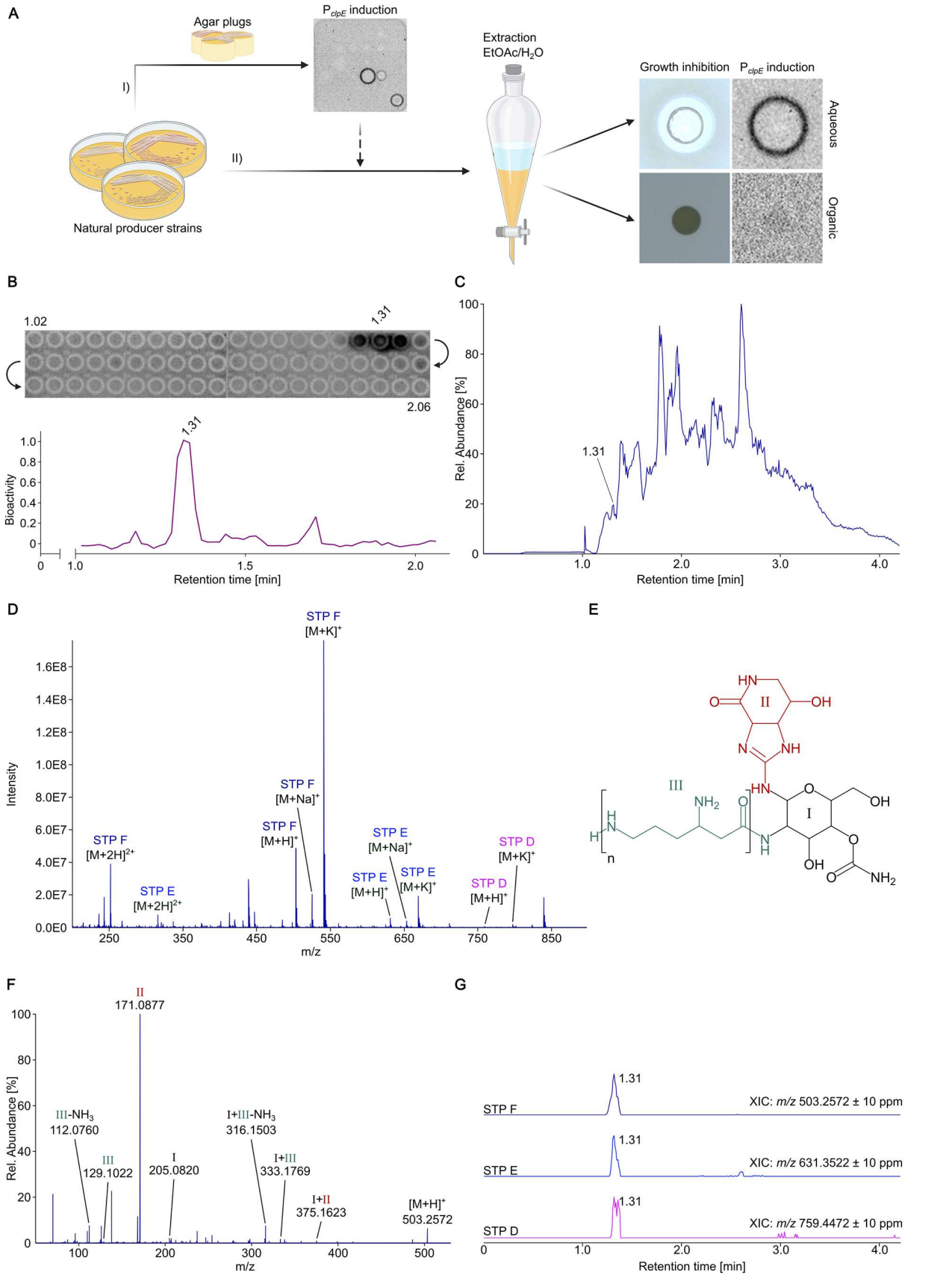

Figure 3. Bioreporter-guided compound dereplication and discovery pipeline. Workflow illustrating the identification of bioactive metabolites from the aqueous extract of producer strain Tue2. (A) Upper route (I), actinomycetes screening using the agar-based P_{clpE}-lux bioreporter assay. Agar plugs from producer strain plates were embedded in P_{clpE}-containing soft agar. Assessment of bioreporter induction (after 180 min) and zones of growth inhibition (after 18 h). Lower route (II), hit confirmation. Biomass was harvested from agar plates grown for 7 days and subjected to

https://doi.org/10.1021/acs.jnatprod.6c00112
J. Nat. Prod. 2026, 89, 1698−1710

Figure 3. continued

liquid−liquid partitioning with 1:1 (v/v) ethyl acetate (EtOAc) and water. Aqueous and organic extracts were evaluated for P_{clpE}-lux induction, using filter discs for organic fractions and soft-agar wells for aqueous fractions. (B) Incubation of the representative μPAD section (spotted in a serpentine path) with the P_{clpE}-lux bioreporter and the corresponding bioreporter activity chromatogram. Induction was detected in 5 of 500 spots within a short elution window (1.30−1.37 min), with maximal induction at 1.31 min. (C) The total ion chromatogram (TIC) shows a prominent peak at 1.31 min, which correlates with the maximal bioreporter response. (D) Mass spectrum at 1.31 min displaying adducts corresponding to streptothricin F (STP F), streptothricin E (STP E), and streptothricin D (STP D). (E) Streptothricin structural moieties, (I) carbamoylated gulosamine (black), (II) streptolidine lactam ring (red), and (III) variable length β-lysine homopolymer (green). (F) Annotated MS/MS fragmentation spectrum of STP F showing diagnostic ions from streptolidine cleavage (II) and β-lysine cleavage (III) relative to the gulosamine core (I). (G) Extracted ion chromatograms (XICs) for STP F (m/z: 503.2573 ± 10 ppm), STP E (m/z: 631.3522 ± 10 ppm), and STP D (m/z: 759.4472 ± 10 ppm), eluting at 1.31 min.

of damaged or misfolded proteins. Bioreporter activation can occur via ribosome-dependent or -independent mechanisms, and proteotoxic effects can be the immediate consequence of engagement of the primary target, downstream effects following target inhibition, or secondary effects that perturb protein homeostasis.

Natural Product Library Screening for Proteotoxic Stress Inducers

A curated collection of 340 diverse natural products from the Tuebingen subset of the German Center for Infection Research (DZIF) natural product library was screened with the P_{clpE}-lux bioreporter to identify additional antibacterial agents that induce proteotoxic stress. This subset contained natural products from actinomycetes (∼88%), fungi (∼6%), and a few agents from myxobacteria, plants, and other bacterial sources, including *Erwinia*, *Pseudomonas*, and *Staphylococcus*. A small number of synthetic compounds (2%) was also included. In total, 22 compounds elicited reproducible inductions, including derivatives of compound families (Figure 2). Consistent with bioreporter validation, the established inducers puromycin and berninamycin D were successfully rediscovered. Bioreporter induction was also observed for cervimycin K, in line with published omics data showing effective derepression of heat-shock response genes and transcriptional profiles resembling gentamicin-induced stress.[46] Comparable to activation patterns observed for other thiol-reactive compounds such as NEM and TMAD, the thiol-reactive enzyme inhibitor naphthomycin A[47] elicited robust induction, whereas its structural analogue naphthomycin B produced a weaker response.

Several compounds whose primary MoAs are not typically associated with proteotoxic stress also induced the P_{clpE}-lux bioreporter. This included the glycoside antibiotic chartreusin,[48,49] whose pleiotropic MoA has previously been noted to induce the three bioreporters that signal DNA and RNA stress, as well as translation stalling.[21] Given that antimicrobial compounds generally activate only a single bioreporter corresponding to their primary MoA, or a second due to overlapping or secondary activities,[21,22] the induction of four distinct bioreporters is an exception, establishing chartreusin as the compound with the broadest bioreporter induction profile that we have observed to date. Structurally related derivatives showed reduced induction intensities, including 1-hydroxychartreusin and norchartreusin. Again, known translation stallers were among the inducing agents, including oxytetracycline, which inhibits aminoacyl-tRNA binding,[50] and the macrolides mycinamicin I, II, and IV, and pikromycin, which interfere with nascent polypeptide progression through the exit tunnel.[51,52] For mycinamicin and pikromycin, the P_{clpE}-lux induction could potentially result from thiol-reactive electrophilic sites that both agents contain. Also, the spirotetronate polyketide chlorothricin, a known pyruvate carboxylase inhibitor,[53] produced a strong response, suggesting protein damage as an additional mechanism. Among DNA gyrase-inhibiting aminocoumarin antibiotics,[54] coumermycin-A1 elicited a moderate and chlorobiocin a weak response. In contrast, novobiocin, which was included in the validation set (Table S4, Figure S4), did not induce the bioreporter, suggesting that aminocoumarins differ in their secondary effects. For β-thujaplicin,[55] we observed a weak induction, adding to the pleiotropic effects already reported for this compound. Additional P_{clpE}-lux responses were triggered by compounds with largely uncharacterized MoAs, including the strong inducer antibiotic A31505-I, and the weak inducers aureothin, cochliodinol, niphithricin B, and sakyomicin B.

Overall, the rediscovery of established proteotoxic stress inducers corroborated the specificity of the P_{clpE}-lux bioreporter. For antibiotic classes not typically associated with proteotoxic stress, P_{clpE}-lux induction points to compound-specific secondary effects beyond their established MoAs. For antibacterial agents with elusive MoAs, the bioreporter helps to build hypotheses for subsequent MoA studies by complementary methods. The superior sensitivity of the bioreporter enabled the detection of weak compound activities that would have been overlooked in classical growth inhibition assays. Because of their relatively low induction levels, such agents are considered putative proteotoxic stress inducers and warrant further confirmation. It is also noteworthy that proteotoxic stress can be caused by a defined protein−target interaction as well as by a more general thiol-reactive (covalent) property of the compound, similar to maleimide-type reactivity.

P_{clpE}-lux Bioreporter-Guided Compound Dereplication and Discovery Pipeline

Following comprehensive validation, the potential of the bioreporter for antibiotic discovery was evaluated by screening natural producer strains from the Tuebingen actinomycetes collection. In a prior bioreporter-guided screening campaign, 137 isolates from the collection exhibited antibacterial activity against *B. subtilis* but did not induce the previous bioreporter panel (signaling DNA, RNA, cell wall, and translation stalling stress).[21] We then applied the P_{clpE}-lux bioreporter to these strains. In the screening phase, strains were cultivated on different solid media to stimulate secondary metabolite production. Agar plugs from well-grown cultures were extracted and embedded in bioreporter-containing agar, thereby circumventing the need for compound isolation (Figure 3A). ISP3 medium supported the most robust production of proteotoxic stress-inducing metabolites among this collection, yielding consistent bioreporter inductions in 53 isolates. Biomass from these strains was subjected to ethyl

https://doi.org/10.1021/acs.jnatprod.6c00112
J. Nat. Prod. 2026, 89, 1698−1710

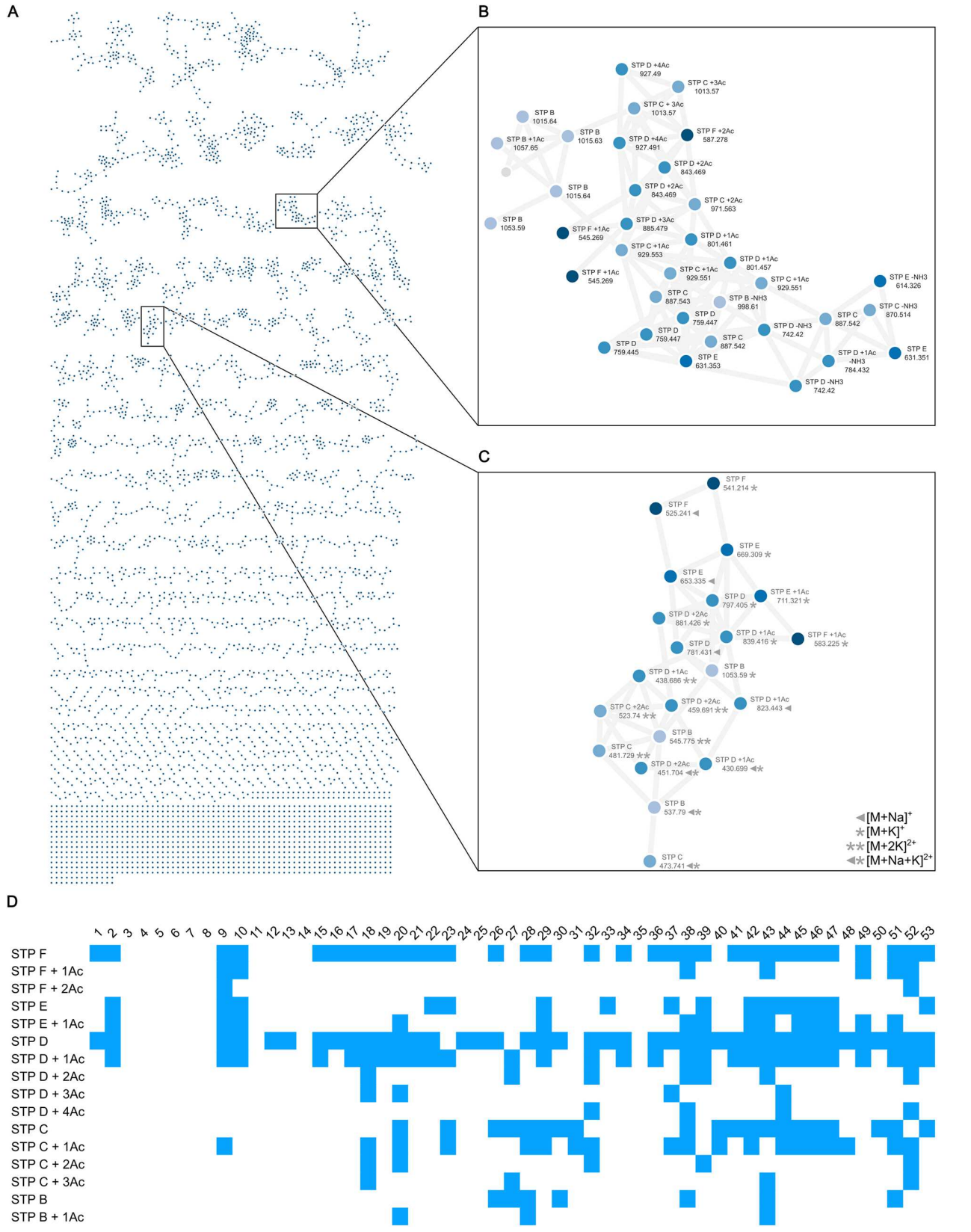

Figure 4. Identification of STP derivatives by molecular networking. (A) Global molecular network generated from LC-MS/MS data of the 53 aqueous extracts from isolates of the Tuebingen strain collection that induced the P_{clpE}-lux bioreporter. Each node represents a unique MS/MS spectrum corresponding to a distinct molecular feature, and edges indicate spectral similarity based on calculated cosine scores. (B, C) Expanded views of two molecular clusters (B, $[M + H]^+$; C, $[M + K]^+/[M + Na]^+$), corresponding to different STP congeners ranging from STP F to STP B (color-coded by congener class), including acetylation modifications; "+xAC" indicates the number of acetylation modifications detected. Edges reflect a high degree of spectral similarity between connected features. (D) A compound-presence matrix was constructed based on precursor

https://doi.org/10.1021/acs.jnatprod.6c00112
J. Nat. Prod. 2026, 89, 1698−1710

Figure 4. continued

masses and the fingerprint fragment (m/z = 171.0877), summarizing the distribution of identified STP derivatives (rows) across the producer strains (columns). In some cases, shifts in retention time occurred, which may indicate the presence of isobaric species. Blue squares indicate the presence of the corresponding molecule as determined by MS/MS analysis and the molecular network. STP identity is defined by β-lysine chain length: STP F (n = 1), STP E (n = 2), STP D (n = 3), STP C (n = 4), and STP B (n = 5).

acetate−water partitioning, and both the aqueous and organic fractions were reassessed for bioreporter induction. Bioreporter signals were mainly observed in the aqueous extracts. For dereplication, we used a novel bioreporter-guided compound dereplication and discovery pipeline. Details of the development, validation, and application of this compound-resolved, bioactivity-based metabolomics workflow were recently reported.[20] Here, we demonstrate its application for the dereplication of the bioactive compound contained in the aqueous extract of producer strain Tue2, using nontargeted high-performance liquid chromatography-tandem mass spectrometry (HPLC-MS/MS) coupled with high-frequency microfractionation onto a microfluidic paper-based analytical device (μPAD). Due to the high polarity of the bioactive metabolites, chromatographic separation was performed on a Hypercarb column, as conventional reversed-phase (RP) failed to retain the bioreporter-active agents. For extract separation, the gradient was held for 2 min at a low initial concentration of the organic modifier (2%) to enhance retention of polar analytes through the polar retention effect on graphite, a characteristic feature of this stationary phase.[56] Microfractionation was performed by splitting the column eluent using a T-piece, enabling μPAD spotting at 1 Hz at a flow rate of 1 mL/min (∼15 μL per spot, splitting ratio 9:1 microspotter/MS), while simultaneously acquiring corresponding MS/MS data.

This approach facilitated the efficient isolation and characterization of highly polar bioactive metabolites that would otherwise be lost due to early elution in the dead volume of RP columns. Following incubation of the μPAD with the P_{clpE}-lux bioreporter, luminescence signals from defined μPAD regions were mapped to their corresponding elution times to generate a bioreporter activity chromatogram (Figure 3B). Bioreporter induction was confined to a short elution window, with maximal induction observed at 1.31 min. Alignment of this bioreporter activity chromatogram with the LC-MS/MS total ion chromatogram (TIC) identified a prominent peak at 1.31 min (Figure 3C), consistent with the induction profile regarding retention time and peak shape. MS1 analysis at this retention time enabled precise identification of the candidate masses responsible for bioreporter induction within this short interval. The dominant feature was assigned to an $[M + K]^+$ ion at m/z 541.2139 (calcd. 541.2137, +0.37 ppm), with the corresponding $[M + H]^+$ ion at m/z 503.2580 (calcd. 503.2578, +0.40 ppm) (Figure 3D). Chemoinformatic analysis via SIRIUS[57] (Figures S7 and S8) predicted these ions as streptothricin F (STP F). Two additional streptothricin analogs were identified by manual annotation, namely streptothricin E (STP E) and streptothricin D (STP D), each represented by multiple ion adducts.

Streptothricins inhibit protein synthesis by binding the 30S ribosomal subunit, blocking translocation, and inducing translational misreading.[58,59] They are frequently encountered in bioactivity-guided natural product screens due to their potent activity and widespread occurrence in microbial extracts, resulting in substantial rediscovery burdens.[60−62] Characteristic structural features include a carbamoylated gulosamine moiety (I), a streptolidine lactam ring (II), and a β-lysine homopolymer of variable length (III) (Figure 3E). Streptothricins naturally occur as mixtures of congeners, with individual members distinguished by the number of β-lysine residues, most commonly STP F (n = 1), STP E (n = 2), and STP D (n = 3). Manual MS/MS analysis, exemplified for STP F, confirmed the chemoinformatic prediction by identifying diagnostic ions corresponding to the individual structural components (Figure 3F). Cleavage of the β-lysine chain (III) generated fragment I + II, consisting of the carbamoylated gulosamine (I) and streptolidine lactam ring (II). Fragment I + III was generated by cleaving off the streptolidine lactam ring (II), resulting in the carbamoylated gulosamine (I) linked to the β-lysine residue (III). The combination of both cleavages produced the carbamoylated gulosamine core (I). Extracted ion chromatograms (XICs) confirmed STP F, STP E, and STP D as the bioactive compounds within the bioreporter induction window, coeluting at approximately 1.31 min (Figure 3G).

Bioreporter-Guided Molecular Networking Reveals Streptothricin Diversity

Molecular networking was performed on the LC-MS/MS data set derived from the 53 aqueous extracts processed using the bioreporter-guided compound dereplication and discovery pipeline. A global molecular network was generated using the classical networking workflow in GNPS2[63] (Figure 4A), enabling retention-time-based integration of bioreporter activity chromatograms for each bacterial isolate. Through this step, it was also possible to detect streptothricin masses in several extracts that did not elicit a bioreporter signal after microfractionation due to low compound abundance. The resulting molecular network revealed two distinct clusters of diverse STP derivatives, as supported by exact mass and diagnostic MS/MS fragmentation patterns (Figure 4B,4C). Within these clusters, a wide variety of STP congeners were dereplicated, ranging from STP F (one β-lysine residue) to STP B (five β-lysine residues), along with multiple derivatives bearing one to four putative acetylations, annotated based on MS/MS fragmentation patterns (level 3). STP resistance is classically attributed to monoacetylation of the β-amino group of the β-lysine moiety by STP acetyltransferases (Sats), which prevents ribosomal binding, representing a mechanism of producer self-resistance.[64] Interestingly, we also detected the exact mass of a doubly acetylated STP F (calcd. 587.2784, found 587.2784, 0.00 ppm). The acetylation sites were confirmed by the distinct fragmentation pattern and by the creation of putative fragments (Figure S9). A similar observation was made for a tetra-acetylated STP D, which contains three β-lysine residues (calcd. 927.4894, found 927.4897, 0.32 ppm). The detection of several STP species with multiple acetylation modifications suggests a more complex modification pattern than previously described, including both multiple singly acetylated lysine residues per molecule and even doubly acetylated lysine residues.

https://doi.org/10.1021/acs.jnatprod.6c00112
J. Nat. Prod. 2026, 89, 1698−1710

To assess the distribution of STP derivatives across all bacterial isolates, a compound-presence matrix was constructed incorporating all dereplicated STP derivatives identified in the global network whose precursor masses and diagnostic fragment ions were consistent with STP structural features (Figure 4D). Among the 53 isolates from the Tuebingen strain collection that consistently induced the P_{clpE}-lux bioreporter, STP derivatives were detected in 45 extracts, while 8 extracts lacked any identifiable STP congener. However, these eight extracts still contained diagnostic ions corresponding to the streptolidine lactam ring within the bioreporter induction window, suggesting the presence of previously uncharacterized STP variants. Ongoing work aims to identify these unknown STP derivatives and correlate metabolite distributions and bioactivity profiles with the phylogenetic taxonomy of the corresponding producer strains.

CONCLUSIONS

This study establishes the P_{clpE}-lux bioreporter as a sensitive diagnostic tool for the discovery of antibacterial compounds that induce proteotoxic stress through the accumulation of damaged or misfolded proteins. Covering this important mechanism shared by many natural products, including marketed antibiotics, broadens the detection capacity and MoA coverage of our bioreporter panel. The new P_{clpE}-lux and our previously described P_{bmrC}-lux[20] bioreporters exhibit complementary activation profiles in response to ribosome-targeting antibiotics, differentiating between the generation of damaged proteins and translation arrest, respectively. The self-sustained luminescence enables continuous, real-time monitoring in both liquid and solid assay formats, supporting rapid screening without the need for extensive sample preparation. Our growing isogenic bioreporter panel in *B. subtilis* allows direct comparison of all induction signals, and the sporulation deficiency of the strain facilitates high-throughput handling. Validation of the P_{clpE}-lux bioreporter performance with more than 430 natural products and antibacterial reference compounds identified several agents whose MoA had not previously been associated with proteotoxic stress. For well-characterized agents, our results hint at putative secondary or downstream effects of primary MoAs and potential mechanistic differences among representatives of the same antibiotic classes. For less investigated compounds, MoA hypotheses emerge. Follow-up investigations, such as transcriptomic profiling or miscoding assays, will be required to confirm these effects and elucidate the underlying molecular mechanisms. In aqueous extracts of producer strains from the Tuebingen actinomycete collection, P_{clpE}-lux-guided analysis of microfractions substantially accelerated the dereplication of hydrophilic bioactive agents. The combination of bioreporter activity profiles with high-resolution MS/MS data in the same dereplication pipeline reduced the data complexity and enabled efficient identification of compounds of interest by aligning retention times with bioactivity peak shapes. This integrative approach allowed the accurate annotation of STP congeners across the producer strain collection and suggests previously unnoted structural diversity. Spectral similarity clustering facilitated the recognition of potentially uncharacterized STP variants and derivative families. Moreover, as STPs are widespread natural products, the comprehensive annotation of their derivative space will improve future de novo dereplication workflows. Collectively, this work presents a flexible platform for the rapid discovery and dereplication of urgently needed novel antibiotics, building on the sensitivity, specificity, and broad applicability of the bioreporter technology. Combining bioreporter-guided microfractionation with molecular networking provides a versatile strategy for identifying bioactive compounds and elucidating their structural relationships. This adaptable pipeline can be readily applied across diverse bioassay formats and screening methodologies to accelerate antibiotic discovery.

EXPERIMENTAL SECTION

General Experimental Procedures

Standard molecular cloning procedures, including restriction−ligation and Gibson assembly, were performed using established protocols. Plasmid DNA was isolated using the GeneJET Plasmid Miniprep Kit (Thermo Scientific) according to the manufacturer's instructions. DNA sequencing was performed using Sanger sequencing (LGC Genomics GmbH). Luminescence imaging in the agar-based bioreporter assay was conducted using a ChemiDoc MP imaging system (Bio-Rad). In the liquid-based bioreporter assay, luminescence and optical density (OD_{600}) were measured using a SPARK multimode microplate reader (Tecan). Microfractionation was conducted using a custom-made high-speed microfractionation device (Microspotter) combined with a microfluidic paper-based analytical device (μPAD), as reported previously.[20] Chromatographic separation was performed on an Agilent 1260 Infinity II system (Agilent Technologies) equipped with a quaternary pump, autosampler, and UV/vis detector. Mass spectrometric detection was performed on a Q Exactive Orbitrap (Thermo Fisher Scientific).

Bioreporter Generation and Cultivation

The P_{clpE}-lux bioreporter was constructed by transforming the sporulation-deficient *B. subtilis* strain 1S34[31] with a modified version of the integrative shuttle reporter vector pBS3Clux.[45] The *clpE* promoter region (P_{clpE}) was amplified from *B. subtilis* 1S34 genomic DNA and cloned into pBS3Clux, positioning P_{clpE} 19 bp upstream of the *P. luminescens luxABCDE* operon. The vector was propagated in *Escherichia coli* XL-10, cultured in Lysogeny Broth (LB) with 100 μg/mL ampicillin, followed by plasmid isolation and verification of correct promoter insertion via sequencing. Naturally competent *B. subtilis* 1S34 cells were prepared by nutrient starvation[65] and transformed with the assembled construct, which integrated into the chromosomal *sacA* locus. Transformants were selected on LB agar containing 5 μg/mL chloramphenicol (CAM), and genomic integration was verified by colony polymerase chain reaction (PCR). Primers used in this study are listed in Table S2. The P_{clpE}-lux bioreporter was routinely cultured in LB with 5 μg/mL CAM at 37 °C and agitation at 190 rpm.

Agar-Based Bioreporter Assay

A glycerol stock of the P_{clpE}-lux bioreporter was used to inoculate a preculture (18 h), which was subsequently diluted to an OD_{600} of 0.05, and the main culture was grown to an OD_{600} of ≈1.0. LB soft agar (0.75% agar, without CAM) was inoculated with the main culture to a final cell count of 3×10^6 CFU/mL, poured into 120 × 120 mm square plates (Sarstedt), and solidified for 20 min. Pure compounds (≤5 μL) were applied directly onto the agar surface, whereas larger sample volumes were applied using sterile filter discs or wells punched into the agar using a cork borer. For natural producer strains, prestamped agar blocks (≥7 days of cultivation) were placed in the plate and embedded in soft agar inoculated with the bioreporter. For μPAD assays, the bioreporter soft agar was poured onto μPAD sheets placed on a thin underlayer of sterile soft agar. Plates were incubated at 37 °C for 180 min, and luminescence (λ = 490 nm) was recorded in a ChemiDoc imager equipped with a cooled charge-coupled device (CCD) detector in chemiluminescent blot 647SP mode with an exposure time of 600 s. Luminescence images were processed using Fiji.[66] Contrast was enhanced for each image using the "Enhance Contrast" function (0.2% saturated pixels, normalization enabled). To ensure consistent visualization of

https://doi.org/10.1021/acs.jnatprod.6c00112
J. Nat. Prod. 2026, 89, 1698−1710

luminescence signals across the DZIF screening plates, a defined background region was selected on a randomly chosen assay plate to measure the baseline luminescence of the P_{clpE}-lux bioreporter. The remaining plates were then adjusted so that their background intensities matched that of the reference plate. Intrinsic CCD detector noise, including readout noise and dark current, becomes more prominent at low signal levels, making assay plates with low overall luminescence appear noisier. After imaging, plates were incubated for 18 h at 30 °C to assess antibacterial activity by measuring zones of inhibition.

Liquid-Based Bioreporter Assay

Precultures and main cultures were prepared as described for the agar assay. Reference antibiotics were serially diluted 2-fold in prewarmed LB using white, clear, flat-bottom 96-well plates (Brand). The P_{clpE}-lux bioreporter was diluted in prewarmed LB medium (without CAM), and 60 μL were added to compound-containing wells to yield a final cell count of 1×10^7 CFU/mL in 120 μL total volume. Luminescence and optical density were recorded in a multimode microplate reader at 5 min intervals over 180 min under incubation conditions specified in Table S3. Bioreporter induction was defined as a ≥500% increase in luminescence within 90 min of antibiotic exposure relative to the baseline signal of the untreated control (100%). This threshold was conservatively defined based on the distribution of induction responses across the panel of reference compounds used for validation, ensuring that all known proteotoxic stress inducers exceeded the cutoff, whereas compounds with unrelated mechanisms consistently remained below it.

Natural Producer Strain Cultivation and Extraction

Natural producer strains from the Tuebingen strain collection were cultivated on ISP2 and ISP3 agar in 120 × 120 mm square plates (Sarstedt) for 7 days at 28 °C. Biomass was harvested using a cell scraper (Sarstedt) and transferred into an equal volume of water/ethyl acetate (1:1). Extraction was performed in an overhead shaker for 18 h, followed by phase separation via centrifugation (4000*g*, 10 min, 4 °C). The aqueous and organic layers were collected separately and lyophilized. Dried organic extracts were reconstituted in 80% methanol, and aqueous extracts were reconstituted in deionized water.

Microfractionation, LC-MS/MS Analysis, and Molecular Networking

Instrumentation for microfractionation, chromatographic separation, and mass spectrometric detection is described under General Experimental Procedures. Due to the strong polarity of the bioactive metabolites, samples were separated on a Hypercarb column (100 × 4.6 mm, 5 μm; Thermo Fisher Scientific). Mobile phases consisted of LC-MS-grade water (A) and acetonitrile (B), both containing 0.1% formic acid. The gradient profile was 0.00−2.00 min, 2% B; 2.00−12.00 min, linear increase to 99% B; 12.00−13.00 min, hold at 99% B; 13.01 min, return to 2% B; total runtime 15 min; flow rate 1 mL/min. Full MS scans were acquired in positive ion mode from m/z 150−2000 at a resolution of 35,000. Source parameters were sheath gas 35 AU, auxiliary gas 5 AU, sweep gas off, spray voltage 3.5 kV, capillary temperature 250 °C, and auxiliary gas heater temperature 250 °C. Molecular networking was conducted using the classical networking workflow in GNPS2[63] with the following parameters: precursor and fragment ion tolerance 0.002 Da; minimum cluster size 2; minimum cosine score (library and network) 0.7; and minimum matched peaks 6. Networks were visualized using Cytoscape. In silico annotation and molecular formula calculations of MS/MS data were performed using SIRIUS 6.[57]

■ ASSOCIATED CONTENT

Data Availability Statement

LC-MS/MS raw and processed files are available through the Zenodo repository: https://zenodo.org/records/18186652 (raw) and https://zenodo.org/records/18198130 (mzML). GNPS2 molecular networking results are available through https://gnps2.org/status?task=f25d1c6bfc3e44fdaebe12d81124b24e.

Supporting Information

The Supporting Information is available free of charge at https://pubs.acs.org/doi/10.1021/acs.jnatprod.6c00112.

Supporting Information File 1: DZIF library compounds (XLSX)

Media composition (Table S1), primer sequences (Table S2), microplate reader settings (Table S3), antibacterial reference compounds (Table S4), bioreporter assay controls (Figures S1−S6), SIRIUS predictions (Figures S7, S8), and STP F + 2Ac prediction (Figure S9) (PDF)

■ AUTHOR INFORMATION

Corresponding Authors

Daniel Petras − *Cluster of Excellence EXC 2124: Controlling Microbes to Fight Infection (CMFI), University of Tuebingen, 72076 Tuebingen, Germany; Department of Biochemistry, University of California Riverside, Riverside, California 92507, United States*; Email: dpetras@ucr.edu

Heike Brötz-Oesterhelt − *Department of Microbial Bioactive Compounds, Interfaculty Institute of Microbiology and Infection Medicine (IMIT), University of Tuebingen, 72076 Tuebingen, Germany; Cluster of Excellence EXC 2124: Controlling Microbes to Fight Infection (CMFI), University of Tuebingen, 72076 Tuebingen, Germany; German Center for Infection Research (DZIF), Partner Site Tuebingen, 72076 Tuebingen, Germany;* orcid.org/0000-0001-9364-1832; Email: heike.broetz-oesterhelt@uni-tuebingen.de

Authors

Julian Schubert − *Department of Microbial Bioactive Compounds, Interfaculty Institute of Microbiology and Infection Medicine (IMIT), University of Tuebingen, 72076 Tuebingen, Germany; Cluster of Excellence EXC 2124: Controlling Microbes to Fight Infection (CMFI), University of Tuebingen, 72076 Tuebingen, Germany;* orcid.org/0009-0005-9382-5945

Christian Geibel − *Department of Microbial Bioactive Compounds, Interfaculty Institute of Microbiology and Infection Medicine (IMIT), University of Tuebingen, 72076 Tuebingen, Germany; Cluster of Excellence EXC 2124: Controlling Microbes to Fight Infection (CMFI), University of Tuebingen, 72076 Tuebingen, Germany;* orcid.org/0009-0002-2044-9422

Anne Berscheid − *Department of Microbial Bioactive Compounds, Interfaculty Institute of Microbiology and Infection Medicine (IMIT), University of Tuebingen, 72076 Tuebingen, Germany; German Center for Infection Research (DZIF), Partner Site Tuebingen, 72076 Tuebingen, Germany;* orcid.org/0000-0003-1585-8715

Katharina W. Wex − *Department of Microbial Bioactive Compounds, Interfaculty Institute of Microbiology and Infection Medicine (IMIT), University of Tuebingen, 72076 Tuebingen, Germany; German Center for Infection Research (DZIF), Partner Site Tuebingen, 72076 Tuebingen, Germany*

Giovanni Andrea Vitale − *Department of Microbial Bioactive Compounds, Interfaculty Institute of Microbiology and Infection Medicine (IMIT), University of Tuebingen, 72076 Tuebingen, Germany; Cluster of Excellence EXC 2124:*

https://doi.org/10.1021/acs.jnatprod.6c00112
J. Nat. Prod. 2026, 89, 1698−1710

Controlling Microbes to Fight Infection (CMFI), University of Tuebingen, 72076 Tuebingen, Germany; orcid.org/0000-0002-7143-6317

Chambers C. Hughes − *Department of Microbial Bioactive Compounds, Interfaculty Institute of Microbiology and Infection Medicine (IMIT), University of Tuebingen, 72076 Tuebingen, Germany; Cluster of Excellence EXC 2124: Controlling Microbes to Fight Infection (CMFI), University of Tuebingen, 72076 Tuebingen, Germany; German Center for Infection Research (DZIF), Partner Site Tuebingen, 72076 Tuebingen, Germany;* orcid.org/0000-0002-7000-6438

Complete contact information is available at: https://pubs.acs.org/10.1021/acs.jnatprod.6c00112

Author Contributions

H.B.-O. conceptualized the approach and supervised the study. A.B. designed, J.S. and K.W.W. constructed, and J.S. validated the bioreporter strain. J.S. screened the libraries, generated extracts, and performed the bioreporter analysis during bioassay-guided fractionation. C.G. and D.P. developed the microfractionation-based metabolomics approach, and C.G. fractionated the extracts. J.S., C.G., G.A.V., and C.C.H. analyzed elution profiles, MS spectra, and the network. H.B.-O. and D.P. provided materials and instrumentation. J.S., H.B.-O., C.G., and G.A.V. wrote the manuscript. All authors edited and approved the final manuscript.

Notes

The authors declare no competing financial interest.

■ ACKNOWLEDGMENTS

We thank M. Wurm and S. Stockert for expert technical assistance, particularly in cultivating and handling the natural producer strains from the Tuebingen strain collection. We thank E. Stegmann for valuable discussions, T.H. Niedermeyer for supplying compounds to the DZIF library, and J. Herrmann for library curation. Funding was provided by the Deutsche Forschungsgemeinschaft (German Research Foundation, DFG) via the Cluster of Excellence EXC 2124: Controlling Microbes to Fight Infection (CMFI, project ID 390838134) to H.B.-O., D.P., C.C.H., and J.S. and via TRR261 (project ID 398967434) to H.B.-O. K.W.W., A.B., J.S., C.C.H., and H.B.-O. received funding from the German Center for Infection Research (project PAACT "Precision access to antibiotic drugs and targets"). This work was supported in part by the National Institute of General Medical Sciences, GM160154, to D.P. and by the Simons Foundation International through award SFI-LS-ECIAMEE-00013858 to D.P.

■ REFERENCES

(1) Cardona, S. T.; Rahman, A. S. M. Z.; Novomisky Nechcoff, J. Innovative Perspectives on the Discovery of Small Molecule Antibiotics. *npj Antimicrob. Resist.* **2025**, *3* (1), No. 19.

(2) Anderson, M.; Panteli, D.; Van Kessel, R.; Ljungqvist, G.; Colombo, F.; Mossialos, E. Challenges and Opportunities for Incentivising Antibiotic Research and Development in Europe. *Lancet Reg. Health - Eur.* **2023**, *33*, No. 100705.

(3) World Health Organization. *2023 Antibacterial Agents in Clinical and Preclinical Development: An Overview and Analysis*; World Health Organization: Geneva, 2024; p 231. https://www.who.int/publications/i/item/9789240094000.

(4) Blaskovich, M. A. T.; Cooper, M. A. Antibiotics Re-Booted—Time to Kick Back against Drug Resistance. *npj Antimicrob. Resist.* **2025**, *3* (1), No. 47.

(5) Payne, D. J.; Gwynn, M. N.; Holmes, D. J.; Pompliano, D. L. Drugs for Bad Bugs: Confronting the Challenges of Antibacterial Discovery. *Nat. Rev. Drug Discovery* **2007**, *6* (1), 29−40.

(6) Perros, M. A Sustainable Model for Antibiotics. *Science* **2015**, *347* (6226), 1062−1064.

(7) Baranova, A. A.; Alferova, V. A.; Korshun, V. A.; Tyurin, A. P. Modern Trends in Natural Antibiotic Discovery. *Life* **2023**, *13* (5), 1073.

(8) Scherlach, K.; Hertweck, C. Mining and Unearthing Hidden Biosynthetic Potential. *Nat. Commun.* **2021**, *12* (1), No. 3864.

(9) Palazzotto, E.; Weber, T. Omics and Multi-Omics Approaches to Study the Biosynthesis of Secondary Metabolites in Microorganisms. *Curr. Opin. Microbiol.* **2018**, *45*, 109−116.

(10) Cesaro, A.; Bagheri, M.; Torres, M.; Wan, F.; de la Fuente-Nunez, C. Deep Learning Tools to Accelerate Antibiotic Discovery. *Expert Opin. Drug Discovery* **2023**, *18* (11), 1245−1257.

(11) Lasch, C.; Myronovskyi, M.; Luzhetskyy, A. *Streptomyces* as a Versatile Host Platform for Heterologous Production of Microbial Natural Products. *Nat. Prod. Rep.* **2026**, *43*, 371−390.

(12) Hedges, M. R.; Di Carlo, C. M.; Wuest, W. M. Combatting Resistance: Natural Products as Tools to Drive the Discovery of Untapped Antibiotic Targets. *Chem. Commun.* **2025**, *61* (74), 14039−14058.

(13) Bognár, B.; Spohn, R.; Lázár, V. Drug Combinations Targeting Antibiotic Resistance. *npj Antimicrob. Resist.* **2024**, *2* (1), No. 29.

(14) Boyd, N. K.; Teng, C.; Frei, C. R. Brief Overview of Approaches and Challenges in New Antibiotic Development: A Focus On Drug Repurposing. *Front. Cell. Infect. Microbiol.* **2021**, *11*, No. 684515.

(15) Leeten, K.; Jacques, N.; Esquembre, L. A.; Schneider, D. C.; Straetener, J.; Henriksen, C.; Musumeci, L.; Putters, F.; Melo, S.; Sánchez-López, E.; Giera, M.; Penoy, N.; Piel, G.; Verlaine, O.; Amoroso, A.; Joris, B.; Slavetinsky, C. J.; Goffin, E.; Pirotte, B.; Frees, D.; Brötz-Oesterhelt, H.; Lancellotti, P.; Oury, C. Ticagrelor Alters the Membrane of *Staphylococcus Aureus* and Enhances the Activity of Vancomycin and Daptomycin without Eliciting Cross-Resistance. *mBio* **2024**, *15* (10), No. e0132224.

(16) Rütten, A.; Kirchner, T.; Musiol-Kroll, E. M. Overview on Strategies and Assays for Antibiotic Discovery. *Pharmaceuticals* **2022**, *15* (10), 1302.

(17) Miethke, M.; Pieroni, M.; Weber, T.; Brönstrup, M.; Hammann, P.; Halby, L.; Arimondo, P. B.; Glaser, P.; Aigle, B.; Bode, H. B.; Moreira, R.; Li, Y.; Luzhetskyy, A.; Medema, M. H.; Pernodet, J.-L.; Stadler, M.; Tormo, J. R.; Genilloud, O.; Truman, A. W.; Weissman, K. J.; Takano, E.; Sabatini, S.; Stegmann, E.; Brötz-Oesterhelt, H.; Wohlleben, W.; Seemann, M.; Empting, M.; Hirsch, A. K. H.; Loretz, B.; Lehr, C.-M.; Titz, A.; Herrmann, J.; Jaeger, T.; Alt, S.; Hesterkamp, T.; Winterhalter, M.; Schiefer, A.; Pfarr, K.; Hoerauf, A.; Graz, H.; Graz, M.; Lindvall, M.; Ramurthy, S.; Karlén, A.; van Dongen, M.; Petkovic, H.; Keller, A.; Peyrane, F.; Donadio, S.; Fraisse, L.; Piddock, L. J. V.; Gilbert, I. H.; Moser, H. E.; Müller, R. Towards the Sustainable Discovery and Development of New Antibiotics. *Nat. Rev. Chem.* **2021**, *5* (10), 726−749.

(18) Landeta, C.; Mejia-Santana, A. Union Is Strength: Target-Based and Whole-Cell High-Throughput Screens in Antibacterial Discovery. *J. Bacteriol.* **2022**, *204* (4), No. e00477-21.

(19) Brötz-Oesterhelt, H.; Sass, P. Postgenomic Strategies in Antibacterial Drug Discovery. *Future Microbiol.* **2010**, *5* (10), 1553−1579.

(20) Geibel, C.; Schubert, J.; Knoblauch, S. B.; Hernandez, A.; Boldt, L.; Schneider, D. C.; Papadopoulos Lambidis, S.; Vitale, G. A.; Fleischer, J.; Haussmann, M.; Gross, H.; Wang, M.; Brötz-Oesterhelt, H.; Petras, D. High-Frequency Microfluidic Fractionation for Compound-Resolved Bioactivity-Based Metabolomics. *Anal. Chem.* **2025**, *97* (43), 24093−24104.

(21) Wex, K. W.; Saur, J. S.; Handel, F.; Ortlieb, N.; Mokeev, V.; Kulik, A.; Niedermeyer, T. H. J.; Mast, Y.; Grond, S.; Berscheid, A.; Brötz-Oesterhelt, H. Bioreporters for Direct Mode of Action-Informed Screening of Antibiotic Producer Strains. *Cell Chem. Biol.* **2021**, *28* (8), 1242−1252.e4.
(22) Urban, A.; Eckermann, S.; Fast, B.; Metzger, S.; Gehling, M.; Ziegelbauer, K.; Rübsamen-Waigmann, H.; Freiberg, C. Novel Whole-Cell Antibiotic Biosensors for Compound Discovery. *Appl. Environ. Microbiol.* **2007**, *73* (20), 6436−6443.
(23) Freiberg, C.; Brunner, N.; Macko, L.; Fischer, H. P. Discovering Antibiotic Efficacy Biomarkers: Toward Mechanism-Specific High Content Compound Screening. *Mol. Cell. Proteomics* **2006**, *5* (12), 2326−2335.
(24) Bandow, J. E.; Brötz, H.; Leichert, L. I. O.; Labischinski, H.; Hecker, M. Proteomic Approach to Understanding Antibiotic Action. *Antimicrob. Agents Chemother.* **2003**, *47* (3), 948−955.
(25) Hutter, B.; Fischer, C.; Jacobi, A.; Schaab, C.; Loferer, H. Panel of *Bacillus Subtilis* Reporter Strains Indicative of Various Modes of Action. *Antimicrob. Agents Chemother.* **2004**, *48* (7), 2588−2594.
(26) Elsholz, A. K. W.; Birk, M. S.; Charpentier, E.; Turgay, K. Functional Diversity of AAA+ Protease Complexes in *Bacillus Subtilis*. *Front. Mol. Biosci.* **2017**, *4*, No. 44.
(27) Elsholz, A. K. W.; Michalik, S.; Zühlke, D.; Hecker, M.; Gerth, U. CtsR, the Gram-Positive Master Regulator of Protein Quality Control, Feels the Heat. *EMBO J.* **2010**, *29* (21), 3621−3629.
(28) Gerth, U.; Kirstein, J.; Mostertz, J.; Waldminghaus, T.; Miethke, M.; Kock, H.; Hecker, M. Fine-Tuning in Regulation of Clp Protein Content in *Bacillus Subtilis*. *J. Bacteriol.* **2004**, *186* (1), 179−191.
(29) Miethke, M.; Hecker, M.; Gerth, U. Involvement of *Bacillus Subtilis* ClpE in CtsR Degradation and Protein Quality Control. *J. Bacteriol.* **2006**, *188* (13), 4610−4619.
(30) Derré, I.; Rapoport, G.; Devine, K.; Rose, M.; Msadek, T. ClpE, a Novel Type of HSP100 ATPase, Is Part of the CtsR Heat Shock Regulon of *Bacillus Subtilis*. *Mol. Microbiol.* **1999**, *32* (3), 581−593.
(31) Piggot, P. J. Mapping of Asporogenous Mutations of Bacillus Subtilis: A Minimum Estimate of the Number of Sporulation Operons. *J. Bacteriol.* **1973**, *114*, 1241−1253.
(32) Vakulenko, S. B.; Mobashery, S. Versatility of Aminoglycosides and Prospects for Their Future. *Clin. Microbiol. Rev.* **2003**, *16* (3), 430−450.
(33) Aviner, R. The Science of Puromycin: From Studies of Ribosome Function to Applications in Biotechnology. *Comput. Struct. Biotechnol. J.* **2020**, *18*, 1074−1083.
(34) Brötz-Oesterhelt, H.; Beyer, D.; Kroll, H.-P.; Endermann, R.; Ladel, C.; Schroeder, W.; Hinzen, B.; Raddatz, S.; Paulsen, H.; Henninger, K.; Bandow, J. E.; Sahl, H.-G.; Labischinski, H. Dysregulation of Bacterial Proteolytic Machinery by a New Class of Antibiotics. *Nat. Med.* **2005**, *11* (10), 1082−1087.
(35) Kirstein, J.; Hoffmann, A.; Lilie, H.; Schmidt, R.; Rübsamen-Waigmann, H.; Brötz-Oesterhelt, H.; Mogk, A.; Turgay, K. The Antibiotic ADEP Reprogrammes ClpP, Switching It from a Regulated to an Uncontrolled Protease. *EMBO Mol. Med.* **2009**, *1* (1), 37−49.
(36) Gregory, J. D. The Stability of N-Ethylmaleimide and Its Reaction with Sulfhydryl Groups. *J. Am. Chem. Soc.* **1955**, *77* (14), 3922−3923.
(37) Tuli, V. Bactericidal Action of Sulfhydryl Binding Compounds. *Antimicrob. Agents Chemother.* **1973**, *3* (2), 157−161.
(38) Harris, J. W.; Power, J. A. Diamide: Mechanisms of Action and Interactions with Other Sensitizers. *Br. J. Cancer, Suppl.* **1978**, *3*, 84−89.
(39) Pöther, D.-C.; Liebeke, M.; Hochgräfe, F.; Antelmann, H.; Becher, D.; Lalk, M.; Lindequist, U.; Borovok, I.; Cohen, G.; Aharonowitz, Y.; Hecker, M. Diamide Triggers Mainly S Thiolations in the Cytoplasmic Proteomes of *Bacillus Subtilis* and *Staphylococcus Aureus*. *J. Bacteriol.* **2009**, *191* (24), 7520−7530.
(40) Borg, A.; Pavlov, M.; Ehrenberg, M. Mechanism of Fusidic Acid Inhibition of RRF- and EF-G-Dependent Splitting of the Bacterial Post-Termination Ribosome. *Nucleic Acids Res.* **2016**, *44* (7), 3264−3275.
(41) Ticu, C.; Nechifor, R.; Nguyen, B.; Desrosiers, M.; Wilson, K. S. Conformational Changes in Switch I of EF-G Drive Its Directional Cycling on and off the Ribosome. *EMBO J.* **2009**, *28* (14), 2053−2065.
(42) Borovinskaya, M. A.; Pai, R. D.; Zhang, W.; Schuwirth, B. S.; Holton, J. M.; Hirokawa, G.; Kaji, H.; Kaji, A.; Cate, J. H. D. Structural Basis for Aminoglycoside Inhibition of Bacterial Ribosome Recycling. *Nat. Struct. Mol. Biol.* **2007**, *14* (8), 727−732.
(43) Reusser, F. Mode of Action of Berninamycin. An Inhibitor of Protein Biosynthesis. *Biochemistry* **1969**, *8* (8), 3303−3308.
(44) Yu, G.; Peng, H.; Cao, J.; Liao, A.; Long, P.; Huang, J.; Hui, M. Avilamycin Production Enhancement by Mutagenesis and Fermentation Optimization in *Streptomyces Viridochromogenes*. *World J. Microbiol. Biotechnol.* **2022**, *38* (3), No. 50.
(45) Radeck, J.; Kraft, K.; Bartels, J.; Cikovic, T.; Dürr, F.; Emenegger, J.; Kelterborn, S.; Sauer, C.; Fritz, G.; Gebhard, S.; Mascher, T. The Bacillus BioBrick Box: Generation and Evaluation of Essential Genetic Building Blocks for Standardized Work with *Bacillus Subtilis*. *J. Biol. Eng.* **2013**, *7* (1), No. 29.
(46) Hoffmann, A.; Steffens, U.; Maček, B.; Franz-Wachtel, M.; Nieselt, K.; Harbig, T. A.; Scherlach, K.; Hertweck, C.; Sahl, H.-G.; Bierbaum, G. The Unusual Mode of Action of the Polyketide Glycoside Antibiotic Cervimycin C. *mSphere* **2024**, *9* (5), No. e00764-23.
(47) Okabe, T.; Yuan, B. D.; Fujio, I.; Sato, I.; Fukazawa, H.; Nishimura, T.; Tanaka, N. Studies on Antineoplastic Activity of Naphthomycin, a Naphthalenic Ansamycin, and Its Mode of Action. *J. Antibiot.* **1985**, *38* (2), 230−235.
(48) Portugal, J. Chartreusin, Elsamicin A and Related Anti-Cancer Antibiotics. *Curr. Med. Chem. Anticancer Agents* **2003**, *3* (6), 411−420.
(49) Li, L. H.; Clark, T. D.; Murch, L. L.; Wooden, J. M.; Pschigoda, L. M.; Krueger, W. C. Biological and Biochemical Effects of Chartreusin on Mammalian Cells. *Cancer Res.* **1978**, *38* (9), 3012−3018.
(50) Chopra, I.; Roberts, M. Tetracycline Antibiotics: Mode of Action, Applications, Molecular Biology, and Epidemiology of Bacterial Resistance. *Microbiol. Mol. Biol. Rev.* **2001**, *65* (2), 232−260.
(51) Breiner-Goldstein, E.; Eyal, Z.; Matzov, D.; Halfon, Y.; Cimicata, G.; Baum, M.; Rokney, A.; Ezernitchi, A. V.; Lowell, A. N.; Schmidt, J. J.; Rozenberg, H.; Zimmerman, E.; Bashan, A.; Valinsky, L.; Anzai, Y.; Sherman, D. H.; Yonath, A. Ribosome-Binding and Anti-Microbial Studies of the Mycinamicins, 16-Membered Macrolide Antibiotics from Micromonospora Griseorubida. *Nucleic Acids Res.* **2021**, *49* (16), 9560−9573.
(52) Almutairi, M. M.; Svetlov, M. S.; Hansen, D. A.; Khabibullina, N. F.; Klepacki, D.; Kang, H.-Y.; Sherman, D. H.; Vázquez-Laslop, N.; Polikanov, Y. S.; Mankin, A. S. Co-Produced Natural Ketolides Methymycin and Pikromycin Inhibit Bacterial Growth by Preventing Synthesis of a Limited Number of Proteins. *Nucleic Acids Res.* **2017**, *45* (16), 9573−9582.
(53) Schindler, P. W.; Zäuhner, H. Mode of Action of the Macrolide-Type Antibiotic, Chlorothricin. *Eur. J. Biochem.* **1973**, *39* (2), 591−600.
(54) Anderle, C.; Stieger, M.; Burrell, M.; Reinelt, S.; Maxwell, A.; Page, M.; Heide, L. Biological Activities of Novel Gyrase Inhibitors of the Aminocoumarin Class. *Antimicrob. Agents Chemother.* **2008**, *52* (6), 1982−1990.
(55) Wyżga, B.; Skóra, M.; Olechowska, K.; Broniatowski, M.; Wydro, P.; Hąc-Wydro, K. Searching for the Role of Membrane Lipids in the Mechanism of Antibacterial Effect of Hinokitiol. *Arch. Biochem. Biophys.* **2024**, *761*, No. 110178.
(56) Russo, M.; Camillo, M. R. T.; La Tella, R.; Rigano, F.; Donato, P.; Mondello, L.; Dugo, P. Principles and Applications of Porous Graphitic Carbon Stationary Phase in Liquid Chromatography: An Update. *J. Chromatogr. A* **2024**, *1719*, No. 464728.
(57) Dührkop, K.; Fleischauer, M.; Ludwig, M.; Aksenov, A. A.; Melnik, A. V.; Meusel, M.; Dorrestein, P. C.; Rousu, J.; Böcker, S.

https://doi.org/10.1021/acs.jnatprod.6c00112
J. Nat. Prod. 2026, 89, 1698−1710

SIRIUS 4: A Rapid Tool for Turning Tandem Mass Spectra into Metabolite Structure Information. *Nat. Methods* **2019**, *16* (4), 299−302.
(58) Franck, E.; Crofts, T. S. History of the Streptothricin Antibiotics and Evidence for the Neglect of the Streptothricin Resistome. *npj Antimicrob. Resist.* **2024**, *2* (1), No. 3.
(59) Morgan, C. E.; Kang, Y.-S.; Green, A. B.; Smith, K. P.; Dowgiallo, M. G.; Miller, B. C.; Chiaraviglio, L.; Truelson, K. A.; Zulauf, K. E.; Rodriguez, S.; Kang, A. D.; Manetsch, R.; Yu, E. W.; Kirby, J. E. Streptothricin F Is a Bactericidal Antibiotic Effective against Highly Drug-Resistant Gram-Negative Bacteria That Interacts with the 30S Subunit of the 70S Ribosome. *PLoS Biol.* **2023**, *21* (5), No. e3002091.
(60) Chevrette, M. G.; Handelsman, J. Needles in Haystacks: Reevaluating Old Paradigms for the Discovery of Bacterial Secondary Metabolites. *Nat. Prod. Rep.* **2021**, *38* (11), 2083−2099.
(61) Cox, G.; Sieron, A.; King, A. M.; Pascale, G. D.; Pawlowski, A. C.; Koteva, K.; Wright, G. D. A Common Platform for Antibiotic Dereplication and Adjuvant Discovery. *Cell Chem. Biol.* **2017**, *24* (1), 98−109.
(62) Ji, Z.; Wei, S.; Zhang, J.; Wu, W.; Wang, M. Identification of Streptothricin Class Antibiotics in the Early-Stage of Antibiotics Screening by Electrospray Ionization Mass Spectrometry. *J. Antibiot.* **2008**, *61* (11), 660−667.
(63) Wang, M.; Carver, J. J.; Phelan, V. V.; et al. Sharing and Community Curation of Mass Spectrometry Data with Global Natural Products Social Molecular Networking. *Nat. Biotechnol.* **2016**, *34* (8), 828−837.
(64) Burckhardt, R. M.; Escalante-Semerena, J. C. In *Bacillus Subtilis*, the SatA (Formerly YyaR) Acetyltransferase Detoxifies Streptothricin via Lysine Acetylation. *Appl. Environ. Microbiol.* **2017**, *83* (21), No. e01590-17.
(65) iGEM Newcastle Team. Transforming into *Bacillus subtilis* 168; iGEM Wiki. https://2009.igem.org/Team:Newcastle/Project/Labwork/OurProtocols/TransformBac (accessed Jan 23, 2026).
(66) Schindelin, J.; Arganda-Carreras, I.; Frise, E.; Kaynig, V.; Longair, M.; Pietzsch, T.; Preibisch, S.; Rueden, C.; Saalfeld, S.; Schmid, B.; Tinevez, J.-Y.; White, D. J.; Hartenstein, V.; Eliceiri, K.; Tomancak, P.; Cardona, A. Fiji: An Open-Source Platform for Biological-Image Analysis. *Nat. Methods* **2012**, *9* (7), 676−682.

https://doi.org/10.1021/acs.jnatprod.6c00112
J. Nat. Prod. 2026, 89, 1698−1710

Supplementary Information

A Proteotoxic Stress Bioreporter Enables Mechanism-Informed Antibiotic Discovery

Julian Schubert[1,2], Christian Geibel[1,2], Anne Berscheid[1,3], Katharina W. Wex[1,3], Giovanni Andrea Vitale[1,2], Chambers C. Hughes[1,2,3], Daniel Petras[2,4,*], Heike Brötz-Oesterhelt[1,2,3,*]

1. Department of Microbial Bioactive Compounds, Interfaculty Institute of Microbiology and Infection Medicine (IMIT), University of Tuebingen, 72076 Tuebingen, Germany
2. Cluster of Excellence EXC 2124: Controlling Microbes to Fight Infection (CMFI), University of Tuebingen, 72076 Tuebingen, Germany
3. German Center for Infection Research (DZIF), Partner Site Tuebingen, 72076 Tuebingen, Germany
4. Department of Biochemistry, University of California Riverside, Riverside, California 92507, USA

*Corresponding authors: dpetras@ucr.edu; heike.broetz-oesterhelt@uni-tuebingen.de

Table of Contents

Table S1. Media composition.

Medium	Composition
LB	1% NaCl, 1% tryptone, 0.5% yeast extract, pH 7.25
LB soft agar	1% NaCl, 1% tryptone, 0.5% yeast extract, 0.75% agar, pH 7.25
ISP2	0.4% D-glucose, 1% malt extract, 0.4% yeast extract, 2% agar, pH 7.3
ISP3	2% oatmeal, 0.5% trace elements, 1.5% agar, pH 7.3
Trace-elements	0.3% $CaCl_2 \cdot 2H_2O$, 0.1% Fe(III)-citrate, 0.02% $MnSO_4 \cdot 1H_2O$, 0.01% $ZnCl_2$, 0.0025% $CuSO_4 \cdot 5H_2O$, 0.002% $Na_2B_4O_7 \cdot 10H_2O$, 0.0004% $CoCl_2 \cdot 6H_2O$, 0.001% $Na_2MoO_4 \cdot 2H_2O$

Table S2. Primers used in this study.

PCR	Nucleotide sequence (5'-3')
ClpE-fwd	GATAAGCTGTCAAACATGAGAATTCATGTTTTACTTTGTAACAAATCAA
ClpE-rev	TTTCATAGAGAGTCCTCCTGTCGACGGAATTTATTTGCATGTTAAGGC
Sequencing	**Nucleotide sequence (5'-3')**
Insert-fwd	TTCGTTTGTTGAACTAATGGGTGC
Insert-rev	AAACCACACTCCTCAGAGATG
Colony PCR	**Nucleotide sequence (5'-3')**
SacA-fwd	CTGATTGGCATGGCGATTGC
SacA-rev	ACAGCTCCAGATCCTCTACG

Table S3. Tecan Spark multimode microplate reader settings.

Parameter	Settings
Lid	Yes
Humidity cassette	No
Temperature control	On, wait for temperature
Temperature	37°C [min: 36°C, max: 38°C]
Measurement	180 min
Interval	5 min
Shaking	60 sec, double orbital, amplitude 2.5 mm (108 rpm)
Wait	10 sec
Luminescence	Integration time 1000 ms
Absorbance	Wavelength 600 nm, bandwidth 3.5 nm, flashes 10, settle time 100 ms, multiple reads per well: XY-line 3 x 3, border 2400 µm
Wait	Wait for interval restart

Table S4. Antibacterial reference compounds used in the validation of the P_{clpE}-lux bioreporter. Compounds eliciting bioreporter induction are denoted by "+", whereas non-inducing compounds are marked with "−".

Compound	Agar	Liquid
Proteotoxic stress inducers and protein synthesis inhibitors		
Abortive translation inducer		
Puromycin	+	+
Misreading inducers		
Amikacin	+	+
Apramycin	+	+
Gentamicin	+	+
Hygromycin B	+	+
Kanamycin	+	+
Neomycin	+	+
Paromomycin	+	+
Streptomycin	+	+
Tobramycin	+	+
Thiol-modifying agents		
N-ethylmaleimide	+**	+
TMAD	+	+
Clp protease dysregulators		
ADEP1	+	+
ADEP2	+	+
ADEP7	+	+
Translation stallers		
Anhydrotetracycline	-	-
Avilamycin B*	-	+
Avilamycin C*	-	+
Azithromycin	-	-
Berninamycin C*	+	+
Chloramphenicol	-	-
Clindamycin	-	-
Doxycycline	-	-
Erythromycin	-	-
Fusidic acid*	+	+
Kirromycin	-	-
Kirrothrycin	-	-
Lincomycin	-	-
Linezolid	-	-
Oxamicetin	-	-
Pactamycin	-	-
Spectinomycin	-	-
Sulfomycin I	-	-
Telithromycin	-	-
Tetracycline	-	-

Compound	Agar	Liquid
Thiostrepton	-	-
Tiamulin	-	-
Tigecycline	-	-
tRNA synthetase inhibitors		
Mupirocin	-	-
Cell envelope inhibitors		
Cell membrane disruptors		
Colistin	-	-
Mefloquine	-	-
Polymyxin B	-	-
Ionophores		
CCCP	-	-
Monensin	-	-
Nigericin	-	-
Salinomycin	-	-
Lipid-II cycle inhibitors		
A-47934	-	-
Bacitracin	-	-
Daptomycin	-	-
Mersacidin	-	-
Nisin	-	-
Ramoplanin	-	-
Teicoplanin	-	-
Vancomycin	-	-
Peptidoglycan synthesis enzyme inhibitors		
Ampicillin	-	-
Benzylpenicillin	-	-
Cefadroxil	-	-
Cefalexin	-	-
Cefotaxime	-	-
Cefoxitin	-	-
Cefuroxime	-	-
D-Cycloserine	-	-
Fosfomycin	-	-
Imipenem	-	-
Meropenem	-	-
Methicillin	-	-
Oxacillin	-	-
Fatty acid synthesis inhibitors		
Triclosan	-	-
DNA synthesis inhibitors		
DNA gyrase binders		
Ciprofloxacin	-	-
Levofloxacin	-	-
Moxifloxacin	-	-

Compound	Agar	Liquid
Nalidixic acid	-	-
Norfloxacin	-	-
Novobiocin	-	-
Nucleotide synthesis inhibitors		
Azaserine	-	-
Trimethoprim	-	-
RNA synthesis inhibitors		
RNA polymerase binders		
Fidaxomicin	-	-
Rifabutin	-	-
Rifampicin	-	-
Intercalators		
Actinomycin D	-	-
Cisplatin	-	-
Doxorubicin	-	-
Echinomycin	-	-
Emodin	-	-
Mitomycin C	-	-
Mitoxantrone	-	-
Netropsin	-	-
Proflavine	-	-
Zeocin	-	-
Diverse mechanisms of action		
5'-Fluorouracil	-	-
Holomycin	-	-
Nitrofurantoin	-	-
Thiolutin	-	-
Derinamycin	-	-
Rinamycin	-	-
Spermidine	-	-
Spermine	-	-
Frigocyclinone	-	-
Quinine	-	-

* Categorized as “translation stallers” per published mechanism of action (MoA); P_{clpE}-lux induction in the current study suggests additional accumulation of damaged or misfolded proteins, a hypothesis requiring assessment by complementary methods.
** Transient induction of P_{clpE}-lux at 90 min after antibiotic exposure.

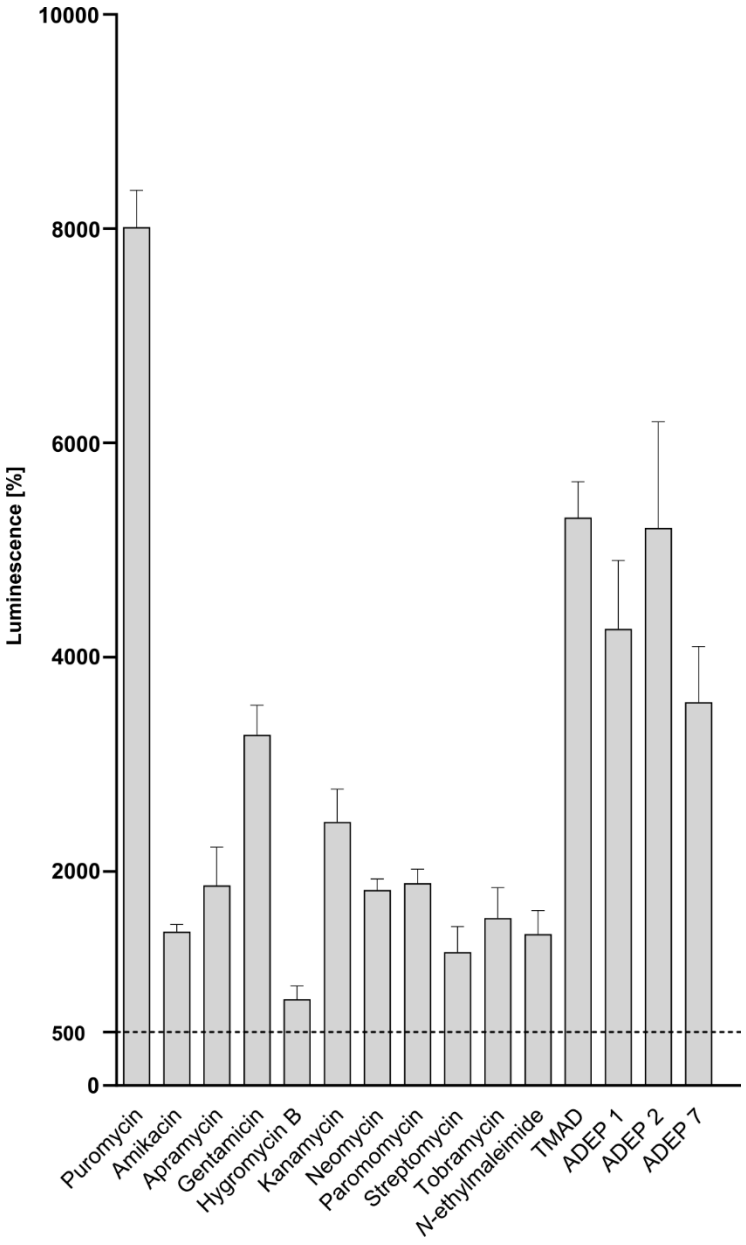

Fig. S1. P_{clpE}-lux bioreporter validation using established proteotoxic stress inducers. Quantitative bioreporter induction by reference compounds in the liquid assay format. The compounds correspond to those summarized in Table S4 and include abortive translation inducers, misreading inducers, thiol-modifying agents, and Clp protease dysregulators. Compounds were tested in two-fold serial dilutions, from below to above their minimal inhibitory concentrations (MIC). Luminescence and OD_{600} (cell mass) were monitored for 180 min, and induction was normalized to the baseline luminescence of the untreated control (100%) and the OD_{600}. The induction threshold was defined as ≥500% luminescence within 90 min of antibiotic exposure (black dotted line). Bars represent maximal normalized luminescence (mean ± SD) from independent biological replicates.

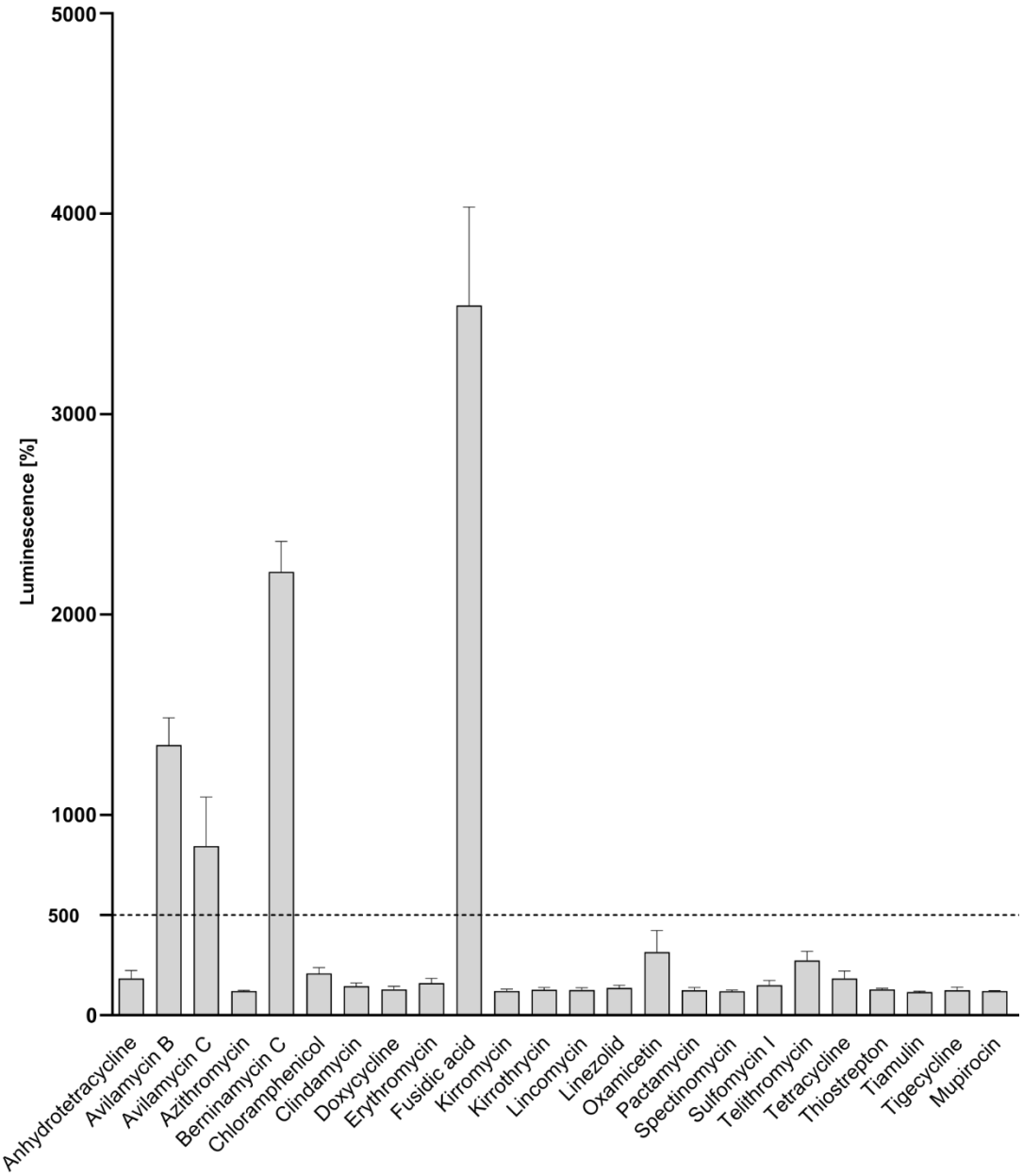

Fig. S2. P*clpE*-lux bioreporter validation using protein synthesis inhibitors. Quantitative bioreporter induction by reference compounds in the liquid assay format. The compounds correspond to those summarized in Table S4 and include translation stallers and tRNA synthetase inhibitors. Compounds were tested in two-fold serial dilutions, from below to above their minimal inhibitory concentrations (MIC). Luminescence and OD_{600} (cell mass) were monitored for 180 min, and induction was normalized to the baseline luminescence of the untreated control (100%) and the OD_{600}. The induction threshold was defined as ≥500% luminescence within 90 min of antibiotic exposure (black dotted line). Bars represent maximal normalized luminescence (mean ± SD) from independent biological replicates.

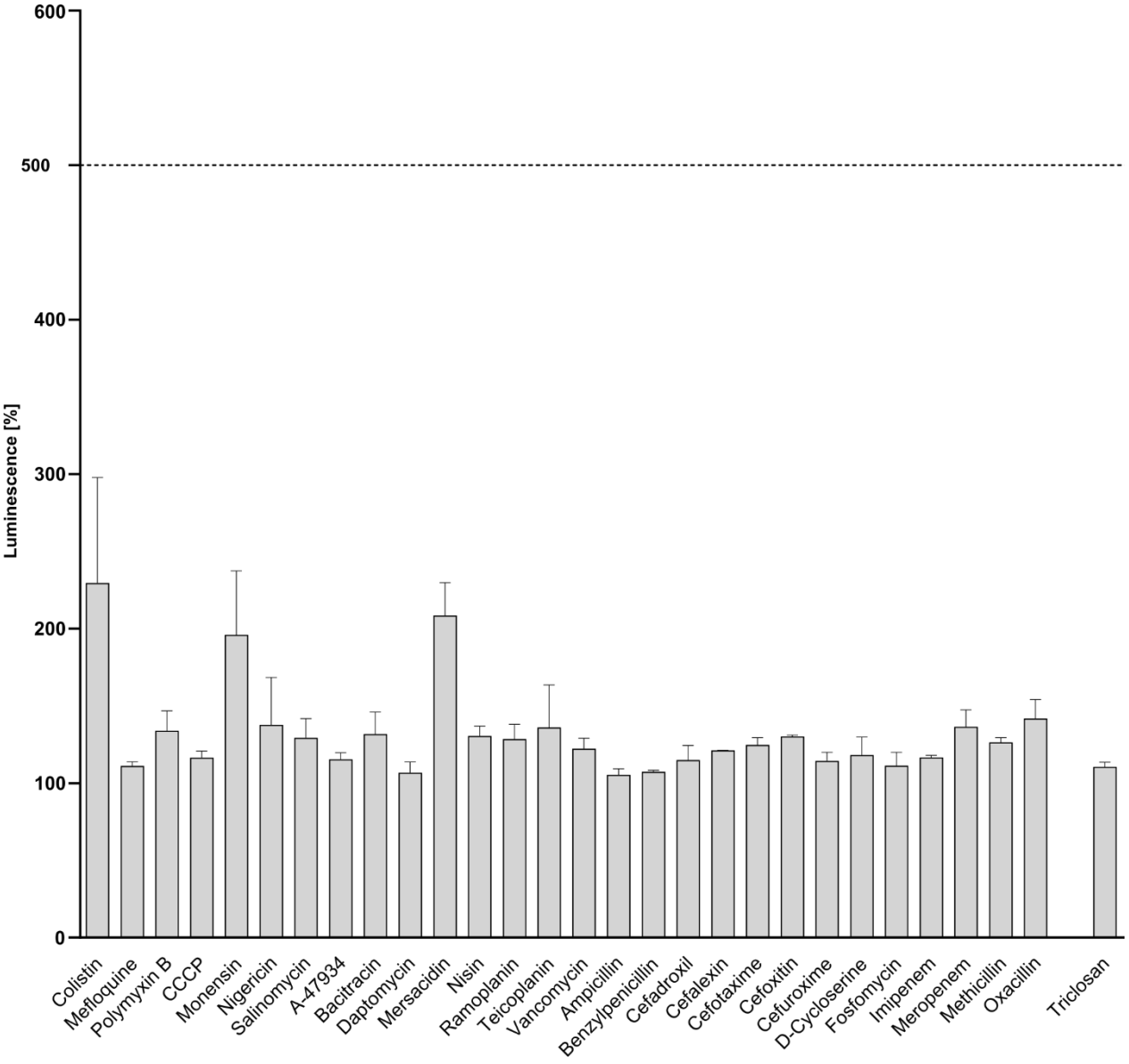

Fig. S3. P_{clpE}-lux bioreporter validation using cell envelope inhibitors and fatty acid synthesis inhibitors. Quantitative bioreporter induction by reference compounds in the liquid assay format. The compounds correspond to those summarized in Table S4 and include cell membrane disruptors, ionophores, lipid-II cycle inhibitors, peptidoglycan synthesis enzyme inhibitors, and the fatty acid synthesis inhibitor triclosan. Compounds were tested in two-fold serial dilutions, from below to above their minimal inhibitory concentrations (MIC). Luminescence and OD_{600} (cell mass) were monitored for 180 min, and induction was normalized to the baseline luminescence of the untreated control (100%) and the OD_{600}. The induction threshold was defined as ≥500% luminescence within 90 min of antibiotic exposure (black dotted line). Bars represent maximal normalized luminescence (mean ± SD) from independent biological replicates.

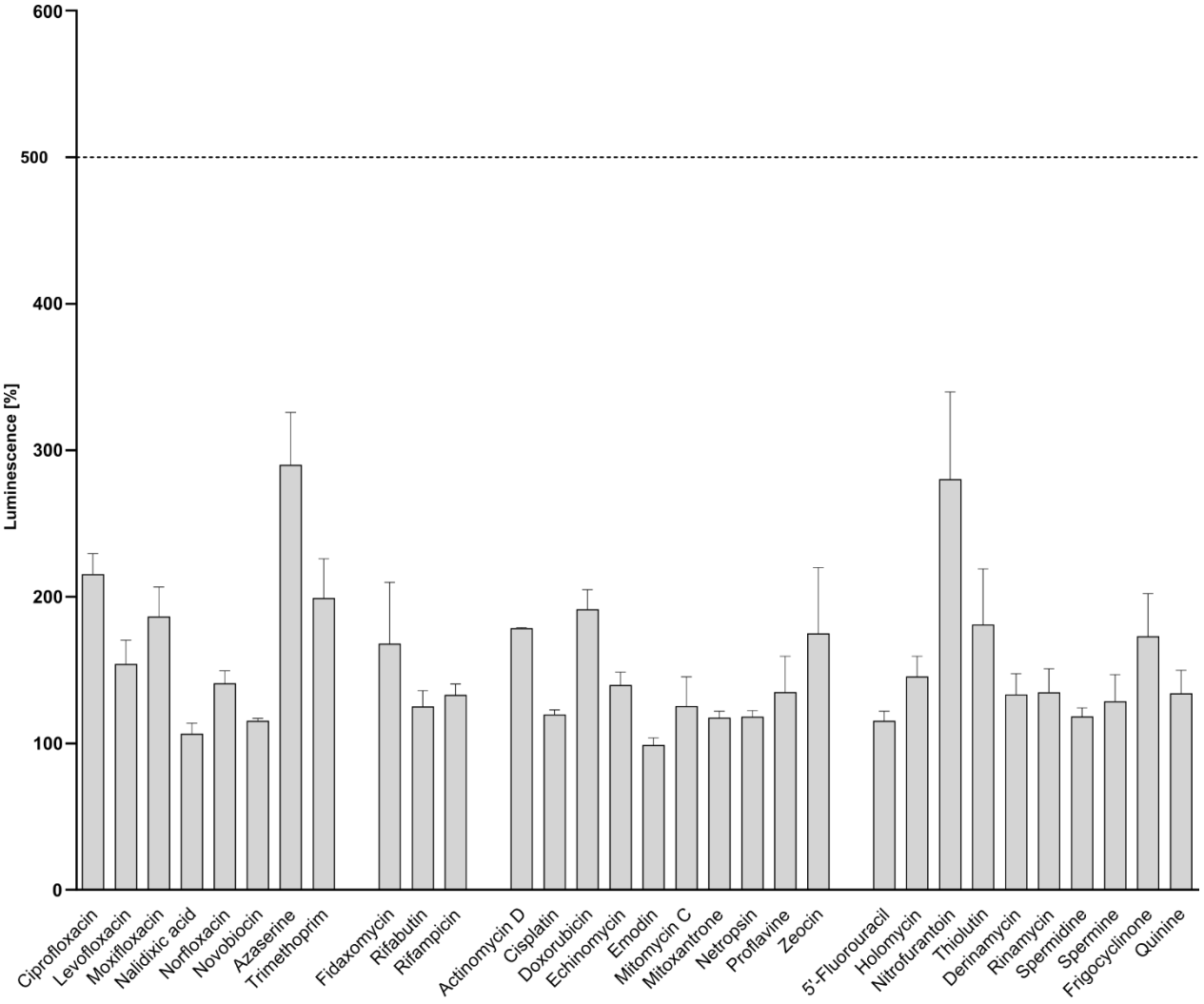

Fig. S4. P_{clpE}-lux bioreporter validation using DNA and RNA synthesis inhibitors, intercalators, and antibacterial agents with diverse MoAs. Quantitative bioreporter induction by reference compounds in the liquid assay format. The compounds correspond to those summarized in Table S4 and include DNA gyrase binders, nucleotide synthesis inhibitors, RNA polymerase binders, intercalators, and compounds with diverse MoAs. Compounds were tested in two-fold serial dilutions, from below to above their minimal inhibitory concentrations (MIC). Luminescence and OD_{600} (cell mass) were monitored for 180 min, and induction was normalized to the baseline luminescence of the untreated control (100%) and the OD_{600}. The induction threshold was defined as ≥500% luminescence within 90 min of antibiotic exposure (black dotted line). Bars represent maximal normalized luminescence (mean ± SD) from independent biological replicates.

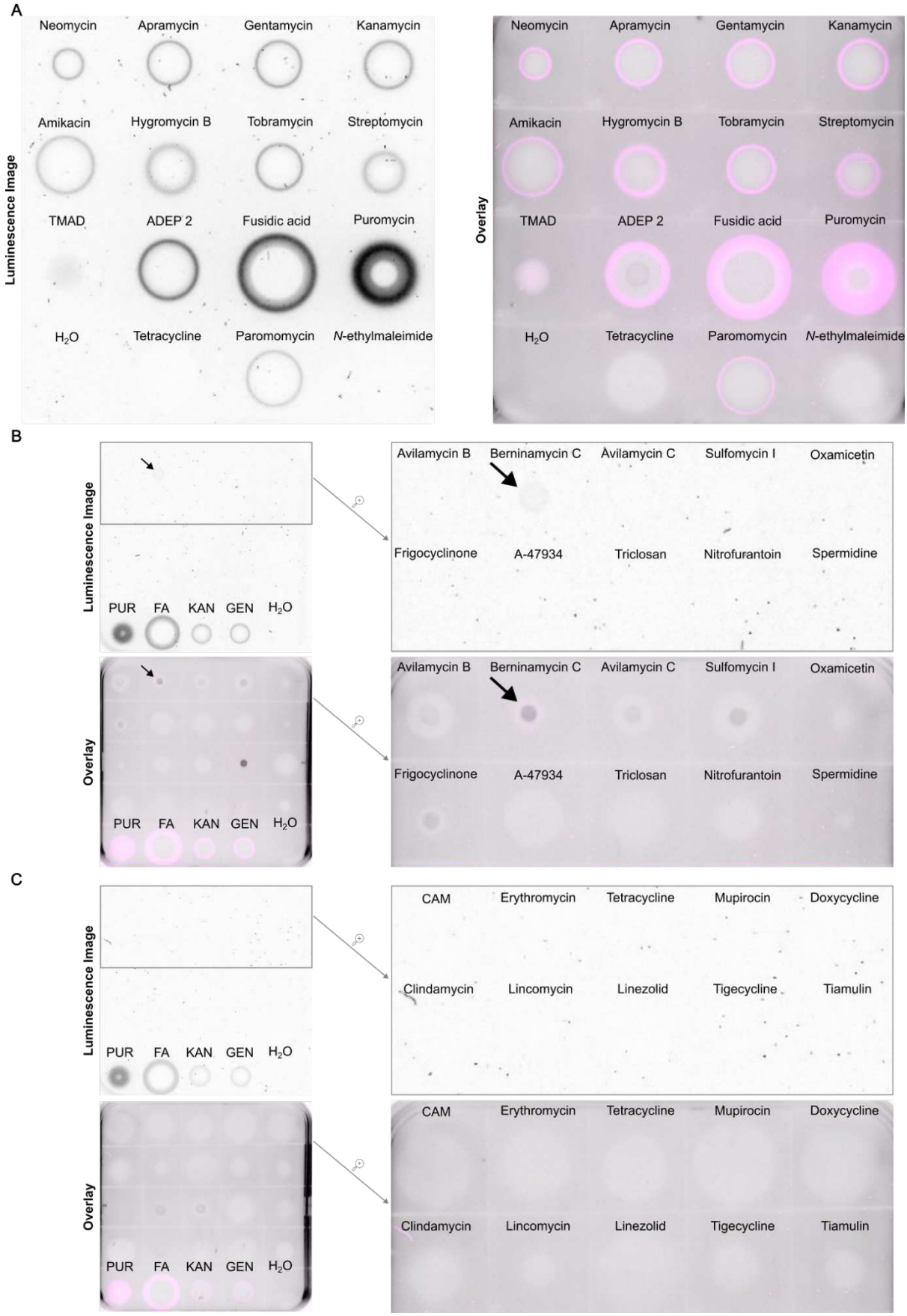
A
Luminescence Image
Neomycin
Apramycin
Gentamycin
Kanamycin
Amikacin
Hygromycin B
Tobramycin
Streptomycin
TMAD
ADEP 2
Fusidic acid
Puromycin
H2O
Tetracycline
Paromomycin
N-ethylmaleimide
Overlay
Neomycin
Apramycin
Gentamycin
Kanamycin
Amikacin
Hygromycin B
Tobramycin
Streptomycin
TMAD
ADEP 2
Fusidic acid
Puromycin
H2O
Tetracycline
Paromomycin
N-ethylmaleimide
B
Luminescence Image
PUR
FA
KAN
GEN
H2O
Avilamycin B
Berninamycin C
Avilamycin C
Sulfomycin I
Oxamicetin
Frigocyclinone
A-47934
Triclosan
Nitrofurantoin
Spermidine
Overlay
PUR
FA
KAN
GEN
H2O
Avilamycin B
Berninamycin C
Avilamycin C
Sulfomycin I
Oxamicetin
Frigocyclinone
A-47934
Triclosan
Nitrofurantoin
Spermidine
C
Luminescence Image
PUR
FA
KAN
GEN
H2O
CAM
Erythromycin
Tetracycline
Mupirocin
Doxycycline
Clindamycin
Lincomycin
Linezolid
Tigecycline
Tiamulin
Overlay
PUR
FA
KAN
GEN
H2O
CAM
Erythromycin
Tetracycline
Mupirocin
Doxycycline
Clindamycin
Lincomycin
Linezolid
Tigecycline
Tiamulin

Fig. S5. Representative agar validation plates. Validation of the P_{clpE}-lux bioreporter using selected reference compounds in the agar-based assay format. Compounds were spotted either directly onto the bioreporter lawn or applied on filter discs in a 4 × 4 (A) or 5 × 5 (B, C) grid and imaged after 180 min. For each agar plate, both the luminescence image (labeled “luminescence image”) and a corresponding overlay image (labeled “overlay”), in which the luminescence image is superimposed in pink onto the epi-luminescence image showing growth inhibition zones, are presented. Selected reference compounds include established proteotoxic stress inducers, non-inducing compounds, and the unexpected inducers fusidic acid and berninamycin C, as well as water (H_2O) as a negative control. The same set of reference compounds was applied to each plate, including puromycin (PUR), fusidic acid (FA), kanamycin (KAN), and gentamicin (GEN). In panels (B) and (C), regions of the agar plates are enlarged to better visualize the weak induction observed for berninamycin C, the absence of induction for avilamycin B and C in the agar-based set-up (while the avilamycin B and C both induced in the liquid setup, Fig. 1 and Fig. S2), and the lack of detectable luminescence on agar for non-inducing reference compounds despite visible zones of growth inhibition.

Based on our prior experience with various bioreporter strains, most inducing agents produce detectable signals in liquid and solid media, but we also encountered exceptional agents that produce signals only in one of these setups.[1] This observation was not specific to the P_{clpE}-lux bioreporter but applied to other bioreporters as well. Such differences may reflect variations in bacterial physiology under these distinct growth conditions, resulting in differential sensitivity to certain compounds or divergent coping mechanisms of the bioreporter strain in these setups.

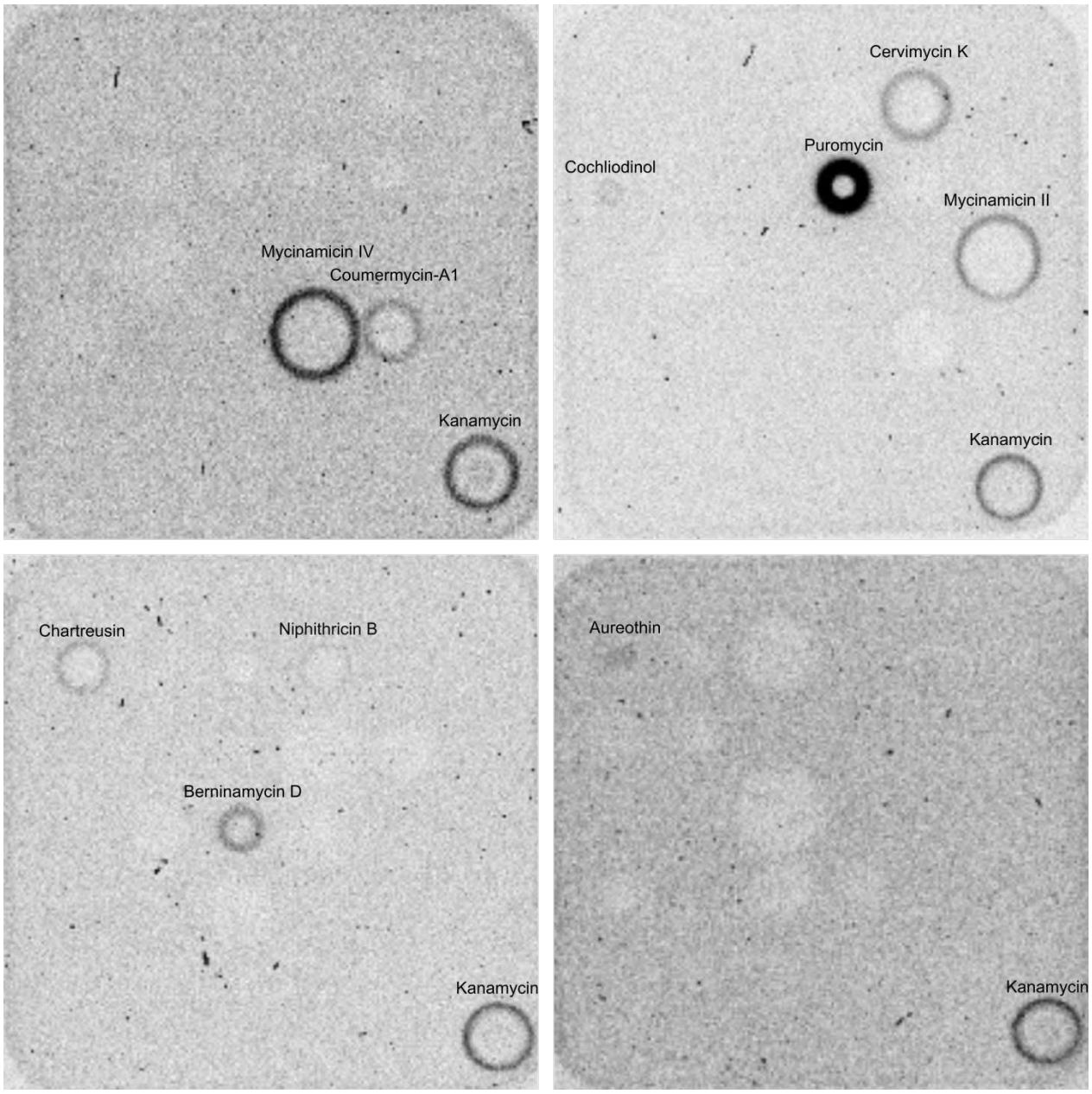

Fig. S6. Exemplary screening plates from the DZIF library. The compounds were directly spotted onto the bioreporter lawn in a 5 × 4 grid, with kanamycin included as a positive control in the bottom-right corner of each plate. Full, uncropped luminescence images of four representative screening plates are shown, acquired after 180 min. Displaying the complete plates allows direct comparison of inducing and non-inducing compounds. Natural variations in background noise arise from the intrinsic properties of the CCD detector (including readout noise and dark current), which become more prominent at low overall signal levels.

Rank	Molecular Formula	Adduct	Zodiac Score	Sirius Score (normalized)	Isotope Score	Tree Score	Explained Peaks	Total Explained Intensity	Median Mass Error (ppm)	Median Mass Error (mDa)
1	C19H34N8O8	[M + H]+	NaN	99,237%	6,219	89,139	49/49	97,955%	1,314	0,255
2	C18H38N4O12	[M + H]+	NaN	0,696%	5,312	85,085	48/49	97,738%	3,461	0,509
3	C24H34N6O6	[M + H]+	NaN	0,067%	2,728	85,332	49/49	97,955%	1,032	0,174
4	C23H38N2O10	[M + H]+	NaN	0,000%	4,371	77,713	47/49	97,463%	-1,400	-0,306
5	C27H35FN2O6	[M + H]+	NaN	0,000%	1,655	63,760	42/49	91,839%	0,727	0,144
6	C16H35FN8O9	[M + H]+	NaN	0,000%	5,878	43,926	32/49	90,650%	1,408	0,259
7	C17H39N6O9P	[M + H]+	NaN	0,000%	5,681	43,443	32/49	90,650%	1,408	0,259
8	C15H30N14O6	[M + H]+	NaN	0,000%	4,272	43,559	32/49	90,650%	2,661	0,370
9	C17H33F3N8O6	[M + H]+	NaN	0,000%	4,882	42,463	32/49	90,650%	2,661	0,370
10	C20H30N12O4	[M + H]+	NaN	0,000%	5,751	40,048	30/49	89,150%	1,489	0,250

Fig. S7. SIRIUS 6 ranking of candidate molecular formulas for the ion at *m/z* 503.2580. C19H34N8O8 is ranked as the most probable formula.

Fig. S8. SIRIUS 6 ranking of candidate structures for the ion at *m/z* 503.2580. STP F is ranked as the most probable structure.

A Putative structure of STP F +2Ac

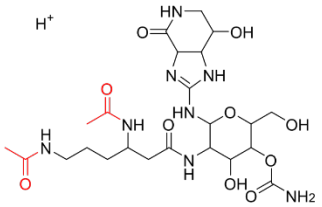

Chemical Formula: $C_{23}H_{39}N_8O_{10}^+$
Exact Mass: 587.2784

B Putative fragments (acetylation sites in red)

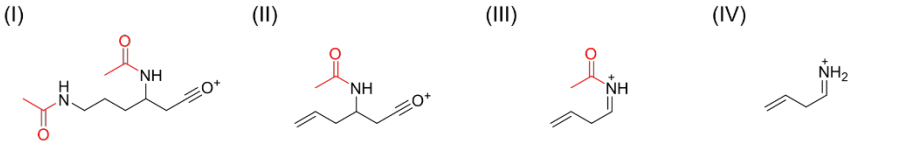

(I) Chemical Formula: $C_{10}H_{17}N_2O_3^+$ Exact Mass: 213.1234

(II) Chemical Formula: $C_8H_{12}NO_2^+$ Exact Mass: 154.0863

(III) Chemical Formula: $C_6H_{10}NO^+$ Exact Mass: 112.0757

(IV) Chemical Formula: $C_4H_8N^+$ Exact Mass: 70.0651

C

Calcd. Mass [Da]	Found Fragments [*m/z*]	Mass Error [ppm/mDa]	Explanation
587.2784	587.2755	-4.94/2.9	Parent mass
213.1234	213.1234	0.00/0	Putative fragment (I)
171.0877	171.0877	0.00/0	STP reporter ion
154.0863	154.0863	0.00/0	Putative fragment (II)
112.0757	112.0760	2.68/0.3	Putative fragment (III)
70.0651	70.0658	9.99/0.7	Putative fragment (IV)

Fig. S9. STP F +2Ac prediction. A) Putative structure of STP F with two acetylation sites on both primary amines of the β-lysine moiety. The mass was confirmed on MS1 level with a mass error of 0.00 ppm. B) Putative fragments for the doubly acetylated β-lysine moiety. Acetylation sites are highlighted in red. C) Overview of the calculated and found *m/z* for the MS2 of 587.2784. Apart from the reporter ion for streptothricins (171.0877), four distinct fragment ions matching the predictions were found.

References

(1) Geibel, C.; Schubert, J.; Knoblauch, S. B.; Hernandez, A.; Boldt, L.; Schneider, D. C.; Papadopoulos Lambidis, S.; Vitale, G. A.; Fleischer, J.; Haussmann, M.; Gross, H.; Wang, M.; Brötz-Oesterhelt, H.; Petras, D. High-Frequency Microfluidic Fractionation for Compound-Resolved Bioactivity-Based Metabolomics. *Anal. Chem.* **2025**, *97* (43), 24093–24104. https://doi.org/10.1021/acs.analchem.5c04612.

GENERAL DISCUSSION

A New Generation of Bioreporters for MoA-Informed Screening

Design and establishment of the new bioreporter panel

The introduction of a new panel of bacterial luciferase-based bioreporters was a central aspect of the development of the bioreporter-guided antibiotic discovery and dereplication platform. Consistent with previously established firefly luciferase- and β-galactosidase-based bioreporter constructs,[83,84] the Gram-positive model organism *B. subtilis* was again used as the strain background for the new panel. Its rapid growth, broad antibiotic susceptibility, and well-characterized physiological stress responses to antibiotics allow reliable bioreporter-based MoA profiling, which is often transferable to clinically relevant pathogenic species.[81,83,88] The use of a sporulation-deficient strain variant[89] further supports applications of the bioreporters in laboratory processes and equipment, including automated and high-throughput screening workflows, without the risk of contamination by heat-resistant endospores. The novelty of the bioreporter panel constructed in the current study lies in the use of a bacterial luciferase operon from *Photorhabdus luminescens*, which enables time-resolved characterization of antibiotic-induced stress responses. The operon encodes both the heterodimeric luciferase and the fatty acid reductase complex required for endogenous substrate synthesis.[90] This supports sustained luminescence production without the need for external substrate addition. At the same time, it allows continuous measurement of bioreporter activity and bacterial growth in a closed system under stable growth conditions. By normalizing the measured luminescence signals to baseline expression and bacterial growth, it is possible to detect inductions even in highly stressed and growth-impaired cells, thereby reducing the likelihood of false-negative results. Furthermore, including growth as an additional detection parameter improves the interpretation of antibiotic effects, making it comparable to that of growth curves and minimum inhibitory concentration (MIC) assays. In contrast, firefly luciferase-based systems depend on the addition of external luciferin and do not account for changes in cell viability.[83] Moreover, the externally added luciferin is rapidly consumed, limiting these systems primarily to single-time-point measurements. Similarly, β-galactosidase-based systems require the addition of a chromogenic substrate to generate a measurable signal. This typically results in the irreversible formation of a blue-colored reaction product, which

prevents a dynamic or time-resolved readout.[84] Additionally, the widespread presence of endogenous β-galactosidases in natural isolates can limit the applicability of these systems for screening natural producer strains or crude extracts,[91,92] as β-galactosidase activity from the tested strains can generate false-positive signals. Finally, the bacterial luciferase-based bioreporter constructs can be applied in both liquid and solid assay formats, allowing a direct comparison of induction profiles across different growth conditions and providing additional bioactivity information. This strategy is especially useful for bioreporter-guided screening or dereplication campaigns, where initial agar-based screening is complemented by quantitative bioactivity analysis of isolated compounds in the liquid-based assay.

The two complementary screening assays that were developed for this bioreporter panel are consistent with the methodical approach used in previous bioreporter systems.[83,84,90,93] For each assay, key experimental parameters were optimized to enhance induction sensitivity and reduce background luminescence. The agar-based approach is an efficient entry point for antibacterial screening efforts due to its simplicity and scalability. Its main advantage is the ability to process large numbers of samples in parallel, achieved through agar-based diffusion gradients that enable simultaneous screening with a single time-point luminescence readout. The assay is compatible with a wide range of sample types, including pure compounds, crude extracts, and natural producer strains, without requiring prior purification or extensive sample processing. This is particularly advantageous in large-scale screenings, as it significantly accelerates the overall workflow (Publication II). In contrast, the liquid-based approach provides higher quantitative resolution, especially for semi-purified extracts or pure compounds. Here, luminescence signals are continuously measured through several generations of exponential growth to obtain a detailed view of the bacterial stress response. The readout times for each format were selected based on the validation data from both publications and generally align with the time points used in corresponding firefly-based constructs.[83] This approach is also consistent with previous transcriptomic analyses that provided the foundation for bioreporter design, where antibiotic-induced expression profiles were analyzed after 10 and 40 min of antibiotic treatment.[81] Importantly, this early detection of bioreporter signals considerably accelerates compound discovery compared with

traditional screening approaches that typically read out bioactivity overnight.[14–16] Of note, extending the incubation beyond the defined readout window generally resulted in nonspecific luminescence signals for both inducing and non-inducing reference compounds. As these effects were observed across the entire bioreporter panel to varying degrees, they most likely reflect general stress responses or changes in gene regulation associated with nutrient depletion or the transition into the stationary growth phase.[94,95] Finally, it is important to emphasize the enhanced detection capability of the bioreporter technology compared with classical bioactivity assays. Traditional screening methods are often limited in their ability to detect weak bioactivities,[96] despite the importance of such signals for identifying previously overlooked candidates. The increased sensitivity of the bioreporter approach was demonstrated by (I) the identification of several weak P_{clpE}-lux inducers that did not produce visible inhibition zones and would have been overlooked with conventional methods (Publication II), and by (II) the substantially lower limit of detection (LOD) of the established bioreporters compared to classical inhibition zone assays (Publication I). Moreover, the bioreporter approach enables the detection of transient or early stress responses, as exemplified by the unusually rapid induction of the P_{clpE}-lux bioreporter by NEM (Publication II), which would not have been identified with conventional firefly-based bioreporters.

The second essential aspect of this thesis was to expand the bioreporter panel and address an important gap in its mechanistic coverage. The rationale for developing the P_{clpE}-lux bioreporter was the observation that the established protein synthesis biomarker *bmrC* reliably detects translation arrest but does not respond to proteotoxic stress resulting from mistranslation, protein misfolding, or other forms of protein damage.[83,84] The newly developed proteotoxic stress bioreporter P_{clpE}-lux now enables the detection of antibiotic-induced accumulation of damaged or misfolded proteins, a fundamental mechanism shared by many antibacterial compounds, including clinically relevant aminoglycosides.[97] Given the specific and complementary activation profiles of the P_{bmrC}-lux and the P_{clpE}-lux bioreporters, the bioreporter panel can distinguish between protein-synthesis stalling and proteotoxic stress, and offers mechanistic insights for compounds that induce both biomarkers (Publication II). Importantly, P_{clpE}-lux helps to address the substantial rediscovery and dereplication burdens associated with commonly

encountered bioactive compounds, such as streptomycin or streptothricin (STP), in natural product screenings (Publication II). These compounds can now be detected early and filtered out, freeing up dereplication capacity to focus on novel bioactive molecules.

The marked specificity of the P_{clpE}-lux bioreporter is consistent with the exclusive expression of ClpE under severe stress conditions, including heat-shock or puromycin treatment.[98,99] Furthermore, because the *clpE* promoter region is tightly regulated by four CtsR DNA-binding domains, this results in constitutive repression under normal growth conditions,[100,101] in line with the generally low basal expression levels observed for the bioreporter. Upon induction, ClpE associates with the proteolytic core ClpP to form the ClpEP protease complex. This complex is essential for maintaining protein quality control and helps restore cellular proteostasis through the degradation of damaged or misfolded proteins.[98–100,102] Additionally, ClpE is crucial for degrading CtsR during the initial heat-shock response, thereby enabling effective derepression of CtsR-regulated genes.[98,103] Given its physiological role, stringent promoter regulation, and highly specific induction in response to the accumulation of damaged or misfolded proteins, *clpE* is an ideal biomarker for detecting protein stress in bacterial cells. Notably, during the search for a candidate proteotoxic stress biomarker, the major heat-shock chaperone DnaK was also investigated, as transcriptomic data indicated a distinct response to aminoglycosides.[81] Similar to ClpE, DnaK plays a central role in the heat-shock stress response, contributing to protein homeostasis, regulation of gene expression, protein folding, membrane translocation, and the degradation of misfolded proteins.[104,105] However, extensive validation experiments and induction profile analyses demonstrated that the P_{dnaK}-lux bioreporter exhibits limited specificity, providing only weak discrimination between predicted inducers and non-inducing compounds (unpublished data by K.W. Wex, A. Berscheid, and the author). This is likely attributable to the comparatively high basal expression of *dnaK*, which aligns with its essential housekeeping function and its relatively weak repression by the autoregulatory transcriptional repressor HcrA.[106–108] This ultimately led to the discontinuation of the P_{dnaK}-lux bioreporter, although it still remains a useful secondary positive control for proteotoxic stress.

The current bioreporter panel now covers the major biosynthetic processes or molecular structures commonly targeted by antibiotics,[27] including fatty acid synthesis (P_{fabHB}-lux),

DNA and folate synthesis (P_{yorB}-lux), cell envelope integrity (P_{ypuA}-lux), lipid II cycling (P_{lial}-lux), translation arrest (P_{bmrC}-lux), and proteotoxic stress (P_{clpE}-lux). In a complementary study, the corresponding RNA stress bioreporter (P_{yppS}-lux) was developed by K.W. Wex. The broad coverage further ensures that, even in the absence of bioreporter induction, mechanistic insights are provided by narrowing the range of possible MoAs. In these cases, the activity may be related to mechanisms not yet represented within the panel, such as ionophore-mediated disruption of cellular ion gradients, or it may indicate an unusual and novel mechanism that requires further MoA profiling.

Mechanistic validation of the bioreporter panel

The bioreporter panel was validated in both the solid- and liquid-assay formats using a curated set of antibacterial reference compounds covering a broad range of mechanistic interactions. Consistent with the established MoAs of the reference compounds, the bioreporters exhibited sensitive and selective induction profiles that closely matched those of previously established firefly-luciferase[83] and β-galactosidase-based bioreporter constructs[84]. Briefly, in accordance with the physiological role of FabHB as a key enzyme in fatty acid biosynthesis,[82,109] the P_{fabHB}-lux bioreporter was induced exclusively by the fatty acid synthesis inhibitors triclosan[59] and cerulenin[57,58]. Likewise, the bioreporter P_{yorB}-lux responded selectively to DNA gyrase inhibitors, nucleotide synthesis inhibitors, DNA-intercalating agents, and the pleiotropic antibiotic nitrofurantoin, which is known to induce DNA damage[110,111]. Although the precise function of YorB has not been fully elucidated, the observed P_{yorB}-lux induction profile is consistent with its involvement in the DNA damage-responsive regulatory LexA network.[82,83,112] A deviation from the expected induction pattern was the absence of P_{yorB}-lux activation by the nucleotide synthesis inhibitor sulfamethoxazole[113] in the liquid-assay format. At this point, we have no clear explanation for this discrepancy. A potential contributing factor may be the previously reported influence of medium composition on sulfonamide activity, where exogenous metabolites have been suggested to modulate antifolate efficacy.[114,115] This effect might be more pronounced under liquid cultivation conditions, as robust inductions by sulfamethoxazole have been observed in the agar-based assay setup.[84,85] Repeating the assay in minimal medium may help determine whether nutrient limitation and reduced

growth rates enhance the bioreporter response to sulfamethoxazole in liquid culture. Similarly, although the native function of YpuA remains unknown, the protein is associated with the SigM regulon and is generally considered part of the cell envelope stress response.[82,116] Accordingly, P_{ypuA}-lux detected compounds that disrupt peptidoglycan biosynthesis and compromise cell membrane integrity. Consistent with previous studies,[84] secondary inductions were also observed for several DNA-active compounds, including DNA gyrase inhibitors and nucleotide synthesis inhibitors. This secondary response may be associated with the SOS-induced cell division inhibitor YneA, which interferes with septal cell wall synthesis and cell division by interacting with peptidoglycan and late divisome proteins following DNA damage.[117] Notably, the ionophore salinomycin[118] induced P_{ypuA}-lux in both assay formats. To follow up on this observation, salinomycin could be tested with the corresponding P_{ypuA}-lacZ bioreporter, since this compound was not included in the validation panel of the β-galactosidase-based constructs.[84] Nevertheless, a general induction of *ypuA* by ionophores can be excluded, since the β-galactosidase bioreporter panel included several ionophores, such as gramicidin A, nigericin, monensin, and valinomycin, none of which produced a bioreporter response.[84] The P_{lial}-lux bioreporter displayed selective induction in response to peptidoglycan precursor binders and cell membrane-disrupting agents, in line with the established role of LiaI within the LiaRS-controlled cell envelope stress response.[84,93] However, the absence of a P_{lial}-lux induction by the glycopeptides vancomycin and teicoplanin[119] in the agar-based assay is contrary to previous observations with the P_{lial}-lacZ bioreporter[84] and warrants further investigation into potential construct-specific effects. Although identical stress-responsive promoter regions were used in the new and the previously established constructs, differences may arise from the modified strain background. In this work, a rifampicin-resistant derivative of *B. subtilis* was used because the previous strain background exhibited an undefined aminoglycoside resistance (preliminary study by K.W. Wex). The translational arrest bioreporter P_{bmrC}-lux, based on the multidrug ABC transporter subunit BmrC, was induced by reference antibiotics that cause translational arrest through diverse mechanisms, including inhibition of translation initiation and tRNA binding, interference with the peptidyl transferase reaction and elongation factors, and obstruction of the peptide exit tunnel.[83,84,120] In contrast, P_{bmrC}-lux did not respond to compounds associated with proteotoxic stress, confirming the specificity of the *bmrC*

promoter for translational arrest[83,84] and underscoring the importance of expanding the bioreporter panel with the P_{clpE}-lux bioreporter.

The novel P_{clpE}-lux bioreporter exhibited sensitive induction in response to all reference compounds whose established MoAs involve the generation of proteotoxic stress, consistent with the physiological role of ClpE discussed earlier. These compounds can be broadly divided into two groups based on their dependence on ribosomal interaction. The first group includes antibiotics with a ribosome-dependent MoA, such as puromycin[74] and aminoglycosides[72], which require interaction with the ribosome to exert their antibacterial activity. Interestingly, although aminoglycosides consistently induced the P_{clpE}-lux bioreporter, the intensity of induction varied among individual compounds, highlighting the ability of the bioreporter to distinguish subtle mechanistic differences within this antibiotic class. While aminoglycosides share a conserved MoA and collectively target the A-site of the 30S ribosomal subunit, structural differences can influence binding interactions and affinities. These differences likely affect the extent of translational misreading and, consequently, the level of the induced bacterial stress response.[73] In addition to ribosomal binding characteristics, differences in cellular uptake kinetics likely contribute to variations in intracellular compound concentrations and the resulting level of proteotoxic stress. Overall, the atypical aminoglycoside hygromycin B produced the weakest P_{clpE}-lux induction. This observation is consistent with its reported mechanism as a ribosomal translocation inhibitor that primarily induces ribosome stalling, while translational misreading occurs only as a secondary effect.[121,122] Notably, this also aligns with the general induction of *bmrC* by hygromycin B, the only aminoglycoside that exhibits this pattern.[84] The second group of proteotoxic stress inducers includes compounds such as ADEPs,[75,76] NEM,[77] and TMAD,[123] which generate protein damage independently of ribosomal involvement. While deregulation of Clp protease activity represents a mechanistic interaction unique to the ADEP antibiotics, thiol-reactive structural moieties similar to those found in maleimides are also present in numerous other antibacterial compounds. Such structural features can likewise promote covalent modification of cysteine residues or disulfide cross-linking, thereby inducing proteotoxic stress. Consequently, the P_{clpE}-lux bioreporter may also be useful for identifying compounds with

thiol-reactive properties and for distinguishing structurally related representatives within the same antibiotic class based on the presence of these reactive moieties.

Importantly, the P_{clpE}-lux bioreporter exhibited high selectivity for proteotoxic stress, as no induction was observed in response to reference compounds targeting DNA replication, RNA transcription, cell wall biosynthesis and integrity, or fatty acid biosynthesis, nor to most ribosome-stalling antibiotics. An unexpected finding was the induction of P_{clpE}-lux by four ribosome-acting agents not previously linked to proteotoxic stress, namely berninamycin C,[124] avilamycin B and C,[125] and fusidic acid[70]. As these compounds were previously characterized as translation stallers, the observed P_{clpE}-lux activation suggests either yet unrecognized mechanistic aspects or secondary effects that lead to the accumulation of damaged or misfolded proteins, as discussed in detail in Publication II. Although bioreporter induction alone does not directly reveal the underlying MoA, it provides a mechanistic hypothesis for subsequent investigations. Given that the induction levels substantially exceeded the predefined threshold and that other translation stallers did not activate the P_{clpE}-lux bioreporter, a nonspecific or artifactual response appears unlikely. This interpretation is further supported by the observation that bioreporter induction was restricted to specific representatives within individual antibiotic classes, whereas structurally related compounds that share the same primary MoA did not elicit comparable responses. For instance, although the thiopeptide berninamycin C produced a strong P_{clpE}-lux response, other representatives of this class, such as thiostrepton and sulfomycin I, did not induce the bioreporter. Interestingly, although all tested thiopeptides contain a thiol-reactive dehydroalanine moiety, only berninamycin C induced proteotoxic stress, making it a notable exception in this class, likely due to its higher thiol reactivity. Evaluating additional thiopeptides, such as nosiheptide[126], or other berninamycin congeners, may provide further insight into structural and mechanistic differences among thiopeptides. Similarly, further characterization of the observed induction for avilamycin B and C could include testing other orthosomycins such as evernimicin, which also binds the 50S ribosomal subunit and prevents interactions with initiation factor 2.[127,128] Promising candidates for comparison with fusidic acid include alternative EF-G binders, such as the cyclic octapeptide argyrin B, which inhibits protein synthesis by trapping EF-G on the ribosome during translocation.[129] Nevertheless,

complementary assays are required to further elucidate how these compounds promote proteotoxic stress, including ribosome and polysome profiling, in vitro translation, and toeprinting assays.[130–132] In addition, follow-up studies could investigate the connection between the unexpected P_{clpE}-lux induction and potential bactericidal effects in *B. subtilis*. Since translation stallers are typically bacteriostatic, time-kill analyses may help determine whether proteotoxic stress represents an additional bactericidal facet of their MoA.

Following the extensive validation, the P_{clpE}-lux bioreporter was used to identify additional proteotoxic stress inducers within a subset of the DZIF natural product library. In addition to rediscovering known proteotoxic stress inducers, including puromycin, cervimycin K,[133] and naphthomycin,[134] multiple compounds not previously associated with proteotoxic stress were identified, as discussed in detail in Publication II. To further characterize these compound-specific effects, transcriptomic profiling could be combined with established proteotoxicity assays, including the quantification of protein aggregation and the analysis of heat-shock and chaperone response induction.[103,135,136] Interestingly, several of the unexpected inducers were again translation inhibitors that carry thiol-reactive structural moieties that may cause proteotoxic stress, such as the macrolides mycinamicins and pikromycin. In addition, multiple chartreusin derivatives induced the P_{clpE}-lux bioreporter, extending previous findings that this compound class activates a broad range of bioreporters (DNA, RNA, and translation arrest).[84] Notably, chartreusin displays the broadest bioreporter induction profile observed by us to date and appears to promote distinct stress responses in a concentration-dependent manner. High concentrations are required to induce the translation arrest bioreporter, whereas DNA- and RNA-associated stress responses are detectable over a wide concentration range.[84] As these results were obtained in the agar-based assay, which relies on the diffusion of chartreusin within the agar, it would be interesting to repeat this analysis in liquid using the new bioreporter panel. This would enable a quantitative assessment of individual bioreporter inductions at defined chartreusin concentrations and help determine the effect of chartreusin on the P_{clpE}-lux bioreporter. The pleiotropic MoA of chartreusin has been reported to involve the inhibition of polypeptide chain elongation by impairing aminoacyl-tRNA binding.[137,138] However, while complete inhibition of aminoacyl-tRNA binding by antibiotics such as tetracycline does not induce a proteotoxic stress response, compounds that promote

mistranslation by allowing incorrect amino acids to bind the decoding center, such as aminoglycosides, cause proteotoxic stress. One possible explanation for the observed P_{clpE}-lux induction by chartreusin could be that, at certain compound concentrations, aminoacyl-tRNA binding to the A-site is impaired but not completely abolished, a hypothesis that requires further validation.

Collectively, the mechanistic validation of the novel bioreporter panel demonstrated the high specificity of the individual bioreporters and the increased coverage achieved through the inclusion of P_{clpE}-lux. Furthermore, the results highlight the utility of the bioreporter panel for identifying mechanistic differences and secondary stress responses that may remain undetected in conventional target-based assays, which typically focus on single enzyme reactions or individual metabolic steps. Of note, although the reference panel included a diverse set of antibacterial compounds, it did not cover representatives of all antibiotic classes. As the induction thresholds in the liquid assay were determined empirically from the current validation dataset, further refinement may be necessary as additional inducing and non-inducing compounds are tested in future studies.

A Bioreporter-Guided Platform for Antibiotic Discovery and Dereplication

Platform design and bioreporter implementation

The development of the bioreporter-guided antibiotic discovery and dereplication platform was a central objective of this thesis. This platform addresses a common limitation in traditional dereplication workflows, namely the disconnect between bioactivity data, early mechanistic insights, and the chemical identity of the corresponding analyte. By integrating these aspects into a single workflow, it supports the rapid identification and preliminary mechanistic characterization of bioactive metabolites. At its core, the platform combines non-targeted liquid chromatography with high-resolution microfractionation, compound-resolved MS/MS data, and an efficient bioreporter readout. Additionally, bioreporter-guided molecular networking of the underlying MS/MS dataset enables rapid dereplication of structurally related compounds. For implementing the bioreporter panel into the platform, several challenges had to be addressed to ensure reliable signal detection. Sufficient analyte deposition in each microspot was an essential prerequisite for the bioreporter readout, as local concentrations determine whether a measurable

signal is generated after microspotting. Accordingly, the splitting ratio of the column eluent was carefully regulated to provide enough material for the collection of high-quality MS/MS data and the simultaneous microfractionation. In this context, the chromatographic conditions for each sample type were also individually adjusted to yield well-resolved peaks. During validation, broad or poorly resolved chromatographic peaks generally resulted in analyte redistribution between adjacent microspots, often reducing local concentrations below the threshold required to elicit a measurable bioreporter response. The same problem occurs for samples containing low concentrations of bioactive metabolites, as observed during natural producer screening (Publication II). In such cases, the signal intensity can be enhanced by concentrating the extract, injecting larger volumes, or repeatedly spotting the same sample on a single µPAD. However, repeated spotting may result in slight peak shifts within one to two microspots that need to be accounted for when assessing the bioreporter signals. Likewise, the physicochemical properties of the sample influenced the overall workflow. For instance, highly hydrophilic compounds such as STP are not effectively retained by conventional reversed-phase chromatography and elute undetected from the column in the dead volume (Publication II). Another challenge was integrating the µPAD into the bioreporter workflow. As organic solvents drastically impair cell viability and lead to false-positive bioactivity signals, a critical step in the workflow was the removal of organic residues deposited during microfractionation. The necessary drying step, however, renders the µPAD uneven and prone to wrinkling. Consequently, an additional rehydration step was introduced, during which the µPAD was flattened on a thin layer of cell-free agar to remove surface irregularities and trapped air bubbles. In practice, incomplete or uneven coverage of the bioreporter layer led to distorted luminescence signals. To prevent diffusion of the analytes into the underlying agar layer during this step, hydrophobic caps were printed on the reverse side of the µPAD, providing an additional diffusion barrier that confines the analytes within the microspots.

Following the successful integration of the bioreporters, the chromatographic resolution of the luminescence signals and the accuracy of compound identification in the combined workflow were validated (Publication I). Using a defined mixture of different reference antibiotics confirmed that (I) the platform efficiently separates and identifies individual antibiotics within a single sample and (II) it generates baseline-separated luminescence

regions corresponding to the sequential elution for each reference compound, even when they induce the same bioreporter. For instance, when multiple bioactive compounds co-elute, this often leads to overlapping luminescence regions on the µPAD. Even in such cases, compound identification remains unambiguous based on peak shape and MS analysis (e.g., STPs, Publication II). The practical applicability of the workflow was further evaluated using a complex extract from a natural producer strain to resemble a realistic dereplication workflow. In addition to the reliable detection of erythromycin A as the primary bioactive metabolite, molecular networking revealed multiple related metabolites clustering with erythromycin A. This highlights the ability of the platform to identify structurally related derivatives beyond the initially detected bioactivity. As discussed in Publication II, molecular networking was particularly valuable for dereplicating the extensive network of STP derivatives and for the discovery of several putatively novel analogues. Across both validation approaches, variations in analyte concentrations along the chromatographic separation were reflected by corresponding changes in inhibition zone size and luminescence intensity. These observations allow the analyte distribution on the µPAD to be traced visually, providing an approximate overview of the underlying peak shape. This is especially useful for optimizing the chromatographic resolution in the early stages of the workflow without requiring detailed MS data analysis. Of note, luminescence signals generally remained confined to the immediate vicinity of each microspot. The absence of detectable interference or luminescence bleed-through between adjacent rows is essential for minimizing false-positive inductions and for an accurate identification of bioreporter signals. Finally, the LOD of the µPAD-based bioreporter readout was determined and compared to the sensitivity of classical inhibition zone assays. The comparison is particularly relevant because the µPAD is positioned beneath the agar surface, in contrast to conventional assays in which compounds are generally applied onto the bacterial lawn. Although *B. subtilis* is capable of anaerobic growth,[139] the majority of bacterial growth occurs at the agar surface. Consequently, analytes must diffuse through an additional agar layer before reaching the bioreporter cells, which may affect local compound concentrations. Despite this additional diffusion barrier, the µPAD-based LODs for all bioreporters were consistently lower than those obtained with the inhibition zone assay, in agreement with the results of the initial bioreporter validation. For compounds with limited diffusion, reducing the thickness of the

top agar layer may further improve sensitivity, provided that robust luminescence production is maintained.

An important bottleneck of the current platform design is the limited throughput of the imaging step. The use of a conventional gel documentation system restricts processing capacity, as only one µPAD can be measured at a time. To scale up the platform for high-throughput screening, an imaging system specifically adapted to the µPAD format or equipped with a more sensitive detector would be beneficial. Alternatively, the µPAD layout could be modified to increase microspot density. However, this would come at the cost of spatial resolution, as smaller microfractionation compartments may reduce the precision with which individual compounds can be assigned to individual bioactive signals. Another option is to shorten the luminescence readout window. While strong bioreporter signals can usually be detected within a few minutes, weaker signals may be missed at shorter acquisition times. Furthermore, the µPAD was generally not sterile when incubated with the bioreporters. Although the relatively high initial inoculum of bioreporter cells typically outcompetes contamination, prolonged incubation (>3 days) occasionally led to the visible formation of foreign colonies during validation. To minimize these environmental contaminations, the µPAD should be subjected to UV treatment before microspotting, and the spotting process should be performed under sterile conditions, for example, by enclosing the microspotter within a laminar-flow-like protective housing. The microspotter itself operates without direct contact between the µPAD surface and the capillary tip. Discrete droplets are generated from the continuous LC flow and deposited onto the µPAD to reduce the risk of mechanical contamination.

Application of the bioreporter-guided platform for natural product discovery

The final aspect of this thesis was the application of the bioreporter-guided platform in a natural producer screening campaign. While evaluating such a labor-intensive workflow was beyond the scope of the initial platform validation (Publication I), the development of the proteotoxic stress bioreporter provided an ideal opportunity to assess the platform under realistic screening conditions (Publication II). For this purpose, a subset of previously uncharacterized natural producer strains from the Tübingen actinomycete strain collection was selected based on prior screening data that demonstrated antibacterial activity against *B. subtilis* but no detectable induction of the previous

bioreporter panel.[84] This curated selection ensured that (I) the strains reliably produce antibacterial metabolites and (II) the likelihood of identifying compounds that induce proteotoxic stress was increased, as this represents a major MoA not covered by the earlier panel. However, the approach inherently excluded strains producing antibacterial metabolites with dual or pleiotropic effects. For example, the natural producers of berninamycin (translation stalling, proteotoxic stress) or chartreusin (DNA and RNA, translation stalling, proteotoxic stress)[84] would be promising candidates for further validation of the P_{clpE}-lux induction profile. In addition, exploring the full bioactive potential of such producer strains using the bioreporter-guided platform might further reveal structurally related congeners, as demonstrated for the erythromycin producer strain (Publication I).

A total of 45 strains produced STP derivatives ranging from STP F to STP B, with STP F and STP D representing the predominant congeners. These observations are consistent with previous reports describing the widespread occurrence of STP-producing actinomycetes and their frequent dereplication in antibiotic screening campaigns.[140,141] As discussed in Publication II, the unexpectedly high degree of acetylation observed in several STP derivatives exceeds the commonly reported monoacetylation of the β-amino group of the β-lysine moiety.[142] Notably, such multiply acetylated congeners have not yet been reported from natural sources. This raises the question of how extended acetylation mechanistically influences the antibacterial potency of the STPs beyond producer self-resistance.[143] The isolation of individual congeners would be required to fully assess their bioactivity, but their low abundance and frequent co-elution with non-acetylated STPs complicate purification. Alternatively, chemical acetylation (e.g., using acetic anhydride) could be considered as a synthetic approach to generate comparable derivatives *in vitro*. However, due to the presence of multiple reactive amino groups, this approach would likely yield heterogeneous mixtures of polyacetylated products, which would again be challenging to resolve chromatographically. Despite these limitations, the observed diversity of acetylated derivatives highlights the value of the platform for uncovering otherwise inaccessible chemical diversity.

In addition to the dereplication of known STPs, several bioactive extracts lacked detectable STP-related compounds within the defined bioactivity window, yet still exhibited

the characteristic diagnostic fragment corresponding to the streptolidine lactam ring. The absence of mass features matching known antibacterial molecules in current databases suggests the presence of previously unreported STP derivatives. To elucidate their structure, the corresponding producer strains could be re-cultured, followed by bioreporter-guided purification and high-resolution structural analysis. Constructing a dedicated molecular network incorporating these extracts alongside authentic STP standards and known derivatives may further reveal structural relationships and site-specific modifications. In addition, screening these strains against a set of reference strains harboring common streptothricin resistance genes, such as streptothricin acetyltransferases,[140] could provide insight into how structural variations or acetylation patterns influence resistance. Further investigation could likewise address the limitation that a single cultivation medium was ultimately selected for the producer strain screening. Since different growth media are known to promote the production of distinct secondary metabolites (OSMAC principle),[144,145] alternative media may reveal additional bioactive compounds. Complementary to the agar-based extraction, selected strains with strong on-plate inductions were cultivated in scaled-up liquid cultures. However, secondary metabolite production varied considerably between cultivations, and no consistent antibacterial activity or reproducible bioreporter signals were observed (data not shown). This led to the discontinuation of the liquid cultivation approach, as robust STP production appeared to be associated with agar-based growth conditions. Of note, a Gram-negative reference strain included in the initial agar-based screening exhibited only limited sensitivity to most producer strains (10/53 strains; data not shown), although STPs are generally active against Gram-negative bacteria.[146,147] This may indicate intrinsic or acquired resistance mechanisms, particularly given that the genome of the reference strain is not fully characterized. To follow up on this, the crude extracts could be tested against a broader panel of Gram-negative strains. Finally, extending the screening workflow to include the corresponding organic fractions could further expand the accessible chemical space. As shown in the publication, bioactivity was mainly detected in the aqueous phase. However, some extracts exhibited bioactivity in the organic phase as well, warranting further investigation. A possible explanation is the presence of residual STPs in the organic extracts due to incomplete phase separation. To verify whether potential unidentified compounds or STPs are responsible for the bioactivity, the extracts

should be separated on a classical reversed-phase column. Since STPs are expected to elute in the dead volume of the column (Publication II), any remaining bioactive signals are likely attributable to non-STP compounds.

GENERAL CONCLUSION

Within the scope of this dissertation, the combined contributions of the two publications resulted in the development of a robust and versatile bioreporter-guided platform for MoA-informed antibiotic discovery and dereplication. Addressing the fundamental limitations of traditional whole-cell screening methods, this work establishes an integrated strategy that combines sensitive bioactivity detection, mechanistic profiling, and analytical dereplication within a single platform. Given the ongoing need for novel antibacterial agents, such mechanism-informed approaches represent an important step towards more efficient antibiotic discovery. Central to this advancement was the construction and validation of a comprehensive stress-responsive bioreporter panel in *B. subtilis*. In particular, the implementation of the proteotoxic stress bioreporter P_{clpE}-lux expanded the mechanistic coverage by capturing a previously unrepresented MoA. This novel bioreporter panel enables sensitive detection of antibiotic-induced stress responses even at subinhibitory concentrations, capturing physiological information that is missed by conventional growth-based assays. Importantly, beyond rapidly identifying established mechanistic interactions, bioreporter inductions provide a rational starting point for targeted follow-up studies of compounds not previously linked to defined MoAs. For example, the unexpected P_{clpE}-lux inducers fusidic acid, berninamycin, and avilamycin are promising candidates for future MoA studies, as discussed earlier. Furthermore, uncharacterized compounds that displayed robust bioactivity and induced the proteotoxic stress bioreporter, such as the antibiotic A 31305-I, warrant further evaluation using the complete bioreporter panel in combination with additional MoA profiling approaches. Finally, integrating the bioreporter panel into the discovery and dereplication platform significantly enhanced its practical utility for natural product screening. The combination of spatially resolved bioreporter activation, chromatographic separation, and MS-based compound identification enables rapid functional classification of bioactive metabolites directly from complex extracts. By assigning localized biological activity to analytical identity in the early stages of the discovery process, the platform reduces rediscovery rates and eases dereplication efforts. The identification of a diverse network of STP derivatives within the Tübingen collection of actinomycete producer strains illustrates both the efficiency of this platform and the importance of rapid functional screening in natural product discovery pipelines. Depositing

this dataset in public repositories supports future screening efforts by enabling early recognition of commonly encountered STP-related features. Furthermore, extending the screening approach to other natural product and producer strain libraries using the complete bioreporter panel will further evaluate the efficiency of the bioreporter-guided platform. In this context, the mechanistic coverage of the P_{clpE}-lux bioreporter makes it well-suited for identifying compounds that induce proteotoxic stress via direct protein damage. As many bioactive natural products contain thiol-reactive functional groups, the bioreporter may also facilitate the early detection of broadly reactive compounds whose nonspecific interactions with cellular proteins should be considered in mechanistic evaluation and subsequent compound optimization. Expansion of the bioreporter-guided platform offers several promising directions, including the incorporation of additional bioreporters to broaden MoA coverage. Furthermore, while many antibacterial mechanisms are transferable between Gram-positive and Gram-negative bacteria, antibacterial effects related to the outer membrane and associated envelope stress responses cannot be captured using *B. subtilis* as the strain background. Investigating such processes would require adapting the system to Gram-negative model organisms, thereby further extending the applicability of the bioreporter platform.

REFERENCES

(1) Hutchings, M. I.; Truman, A. W.; Wilkinson, B. Antibiotics: Past, Present and Future. *Curr. Opin. Microbiol.* **2019**, *51*, 72–80. https://doi.org/10.1016/j.mib.2019.10.008.

(2) Lewis, K. Platforms for Antibiotic Discovery. *Nat. Rev. Drug Discov.* **2013**, *12* (5), 371–387. https://doi.org/10.1038/nrd3975.

(3) Silver, L. L. Challenges of Antibacterial Discovery. *Clin. Microbiol. Rev.* **2011**, *24* (1), 71–109. https://doi.org/10.1128/CMR.00030-10.

(4) Cook, M. A.; Wright, G. D. The Past, Present, and Future of Antibiotics. *Sci. Transl. Med.* **2022**, *14* (657), eabo7793. https://doi.org/10.1126/scitranslmed.abo7793.

(5) Wasan, H.; Singh, D.; Reeta, K. H.; Gupta, Y. K. Landscape of Push Funding in Antibiotic Research: Current Status and Way Forward. *Biology* **2023**, *12* (1), 101. https://doi.org/10.3390/biology12010101.

(6) Projan, S. J. Why Is Big Pharma Getting out of Antibacterial Drug Discovery? *Curr. Opin. Microbiol.* **2003**, *6* (5), 427–430. https://doi.org/10.1016/j.mib.2003.08.003.

(7) Butler, M. S.; Henderson, I. R.; Capon, R. J.; Blaskovich, M. A. T. Antibiotics in the Clinical Pipeline as of December 2022. *J. Antibiot. (Tokyo)* **2023**, *76* (8), 431–473. https://doi.org/10.1038/s41429-023-00629-8.

(8) Gwynn, M. N.; Portnoy, A.; Rittenhouse, S. F.; Payne, D. J. Challenges of Antibacterial Discovery Revisited. *Ann. N. Y. Acad. Sci.* **2010**, *1213* (1), 5–19. https://doi.org/10.1111/j.1749-6632.2010.05828.x.

(9) Imai, Y.; Meyer, K. J.; Iinishi, A.; Favre-Godal, Q.; Green, R.; Manuse, S.; Caboni, M.; Mori, M.; Niles, S.; Ghiglieri, M.; Honrao, C.; Ma, X.; Guo, J. J.; Makriyannis, A.; Linares-Otoya, L.; Böhringer, N.; Wuisan, Z. G.; Kaur, H.; Wu, R.; Mateus, A.; Typas, A.; Savitski, M. M.; Espinoza, J. L.; O'Rourke, A.; Nelson, K. E.; Hiller, S.; Noinaj, N.; Schäberle, T. F.; D'Onofrio, A.; Lewis, K. A New Antibiotic Selectively Kills Gram-Negative Pathogens. *Nature* **2019**, *576* (7787), 459–464. https://doi.org/10.1038/s41586-019-1791-1.

(10) Ling, L. L.; Schneider, T.; Peoples, A. J.; Spoering, A. L.; Engels, I.; Conlon, B. P.; Mueller, A.; Schäberle, T. F.; Hughes, D. E.; Epstein, S.; Jones, M.; Lazarides, L.; Steadman, V. A.; Cohen, D. R.; Felix, C. R.; Fetterman, K. A.; Millett, W. P.; Nitti, A. G.; Zullo, A. M.; Chen, C.; Lewis, K. A New Antibiotic Kills Pathogens without Detectable Resistance. *Nature* **2015**, *517* (7535), 455–459. https://doi.org/10.1038/nature14098.

(11) Walsh, T. R.; Gales, A. C.; Laxminarayan, R.; Dodd, P. C. Antimicrobial Resistance: Addressing a Global Threat to Humanity. *PLoS Med.* **2023**, *20* (7), e1004264. https://doi.org/10.1371/journal.pmed.1004264.

(12) Aljeldah, M. M. Antimicrobial Resistance and Its Spread Is a Global Threat. *Antibiotics* **2022**, *11* (8), 1082. https://doi.org/10.3390/antibiotics11081082.

(13)Brötz-Oesterhelt, H.; Sass, P. Postgenomic Strategies in Antibacterial Drug Discovery. *Future Microbiol.* **2010**, *5* (10), 1553–1579. https://doi.org/10.2217/fmb.10.119.

(14) Landeta, C.; Mejia-Santana, A. Union Is Strength: Target-Based and Whole-Cell High-Throughput Screens in Antibacterial Discovery. *J. Bacteriol.* **2022**, *204* (4), e00477-21. https://doi.org/10.1128/jb.00477-21.

(15) Rütten, A.; Kirchner, T.; Musiol-Kroll, E. M. Overview on Strategies and Assays for Antibiotic Discovery. *Pharmaceuticals* **2022**, *15* (10), 1302. https://doi.org/10.3390/ph15101302.

(16) Miethke, M.; Pieroni, M.; Weber, T.; Brönstrup, M.; Hammann, P.; Halby, L.; Arimondo, P. B.; Glaser, P.; Aigle, B.; Bode, H. B.; Moreira, R.; Li, Y.; Luzhetskyy, A.; Medema, M. H.; Pernodet, J.-L.; Stadler, M.; Tormo, J. R.; Genilloud, O.; Truman, A. W.; Weissman, K. J.; Takano, E.; Sabatini, S.; Stegmann, E.; Brötz-Oesterhelt, H.; Wohlleben, W.; Seemann, M.; Empting, M.; Hirsch, A. K. H.; Loretz, B.; Lehr, C.-M.; Titz, A.; Herrmann, J.; Jaeger, T.; Alt, S.; Hesterkamp, T.; Winterhalter, M.; Schiefer, A.; Pfarr, K.; Hoerauf, A.; Graz, H.; Graz, M.; Lindvall, M.; Ramurthy, S.; Karlén, A.; van Dongen, M.; Petkovic, H.; Keller, A.; Peyrane, F.; Donadio, S.; Fraisse, L.; Piddock, L. J. V.; Gilbert, I. H.; Moser, H. E.; Müller, R. Towards the Sustainable Discovery and Development of New Antibiotics. *Nat. Rev. Chem.* **2021**, *5* (10), 726–749. https://doi.org/10.1038/s41570-021-00313-1.

(17) Baranova, A. A.; Alferova, V. A.; Korshun, V. A.; Tyurin, A. P. Modern Trends in Natural Antibiotic Discovery. *Life* **2023**, *13* (5), 1073. https://doi.org/10.3390/life13051073.

(18) Wohlleben, W.; Mast, Y.; Stegmann, E.; Ziemert, N. Antibiotic Drug Discovery. *Microb. Biotechnol.* **2016**, *9* (5), 541–548. https://doi.org/10.1111/1751-7915.12388.

(19) Li, L. Accessing Hidden Microbial Biosynthetic Potential from Underexplored Sources for Novel Drug Discovery. *Biotechnol. Adv.* **2023**, *66*, 108176. https://doi.org/10.1016/j.biotechadv.2023.108176.

(20) Seyedsayamdost, M. R. High-Throughput Platform for the Discovery of Elicitors of Silent Bacterial Gene Clusters. *Proc. Natl. Acad. Sci.* **2014**, *111* (20), 7266–7271. https://doi.org/10.1073/pnas.1400019111.

(21) Asamizu, S. Co-Cultivation Strategies for Natural Product Discovery from Actinomycetes: Unlocking Silent Secondary Metabolism with Mycolic Acid-Containing Bacteria. *World J. Microbiol. Biotechnol.* **2025**, *41* (7), 217. https://doi.org/10.1007/s11274-025-04406-7.

(22) Scherlach, K.; Hertweck, C. Mining and Unearthing Hidden Biosynthetic Potential. *Nat. Commun.* **2021**, *12* (1), 3864. https://doi.org/10.1038/s41467-021-24133-5.

(23) Payne, D. J.; Gwynn, M. N.; Holmes, D. J.; Pompliano, D. L. Drugs for Bad Bugs: Confronting the Challenges of Antibacterial Discovery. *Nat. Rev. Drug Discov.* **2007**, *6* (1), 29–40. https://doi.org/10.1038/nrd2201.

(24)Perros, M. A Sustainable Model for Antibiotics. *Science* **2015**, *347* (6226), 1062–1064. https://doi.org/10.1126/science.aaa3048.

(25) McDowell, L. L.; Quinn, C. L.; Leeds, J. A.; Silverman, J. A.; Silver, L. L. Perspective on Antibacterial Lead Identification Challenges and the Role of Hypothesis-Driven Strategies. *SLAS Discov.* **2019**, *24* (4), 440–456. https://doi.org/10.1177/2472555218818786.

(26) Roemhild, R.; Bollenbach, T.; Andersson, D. I. The Physiology and Genetics of Bacterial Responses to Antibiotic Combinations. *Nat. Rev. Microbiol.* **2022**, *20* (8), 478–490. https://doi.org/10.1038/s41579-022-00700-5.

(27) Lade, H.; Kim, J.-S. Bacterial Targets of Antibiotics in Methicillin-Resistant *Staphylococcus Aureus*. *Antibiotics* **2021**, *10* (4), 398. https://doi.org/10.3390/antibiotics10040398.

(28) Aldred, K. J.; Kerns, R. J.; Osheroff, N. Mechanism of Quinolone Action and Resistance. *Biochemistry* **2014**, *53* (10), 1565–1574. https://doi.org/10.1021/bi5000564.

(29) Drlica, K.; Malik, M.; Kerns, R. J.; Zhao, X. Quinolone-Mediated Bacterial Death. *Antimicrob. Agents Chemother.* **2008**, *52* (2), 385–392. https://doi.org/10.1128/AAC.01617-06.
(30) Anderle, C.; Stieger, M.; Burrell, M.; Reinelt, S.; Maxwell, A.; Page, M.; Heide, L. Biological Activities of Novel Gyrase Inhibitors of the Aminocoumarin Class. *Antimicrob. Agents Chemother.* **2008**, *52* (6), 1982–1990. https://doi.org/10.1128/AAC.01235-07.
(31) Estrada, A.; Wright, D. L.; Anderson, A. C. Antibacterial Antifolates: From Development through Resistance to the Next Generation. *Cold Spring Harb. Perspect. Med.* **2016**, *6* (8), a028324. https://doi.org/10.1101/cshperspect.a028324.
(32) Wormser, G. P.; Keusch, G. T.; Heel, R. C. Co-Trimoxazole (Trimethoprim-Sulfamethoxazole): An Updated Review of Its Antibacterial Activity and Clinical Efficacy. *Drugs* **1982**, *24* (6), 459–518. https://doi.org/10.2165/00003495-198224060-00002.
(33) Campbell, E. A.; Korzheva, N.; Mustaev, A.; Murakami, K.; Nair, S.; Goldfarb, A.; Darst, S. A. Structural Mechanism for Rifampicin Inhibition of Bacterial RNA Polymerase. *Cell* **2001**, *104* (6), 901–912. https://doi.org/10.1016/S0092-8674(01)00286-0.
(34) Artsimovitch, I.; Seddon, J.; Sears, P. Fidaxomicin Is an Inhibitor of the Initiation of Bacterial RNA Synthesis. *Clin Infect Dis* **2012**, *55 Suppl 2* (Suppl 2), S127-131. https://doi.org/10.1093/cid/cis358.
(35) Lo, Y.-S.; Tseng, W.-H.; Chuang, C.-Y.; Hou, M.-H. The Structural Basis of Actinomycin D-Binding Induces Nucleotide Flipping out, a Sharp Bend and a Left-Handed Twist in CGG Triplet Repeats. *Nucleic Acids Res.* **2013**, *41* (7), 4284–4294. https://doi.org/10.1093/nar/gkt084.
(36) Yang, F.; Teves, S. S.; Kemp, C. J.; Henikoff, S. Doxorubicin, DNA Torsion, and Chromatin Dynamics. *Biochim. Biophys. Acta* **2014**, *1845* (1), 84–89. https://doi.org/10.1016/j.bbcan.2013.12.002.
(37) Kelland, L. The Resurgence of Platinum-Based Cancer Chemotherapy. *Nat. Rev. Cancer* **2007**, *7* (8), 573–584. https://doi.org/10.1038/nrc2167.
(38) Tomasz, M. Mitomycin C: Small, Fast and Deadly (but Very Selective). *Chem. Biol.* **1995**, *2* (9), 575–579. https://doi.org/10.1016/1074-5521(95)90120-5.
(39) Barrett, M. P.; Gemmell, C. G.; Suckling, C. J. Minor Groove Binders as Anti-Infective Agents. *Pharmacol. Ther.* **2013**, *139* (1), 12–23. https://doi.org/10.1016/j.pharmthera.2013.03.002.
(40) Ntallis, C.; Martin, N. I.; Edwards, A. M.; Weingarth, M. Bacterial Cell Envelope-Targeting Antibiotics. *Nat. Rev. Microbiol.* **2026**, *24* (3), 183–196. https://doi.org/10.1038/s41579-025-01247-x.
(41) Egan, A. J. F.; Errington, J.; Vollmer, W. Regulation of Peptidoglycan Synthesis and Remodelling. *Nat. Rev. Microbiol.* **2020**, *18* (8), 446–460. https://doi.org/10.1038/s41579-020-0366-3.
(42) Silver, L. L. Fosfomycin: Mechanism and Resistance. *Cold Spring Harb. Perspect. Med.* **2017**, *7* (2), a025262. https://doi.org/10.1101/cshperspect.a025262.
(43) Batson, S.; De Chiara, C.; Majce, V.; Lloyd, A. J.; Gobec, S.; Rea, D.; Fülöp, V.; Thoroughgood, C. W.; Simmons, K. J.; Dowson, C. G.; Fishwick, C. W. G.; De Carvalho, L. P. S.; Roper, D. I. Inhibition of D-Ala:D-Ala Ligase through a

Phosphorylated Form of the Antibiotic D-Cycloserine. *Nat. Commun.* **2017**, *8* (1), 1939. https://doi.org/10.1038/s41467-017-02118-7.
(44) Kingston, A. W.; Zhao, H.; Cook, G. M.; Helmann, J. D. Accumulation of Heptaprenyl Diphosphate Sensitizes *Bacillus Subtilis* to Bacitracin: Implications for the Mechanism of Resistance Mediated by the BceAB Transporter. *Mol. Microbiol.* **2014**, *93* (1), 37–49. https://doi.org/10.1111/mmi.12637.
(45) Fang, X.; Tiyanont, K.; Zhang, Y.; Wanner, J.; Boger, D.; Walker, S. The Mechanism of Action of Ramoplanin and Enduracidin. *Mol. Biosyst.* **2005**, *2* (1), 69–76. https://doi.org/10.1039/B515328J.
(46) Schneider, T.; Sahl, H.-G. An Oldie but a Goodie – Cell Wall Biosynthesis as Antibiotic Target Pathway. *Int. J. Med. Microbiol.* **2010**, *300* (2–3), 161–169. https://doi.org/10.1016/j.ijmm.2009.10.005.
(47) Bush, K.; Bradford, P. A. β-Lactams and β-Lactamase Inhibitors: An Overview. *Cold Spring Harb. Perspect. Med.* **2016**, *6* (8), a025247. https://doi.org/10.1101/cshperspect.a025247.
(48) Kahne, D.; Leimkuhler, C.; Lu, W.; Walsh, C. Glycopeptide and Lipoglycopeptide Antibiotics. *Chem. Rev.* **2005**, *105* (2), 425–448. https://doi.org/10.1021/cr030103a.
(49) Valkenier, H.; Davis, A. P. Making a Match for Valinomycin: Steroidal Scaffolds in the Design of Electroneutral, Electrogenic Anion Carriers. *Acc. Chem. Res.* **2013**, *46* (12), 2898–2909. https://doi.org/10.1021/ar4000345.
(50) Kelkar, D. A.; Chattopadhyay, A. The Gramicidin Ion Channel: A Model Membrane Protein. *Biochim. Biophys. Acta BBA - Biomembr.* **2007**, *1768* (9), 2011–2025. https://doi.org/10.1016/j.bbamem.2007.05.011.
(51) Kasianowicz, J.; Benz, R.; McLaughlin, S. The Kinetic Mechanism by Which CCCP (Carbonyl Cyanidem-Chlorophenylhydrazone) Transports Protons across Membranes. *J. Membr. Biol.* **1984**, *82* (2), 179–190. https://doi.org/10.1007/BF01868942.
(52) Grein, F.; Müller, A.; Scherer, K. M.; Liu, X.; Ludwig, K. C.; Klöckner, A.; Strach, M.; Sahl, H.-G.; Kubitscheck, U.; Schneider, T. Ca2+-Daptomycin Targets Cell Wall Biosynthesis by Forming a Tripartite Complex with Undecaprenyl-Coupled Intermediates and Membrane Lipids. *Nat. Commun.* **2020**, *11* (1), 1455. https://doi.org/10.1038/s41467-020-15257-1.
(53) Taylor, S. D.; Palmer, M. The Action Mechanism of Daptomycin. *Bioorg. Med. Chem.* **2016**, *24* (24), 6253–6268. https://doi.org/10.1016/j.bmc.2016.05.052.
(54) Velkov, T.; Roberts, K. D.; Thompson, P. E.; Li, J. Polymyxins: A New Hope in Combating Gram-Negative Superbugs? *Future Med. Chem.* **2016**, *8* (10), 1017–1025. https://doi.org/10.4155/fmc-2016-0091.
(55) Heath, R. J.; Rock, C. O. Fatty Acid Biosynthesis as a Target for Novel Antibacterials. *Curr. Opin. Investig. Drugs* **2004**, *5* (2), 146–153.
(56) Price, A. C.; Choi, K.-H.; Heath, R. J.; Li, Z.; White, S. W.; Rock, C. O. Inhibition of β-Ketoacyl-Acyl Carrier Protein Synthases by Thiolactomycin and Cerulenin. *J. Biol. Chem.* **2001**, *276* (9), 6551–6559. https://doi.org/10.1074/jbc.M007101200.
(57) Buttke, T. M.; Ingram, L. O. Inhibition of Unsaturated Fatty Acid Synthesis in *Escherichia Coli* by the Antibiotic Cerulenin. *Biochemistry* **1978**, *17* (24), 5282–5286. https://doi.org/10.1021/bi00617a031.

(58) D'agnony, G.; Rosenfeld, I. S.; Awaya, J.; Ōmura, S.; Vagelos, P. R. Inhibition of Fatty Acid Synthesis by the Antibiotic Cerulenin. *Biochim. Biophys. Acta BBA - Lipids Lipid Metab.* **1973**, *326* (2), 155–166. https://doi.org/10.1016/0005-2760(73)90241-5.
(59) Heath, R. J.; Rubin, J. R.; Holland, D. R.; Zhang, E.; Snow, M. E.; Rock, C. O. Mechanism of Triclosan Inhibition of Bacterial Fatty Acid Synthesis. *J. Biol. Chem.* **1999**, *274* (16), 11110–11114. https://doi.org/10.1074/jbc.274.16.11110.
(60) Rodnina, M. V.; Wintermeyer, W. Recent Mechanistic Insights into Eukaryotic Ribosomes. *Curr. Opin. Cell Biol.* **2009**, *21* (3), 435–443. https://doi.org/10.1016/j.ceb.2009.01.023.
(61) Noller, H. F. RNA Structure: Reading the Ribosome. *Science* **2005**, *309* (5740), 1508–1514. https://doi.org/10.1126/science.1111771.
(62) Wilson, D. N. Ribosome-Targeting Antibiotics and Mechanisms of Bacterial Resistance. *Nat. Rev. Microbiol.* **2014**, *12* (1), 35–48. https://doi.org/10.1038/nrmicro3155.
(63) Wilson, D. N.; Schluenzen, F.; Harms, J. M.; Starosta, A. L.; Connell, S. R.; Fucini, P. The Oxazolidinone Antibiotics Perturb the Ribosomal Peptidyl-Transferase Center and Effect tRNA Positioning. *Proc. Natl. Acad. Sci. U. S. A.* **2008**, *105* (36), 13339–13344. https://doi.org/10.1073/pnas.0804276105.
(64) Brodersen, D. E.; Clemons, W. M.; Carter, A. P.; Morgan-Warren, R. J.; Wimberly, B. T.; Ramakrishnan, V. The Structural Basis for the Action of the Antibiotics Tetracycline, Pactamycin, and Hygromycin B on the 30S Ribosomal Subunit. *Cell* **2000**, *103* (7), 1143–1154. https://doi.org/10.1016/S0092-8674(00)00216-6.
(65) Chopra, I.; Roberts, M. Tetracycline Antibiotics: Mode of Action, Applications, Molecular Biology, and Epidemiology of Bacterial Resistance. *Microbiol. Mol. Biol. Rev.* **2001**, *65* (2), 232–260. https://doi.org/10.1128/MMBR.65.2.232-260.2001.
(66) Schlünzen, F.; Zarivach, R.; Harms, J.; Bashan, A.; Tocilj, A.; Albrecht, R.; Yonath, A.; Franceschi, F. Structural Basis for the Interaction of Antibiotics with the Peptidyl Transferase Centre in Eubacteria. *Nature* **2001**, *413* (6858), 814–821. https://doi.org/10.1038/35101544.
(67) Tenson, T.; Lovmar, M.; Ehrenberg, M. The Mechanism of Action of Macrolides, Lincosamides and Streptogramin B Reveals the Nascent Peptide Exit Path in the Ribosome. *J. Mol. Biol.* **2003**, *330* (5), 1005–1014. https://doi.org/10.1016/S0022-2836(03)00662-4.
(68) Kostopoulou, O. N.; Papadopoulos, G.; Kouvela, E. C.; Kalpaxis, D. L. Clindamycin Binding to Ribosomes Revisited: Foot Printing and Computational Detection of Two Binding Sites within the Peptidyl Transferase Center. *Pharm.* **2013**, *68* (7), 616–621.
(69) Beyer, D.; Pepper, K. The Streptogramin Antibiotics: Update on Their Mechanism of Action. *Expert Opin. Investig. Drugs* **1998**, *7* (4), 591–599. https://doi.org/10.1517/13543784.7.4.591.
(70) Borg, A.; Holm, M.; Shiroyama, I.; Hauryliuk, V.; Pavlov, M.; Sanyal, S.; Ehrenberg, M. Fusidic Acid Targets Elongation Factor G in Several Stages of Translocation on the Bacterial Ribosome. *J. Biol. Chem.* **2015**, *290* (6), 3440–3454. https://doi.org/10.1074/jbc.M114.611608.
(71) Khoshnood, S.; Heidary, M.; Asadi, A.; Soleimani, S.; Motahar, M.; Savari, M.; Saki, M.; Abdi, M. A Review on Mechanism of Action, Resistance, Synergism, and Clinical Implications of Mupirocin against *Staphylococcus Aureus*. *Biomed. Pharmacother.* **2019**, *109*, 1809–1818. https://doi.org/10.1016/j.biopha.2018.10.131.

(72) Vakulenko, S. B.; Mobashery, S. Versatility of Aminoglycosides and Prospects for Their Future. *Clin. Microbiol. Rev.* **2003**, *16* (3), 430–450. https://doi.org/10.1128/CMR.16.3.430-450.2003.
(73) Krause, K. M.; Serio, A. W.; Kane, T. R.; Connolly, L. E. Aminoglycosides: An Overview. *Cold Spring Harb. Perspect. Med.* **2016**, *6* (6), a027029. https://doi.org/10.1101/cshperspect.a027029.
(74) Aviner, R. The Science of Puromycin: From Studies of Ribosome Function to Applications in Biotechnology. *Comput. Struct. Biotechnol. J.* **2020**, *18*, 1074–1083. https://doi.org/10.1016/j.csbj.2020.04.014.
(75) Brötz-Oesterhelt, H.; Beyer, D.; Kroll, H.-P.; Endermann, R.; Ladel, C.; Schroeder, W.; Hinzen, B.; Raddatz, S.; Paulsen, H.; Henninger, K.; Bandow, J. E.; Sahl, H.-G.; Labischinski, H. Dysregulation of Bacterial Proteolytic Machinery by a New Class of Antibiotics. *Nat. Med.* **2005**, *11* (10), 1082–1087. https://doi.org/10.1038/nm1306.
(76) Kirstein, J.; Hoffmann, A.; Lilie, H.; Schmidt, R.; Rübsamen-Waigmann, H.; Brötz-Oesterhelt, H.; Mogk, A.; Turgay, K. The Antibiotic ADEP Reprogrammes ClpP, Switching It from a Regulated to an Uncontrolled Protease. *EMBO Mol. Med.* **2009**, *1* (1), 37–49. https://doi.org/10.1002/emmm.200900002.
(77) Gregory, J. D. The Stability of N-Ethylmaleimide and Its Reaction with Sulfhydryl Groups. *J. Am. Chem. Soc.* **1955**, *77* (14), 3922–3923. https://doi.org/10.1021/ja01619a073.
(78) Tuli, V. Bactericidal Action of Sulfhydryl Binding Compounds. *Antimicrob. Agents Chemother.* **1973**, *3* (2), 157–161. https://doi.org/10.1128/AAC.3.2.157.
(79) Pöther, D.-C.; Liebeke, M.; Hochgräfe, F.; Antelmann, H.; Becher, D.; Lalk, M.; Lindequist, U.; Borovok, I.; Cohen, G.; Aharonowitz, Y.; Hecker, M. Diamide Triggers Mainly S Thiolations in the Cytoplasmic Proteomes of *Bacillus Subtilis* and *Staphylococcus Aureus*. *J. Bacteriol.* **2009**, *191* (24), 7520–7530. https://doi.org/10.1128/JB.00937-09.
(80) Kohanski, M. A.; Dwyer, D. J.; Collins, J. J. How Antibiotics Kill Bacteria: From Targets to Networks. *Nat. Rev. Microbiol.* **2010**, *8* (6), 423–435. https://doi.org/10.1038/nrmicro2333.
(81) Freiberg, C.; Brunner, N.; Macko, L.; Fischer, H. P. Discovering Antibiotic Efficacy Biomarkers: Toward Mechanism-Specific High Content Compound Screening. *Mol. Cell. Proteomics* **2006**, *5* (12), 2326–2335. https://doi.org/10.1074/mcp.M600127-MCP200.
(82) Hutter, B.; Fischer, C.; Jacobi, A.; Schaab, C.; Loferer, H. Panel of *Bacillus Subtilis* Reporter Strains Indicative of Various Modes of Action. *Antimicrob. Agents Chemother.* **2004**, *48* (7), 2588–2594. https://doi.org/10.1128/AAC.48.7.2588-2594.2004.
(83) Urban, A.; Eckermann, S.; Fast, B.; Metzger, S.; Gehling, M.; Ziegelbauer, K.; Rübsamen-Waigmann, H.; Freiberg, C. Novel Whole-Cell Antibiotic Biosensors for Compound Discovery. *Appl. Environ. Microbiol.* **2007**, *73* (20), 6436–6443. https://doi.org/10.1128/AEM.00586-07.
(84) Wex, K. W.; Saur, J. S.; Handel, F.; Ortlieb, N.; Mokeev, V.; Kulik, A.; Niedermeyer, T. H. J.; Mast, Y.; Grond, S.; Berscheid, A.; Brötz-Oesterhelt, H. Bioreporters for Direct Mode of Action-Informed Screening of Antibiotic Producer Strains. *Cell Chem. Biol.* **2021**, *28* (8), 1242-1252.e4. https://doi.org/10.1016/j.chembiol.2021.02.022.

(85) Geibel, C.; Schubert, J.; Knoblauch, S. B.; Hernandez, A.; Boldt, L.; Schneider, D. C.; Papadopoulos Lambidis, S.; Vitale, G. A.; Fleischer, J.; Haussmann, M.; Gross, H.; Wang, M.; Brötz-Oesterhelt, H.; Petras, D. High-Frequency Microfluidic Fractionation for Compound-Resolved Bioactivity-Based Metabolomics. *Anal. Chem.* **2025**, *97* (43), 24093–24104. https://doi.org/10.1021/acs.analchem.5c04612.
(86) Gaudêncio, S. P.; Pereira, F. Dereplication: Racing to Speed up the Natural Products Discovery Process. *Nat. Prod. Rep.* **2015**, *32* (6), 779–810. https://doi.org/10.1039/C4NP00134F.
(87) Wolfender, J.-L.; Marti, G.; Thomas, A.; Bertrand, S. Current Approaches and Challenges for the Metabolite Profiling of Complex Natural Extracts. *J. Chromatogr. A* **2015**, *1382*, 136–164. https://doi.org/10.1016/j.chroma.2014.10.091.
(88) Bandow, J. E.; Brötz, H.; Leichert, L. I. O.; Labischinski, H.; Hecker, M. Proteomic Approach to Understanding Antibiotic Action. *Antimicrob. Agents Chemother.* **2003**, *47* (3), 948–955. https://doi.org/10.1128/AAC.47.3.948-955.2003.
(89) Piggot, P. J. Mapping of Asporogenous Mutations of *Bacillus Subtilis*: A Minimum Estimate of the Number of Sporulation Operons. *J. Bacteriol.* **1973**, *114*, 1241–1253.
(90) Radeck, J.; Kraft, K.; Bartels, J.; Cikovic, T.; Dürr, F.; Emenegger, J.; Kelterborn, S.; Sauer, C.; Fritz, G.; Gebhard, S.; Mascher, T. The Bacillus BioBrick Box: Generation and Evaluation of Essential Genetic Building Blocks for Standardized Work with *Bacillus Subtilis*. *J. Biol. Eng.* **2013**, *7* (1), 29. https://doi.org/10.1186/1754-1611-7-29.
(91) King, A. A.; Chater, K. F. The Expression of the *Escherichia Coli* lacZ Gene in Streptomyces. *Microbiology* **1986**, *132* (6), 1739–1752. https://doi.org/10.1099/00221287-132-6-1739.
(92) Eckhardt, T.; Strickler, J.; Gorniak, L.; Burnett, W. V.; Fare, L. R. Characterization of the Promoter, Signal Sequence, and Amino Terminus of a Secreted Beta-Galactosidase from *Streptomyces Lividans*. *J. Bacteriol.* **1987**, *169* (9), 4249–4256. https://doi.org/10.1128/jb.169.9.4249-4256.1987.
(93) Mascher, T.; Zimmer, S. L.; Smith, T. A.; Helmann, J. D. Antibiotic-Inducible Promoter Regulated by the Cell Envelope Stress-Sensing Two-Component System LiaRS of *Bacillus Subtilis*. *Antimicrob. Agents Chemother.* **2004**, *48* (8), 2888–2896. https://doi.org/10.1128/AAC.48.8.2888-2896.2004.
(94) Eymann, C.; Homuth, G.; Scharf, C.; Hecker, M. *Bacillus Subtilis* Functional Genomics: Global Characterization of the Stringent Response by Proteome and Transcriptome Analysis. *J. Bacteriol.* **2002**, *184* (9), 2500–2520. https://doi.org/10.1128/JB.184.9.2500-2520.2002.
(95) Ratnayake-Lecamwasam, M.; Serror, P.; Wong, K.-W.; Sonenshein, A. L. *Bacillus Subtilis* CodY Represses Early-Stationary-Phase Genes by Sensing GTP Levels. *Genes Dev.* **2001**, *15* (9), 1093–1103. https://doi.org/10.1101/gad.874201.
(96) Gajic, I.; Kabic, J.; Kekic, D.; Jovicevic, M.; Milenkovic, M.; Mitic Culafic, D.; Trudic, A.; Ranin, L.; Opavski, N. Antimicrobial Susceptibility Testing: A Comprehensive Review of Currently Used Methods. *Antibiotics* **2022**, *11* (4), 427. https://doi.org/10.3390/antibiotics11040427.
(97) Krawczyk, S. J.; Leśniczak-Staszak, M.; Gowin, E.; Szaflarski, W. Mechanistic Insights into Clinically Relevant Ribosome-Targeting Antibiotics. *Biomolecules* **2024**, *14* (10), 1263. https://doi.org/10.3390/biom14101263.

(98) Derré, I.; Rapoport, G.; Devine, K.; Rose, M.; Msadek, T. ClpE, a Novel Type of HSP100 ATPase, Is Part of the CtsR Heat Shock Regulon of *Bacillus Subtilis*. *Mol. Microbiol.* **1999**, *32* (3), 581–593. https://doi.org/10.1046/j.1365-2958.1999.01374.x.
(99) Gerth, U.; Kirstein, J.; Mostertz, J.; Waldminghaus, T.; Miethke, M.; Kock, H.; Hecker, M. Fine-Tuning in Regulation of Clp Protein Content in *Bacillus Subtilis*. *J. Bacteriol.* **2004**, *186* (1), 179–191. https://doi.org/10.1128/JB.186.1.179-191.2004.
(100) Elsholz, A. K. W.; Michalik, S.; Zühlke, D.; Hecker, M.; Gerth, U. CtsR, the Gram-Positive Master Regulator of Protein Quality Control, Feels the Heat. *EMBO J.* **2010**, *29* (21), 3621–3629. https://doi.org/10.1038/emboj.2010.228.
(101) Fuhrmann, J.; Schmidt, A.; Spiess, S.; Lehner, A.; Turgay, K.; Mechtler, K.; Charpentier, E.; Clausen, T. McsB Is a Protein Arginine Kinase That Phosphorylates and Inhibits the Heat-Shock Regulator CtsR. *Science* **2009**, *324* (5932), 1323–1327. https://doi.org/10.1126/science.1170088.
(102) Yan, W.; Cai, Y.; Zhang, Q.; Liu, Y.; Xu, W.; Yin, Y.; He, Y.; Wang, H.; Zhang, X. Screening and Identification of ClpE Interaction Proteins in Streptococcus Pneumoniae by a Bacterial Two-Hybrid System and Co-Immunoprecipitation. *J. Microbiol.* **2013**, *51* (4), 453–460. https://doi.org/10.1007/s12275-013-3001-4.
(103) Miethke, M.; Hecker, M.; Gerth, U. Involvement of *Bacillus Subtilis* ClpE in CtsR Degradation and Protein Quality Control. *J. Bacteriol.* **2006**, *188* (13), 4610–4619. https://doi.org/10.1128/JB.00287-06.
(104) Liang, W.-C.; Wang, X.-H.; Lin, M.-G.; Lin, L.-L. A 70-kDa Molecular Chaperone, DnaK, from the Industrial Bacterium *Bacillus Licheniformis*: Gene Cloning, Purification and Molecular Characterization of the Recombinant Protein. *Indian J. Microbiol.* **2009**, *49* (2), 151–160. https://doi.org/10.1007/s12088-009-0029-6.
(105) Schramm, F. D.; Heinrich, K.; Thüring, M.; Bernhardt, J.; Jonas, K. An Essential Regulatory Function of the DnaK Chaperone Dictates the Decision between Proliferation and Maintenance in Caulobacter Crescentus. *PLOS Genet.* **2017**, *13* (12), e1007148. https://doi.org/10.1371/journal.pgen.1007148.
(106) Mogk, A.; Völker, A.; Engelmann, S.; Hecker, M.; Schumann, W.; Völker, U. Nonnative Proteins Induce Expression of the *Bacillus Subtilis* CIRCE Regulon. *J. Bacteriol.* **1998**, *180* (11), 2895–2900. https://doi.org/10.1128/JB.180.11.2895-2900.1998.
(107) Zuber, U.; Schumann, W. CIRCE, a Novel Heat Shock Element Involved in Regulation of Heat Shock Operon dnaK of *Bacillus Subtilis*. *J. Bacteriol.* **1994**, *176* (5), 1359–1363. https://doi.org/10.1128/jb.176.5.1359-1363.1994.
(108) Schröder, H.; Langer, T.; Hartl, F. U.; Bukau, B. DnaK, DnaJ and GrpE Form a Cellular Chaperone Machinery Capable of Repairing Heat-Induced Protein Damage. *EMBO J.* **1993**, *12* (11), 4137–4144. https://doi.org/10.1002/j.1460-2075.1993.tb06097.x.
(109) Schujman, G. E.; Paoletti, L.; Grossman, A. D.; De Mendoza, D. FapR, a Bacterial Transcription Factor Involved in Global Regulation of Membrane Lipid Biosynthesis. *Dev. Cell* **2003**, *4* (5), 663–672. https://doi.org/10.1016/S1534-5807(03)00123-0.
(110) McOsker, C. C.; Fitzpatrick, P. M. Nitrofurantoin: Mechanism of Action and Implications for Resistance Development in Common Uropathogens. *J. Antimicrob. Chemother.* **1994**, *33* (suppl A), 23–30. https://doi.org/10.1093/jac/33.suppl_A.23.

(111) Kettlewell, R.; Jones, C.; Felton, T. W.; Lagator, M.; Gifford, D. R. Insights into Durability against Resistance from the Antibiotic Nitrofurantoin. *Npj Antimicrob. Resist.* **2024**, *2* (1), 41. https://doi.org/10.1038/s44259-024-00056-1.
(112) Au, N.; Kuester-Schoeck, E.; Mandava, V.; Bothwell, L. E.; Canny, S. P.; Chachu, K.; Colavito, S. A.; Fuller, S. N.; Groban, E. S.; Hensley, L. A.; O'Brien, T. C.; Shah, A.; Tierney, J. T.; Tomm, L. L.; O'Gara, T. M.; Goranov, A. I.; Grossman, A. D.; Lovett, C. M. Genetic Composition of the *Bacillus Subtilis* SOS System. *J. Bacteriol.* **2005**, *187* (22), 7655–7666. https://doi.org/10.1128/JB.187.22.7655-7666.2005.
(113) Hitchings, G. H. Mechanism of Action of Trimethoprim-Sulfamethoxazole–I. *J. Infect. Dis.* **1973**, *128* (Supplement 3), S433–S436. https://doi.org/10.1093/infdis/128.Supplement_3.S433.
(114) Sköld, O. Sulfonamide Resistance: Mechanisms and Trends. *Drug Resist. Updat.* **2000**, *3* (3), 155–160. https://doi.org/10.1054/drup.2000.0146.
(115) Koch, A. E.; Burchall, J. J. Reversal of the Antimicrobial Activity of Trimethoprim by Thymidine in Commercially Prepared Media. *Appl. Microbiol.* **1971**, *22* (5), 812–817. https://doi.org/10.1128/am.22.5.812-817.1971.
(116) Jervis, A. J.; Thackray, P. D.; Houston, C. W.; Horsburgh, M. J.; Moir, A. SigM-Responsive Genes of *Bacillus Subtilis* and Their Promoters. *J. Bacteriol.* **2007**, *189* (12), 4534–4538. https://doi.org/10.1128/JB.00130-07.
(117) Masser, E. A.; Burby, P. E.; Hawkins, W. D.; Gustafson, B. R.; Lenhart, J. S.; Simmons, L. A. DNA Damage Checkpoint Activation Affects Peptidoglycan Synthesis and Late Divisome Components in *Bacillus Subtilis*. *Mol. Microbiol.* **2021**, *116* (2), 707–722. https://doi.org/10.1111/mmi.14765.
(118) Miyazaki, Y.; Shibuya, M.; Sugawara, H.; Kawaguchi, O.; Hirose, C.; Nagatsu, J.; Esumi, S. Salinomycin, a New Polyether Antibiotic. *J. Antibiot. (Tokyo)* **1974**, *27* (11), 814–821. https://doi.org/10.7164/antibiotics.27.814.
(119) Reynolds, P. E. Structure, Biochemistry and Mechanism of Action of Glycopeptide Antibiotics. *Eur. J. Clin. Microbiol. Infect. Dis.* **1989**, *8* (11), 943–950. https://doi.org/10.1007/BF01967563.
(120) Torres, C.; Galián, C.; Freiberg, C.; Fantino, J. R.; Jault, J. M. The YheI/YheH Heterodimer from *Bacillus Subtilis* Is a Multidrug ABC Transporter. *Biochim. Biophys. Acta - Biomembr.* **2009**, *1788* (3), 615–622. https://doi.org/10.1016/j.bbamem.2008.12.012.
(121) McGaha, S. M.; Champney, W. S. Hygromycin B Inhibition of Protein Synthesis and Ribosome Biogenesis in *Escherichia Coli*. *Antimicrob. Agents Chemother.* **2007**, *51* (2), 591–596. https://doi.org/10.1128/AAC.01116-06.
(122) Borovinskaya, M. A.; Shoji, S.; Fredrick, K.; Cate, J. H. D. Structural Basis for Hygromycin B Inhibition of Protein Biosynthesis. *RNA* **2008**, *14* (8), 1590–1599. https://doi.org/10.1261/rna.1076908.
(123) Harris, J. W.; Power, J. A. Diamide: Mechanisms of Action and Interactions with Other Sensitizers. *Br. J. Cancer* **1978**, *3*, 84–89.
(124) Reusser, F. Mode of Action of Berninamycin. An Inhibitor of Protein Biosynthesis. *Biochemistry* **1969**, *8* (8), 3303–3308. https://doi.org/10.1021/bi00836a026.
(125) Yu, G.; Peng, H.; Cao, J.; Liao, A.; Long, P.; Huang, J.; Hui, M. Avilamycin Production Enhancement by Mutagenesis and Fermentation Optimization in *Streptomyces Viridochromogenes*. *World J. Microbiol. Biotechnol.* **2022**, *38* (3), 50. https://doi.org/10.1007/s11274-021-03191-3.

(126) Just-Baringo, X.; Albericio, F.; Álvarez, M. Thiopeptide Antibiotics: Retrospective and Recent Advances. *Mar. Drugs* **2014**, *12* (1), 317–351. https://doi.org/10.3390/md12010317.
(127) Arenz, S.; Juette, M. F.; Graf, M.; Nguyen, F.; Huter, P.; Polikanov, Y. S.; Blanchard, S. C.; Wilson, D. N. Structures of the Orthosomycin Antibiotics Avilamycin and Evernimicin in Complex with the Bacterial 70S Ribosome. *Proc. Natl. Acad. Sci.* **2016**, *113* (27), 7527–7532. https://doi.org/10.1073/pnas.1604790113.
(128) McNicholas, P. M.; Najarian, D. J.; Mann, P. A.; Hesk, D.; Hare, R. S.; Shaw, K. J.; Black, T. A. Evernimicin Binds Exclusively to the 50S Ribosomal Subunit and Inhibits Translation in Cell-Free Systems Derived from Both Gram-Positive and Gram-Negative Bacteria. *Antimicrob. Agents Chemother.* **2000**, *44* (5), 1121–1126. https://doi.org/10.1128/AAC.44.5.1121-1126.2000.
(129) Wieland, M.; Holm, M.; Rundlet, E. J.; Morici, M.; Koller, T. O.; Maviza, T. P.; Pogorevc, D.; Osterman, I. A.; Müller, R.; Blanchard, S. C.; Wilson, D. N. The Cyclic Octapeptide Antibiotic Argyrin B Inhibits Translation by Trapping EF-G on the Ribosome during Translocation. *Proc. Natl. Acad. Sci.* **2022**, *119* (19), e2114214119. https://doi.org/10.1073/pnas.2114214119.
(130) Seip, B.; Sacheau, G.; Dupuy, D.; Innis, C. A. Ribosomal Stalling Landscapes Revealed by High-Throughput Inverse Toeprinting of mRNA Libraries. *Life Sci. Alliance* **2018**, *1* (5), e201800148. https://doi.org/10.26508/lsa.201800148.
(131) Rodriguez-Martinez, A.; Young-Baird, S. K. Polysome Profiling Is an Extensible Tool for the Analysis of Bulk Protein Synthesis, Ribosome Biogenesis, and the Specific Steps in Translation. *Mol. Biol. Cell* **2025**, *36* (4), mr2. https://doi.org/10.1091/mbc.E24-08-0341.
(132) Ingolia, N. T.; Hussmann, J. A.; Weissman, J. S. Ribosome Profiling: Global Views of Translation. *Cold Spring Harb. Perspect. Biol.* **2019**, *11* (5), a032698. https://doi.org/10.1101/cshperspect.a032698.
(133) Hoffmann, A.; Steffens, U.; Maček, B.; Franz-Wachtel, M.; Nieselt, K.; Harbig, T. A.; Scherlach, K.; Hertweck, C.; Sahl, H.-G.; Bierbaum, G. The Unusual Mode of Action of the Polyketide Glycoside Antibiotic Cervimycin C. *mSphere* **2024**, *9* (5), e00764-23. https://doi.org/10.1128/msphere.00764-23.
(134) Okabe, T.; Yuan, B. D.; Fujio, I.; Sato, I.; Fukazawa, H.; Nishimura, T.; Tanaka, N. Studies on Antineoplastic Activity of Naphthomycin, a Naphthalenic Ansamycin, and Its Mode of Action. *J. Antibiot. (Tokyo)* **1985**, *38* (2), 230–235. https://doi.org/10.7164/antibiotics.38.230.
(135) Mortier, J.; Cambré, A.; Schack, S.; Christie, G.; Aertsen, A. Impact of Protein Aggregates on Sporulation and Germination of *Bacillus Subtilis*. *Microorganisms* **2023**, *11* (9), 2365. https://doi.org/10.3390/microorganisms11092365.
(136) Matavacas, J.; von Wachenfeldt, C. Update on the Protein Homeostasis Network in *Bacillus Subtilis*. *Front. Microbiol.* **2022**, *13*, 865141. https://doi.org/10.3389/fmicb.2022.865141.
(137) Gregg, R. E.; Heintz, R. L. The Inhibition of Eukaryotic Aminoacyl Transferase I by Chartreusin. *Arch. Biochem. Biophys.* **1972**, *152* (2), 451–456. https://doi.org/10.1016/0003-9861(72)90238-X.
(138) Portugal, J. Chartreusin, Elsamicin A and Related Anti-Cancer Antibiotics. *Contin. Anti-Cancer Agents Med. Chem.* **2003**, *3* (6), 411–420. https://doi.org/10.2174/1568011033482215.

(139) Hoffmann, T.; Troup, B.; Szabo, A.; Hungerer, C.; Jahn, D. The Anaerobic Life of *Bacillus Subtilis* : Cloning of the Genes Encoding the Respiratory Nitrate Reductase System. *FEMS Microbiol. Lett.* **1995**, *131* (2), 219–225. https://doi.org/10.1111/j.1574-6968.1995.tb07780.x.
(140) Cox, G.; Sieron, A.; King, A. M.; Pascale, G. D.; Pawlowski, A. C.; Koteva, K.; Wright, G. D. A Common Platform for Antibiotic Dereplication and Adjuvant Discovery. *Cell Chem. Biol.* **2017**, *24* (1), 98–109. https://doi.org/10.1016/j.chembiol.2016.11.011.
(141) Baltz, R. Renaissance in Antibacterial Discovery from Actinomycetes. *Curr. Opin. Pharmacol.* **2008**, *8* (5), 557–563. https://doi.org/10.1016/j.coph.2008.04.008.
(142) Burckhardt, R. M.; Escalante-Semerena, J. C. In *Bacillus Subtilis*, the SatA (Formerly YyaR) Acetyltransferase Detoxifies Streptothricin via Lysine Acetylation. *Appl. Environ. Microbiol.* **2017**, *83* (21), e01590-17. https://doi.org/10.1128/AEM.01590-17.
(143) Keeratipibul, S.; Sugiyama, M.; Nomi, R. Mechanism of Resistance to Streptothricin of a Producing Microorganism. *Biotechnol. Lett.* **1983**, *5* (7), 441–446. https://doi.org/10.1007/BF00132225.
(144) Jakubiec-Krzesniak, K.; Rajnisz-Mateusiak, A.; Guspiel, A.; Ziemska, J.; Solecka, J. Secondary Metabolites of Actinomycetes and Their Antibacterial, Antifungal and Antiviral Properties. *Pol. J. Microbiol.* **2018**, *67* (3), 259–272. https://doi.org/10.21307/pjm-2018-048.
(145) Bundale, S.; Begde, D.; Nashikkar, N.; Kadam, T.; Upadhyay, A. Optimization of Culture Conditions for Production of Bioactive Metabolites by *Streptomyces* Spp. Isolated from Soil. *Adv. Microbiol.* **2015**, *05* (06), 441–451. https://doi.org/10.4236/aim.2015.56045.
(146) Waksman, S. A.; Woodruff, H. B. Streptothricin, a New Selective Bacteriostatic and Bactericidal Agent, Particularly Active Against Gram-Negative Bacteria. *Exp. Biol. Med.* **1942**, *49* (2), 207–210. https://doi.org/10.3181/00379727-49-13515.
(147) Morgan, C. E.; Kang, Y.-S.; Green, A. B.; Smith, K. P.; Dowgiallo, M. G.; Miller, B. C.; Chiaraviglio, L.; Truelson, K. A.; Zulauf, K. E.; Rodriguez, S.; Kang, A. D.; Manetsch, R.; Yu, E. W.; Kirby, J. E. Streptothricin F Is a Bactericidal Antibiotic Effective against Highly Drug-Resistant Gram-Negative Bacteria That Interacts with the 30S Subunit of the 70S Ribosome. *PLOS Biol.* **2023**, *21* (5), e3002091. https://doi.org/10.1371/journal.pbio.3002091.